UNIVERSITY OF CALIFORNIA

Santa Barbara

Translating electrochemical aptamer-based sensors to real-world applications

A dissertation submitted in partial satisfaction of the

requirements for the degree Doctor of Philosophy

in Biochemistry and Molecular Biology

by

Jacob Somerson

Committee in charge:

Professor Kevin Plaxco, Chair

Professor Irene Chen

Professor David Low

Professor Omar Saleh

June 2018

The dissertation of Jacob Somerson is approved.

_____

Irene Chen

_____

David Low

_____

Omar Saleh

_____

Kevin Plaxco, Committee Chair

May 2018

ACKNOWLEDGEMENTS

No work exists in isolation and no person is an island. None of this would be possible without my many skilled collaborators and teachers and the many, many people who supported me.

Thanks to my advisor, Kevin Plaxco, for creating a collaborative, open, communicative environment filled with some of the best scientists I've known. Thank you for your commitment to my professional, scientific, literary and personal growth.

Thanks to my committee members, Professors Irene Chen, David Low and Omar Saleh for their helpful continued guidance.

Thank you to everyone at the Institute for Collaborative Biotechnologies. Without their joyful, caring abject competence, none of this work could even have begun.

I am indebted to so many collaborators, benchmates, visiting scientists, generators of interesting conversations, people who were willing to listen as I tried to verbalize new models, people who went on coffee breaks, people who kindly listened to my complaints when experiments failed, people who kindly listened to my complaints when experiments worked and to all the people who gave me things to think about. There are far too many to name, but particular thanks to Prof. Hui Li, Dr. Herschel Watkins, and Prof. Ryan White.

I'm fortunate to have a family who has always believed that I could accomplish anything and gave me the best tools possible. Thank you, Dad for showing me the healing power of the blend of science and human connection. Thank you, Mom for teaching me how to perpetually accomplish. Thank you, Katie for leading the way. Thank you, Joy for teaching me the transformative value of empathy. Thank you, Jeremy for giving me an amazing role

model to try to grow towards. Thank you, Rosanne for the nurturing and the inspiration. And unending thanks to Betty, our grande dame, for conversation, insight and love.

This work can seem thankless and unending without a nurturing, supportive community. Thank you to everyone who has held me up and helped me to be a little more beloved through these years, with special thanks to Christine, Bill, Tegan, Kristen, Baker, Borgia and Jackie.

Rick, thank you for believing in me, having my back and demonstrating both a vision and the execution of how to be a better person. Thank you for all of the joy, support, comfort and unconditional love. I love you too, babe.

To Björk, Liza Minnelli and Stephen Sondheim for teaching me the value of unabashed self-expression, the perpetual capacity for reinvention and the many ways to tell a great story.

To Margaret Atwood, Madeleine L'Engle, Bill Watterson, Gary Larson and all the other writers who taught me to imagine bigger than the world could be.

This work owes a great deal to the fifteenth century Sufi mystics who originated the cultivation and brewing of the coffee bean. My heartfelt thanks to them.

In loving memory of Dr. Michael Somerson, D.O. (1951-2007).

VITA OF JACOB SOMERSON
May 2018

EDUCATION

Bachelor of Science in Materials Science and Engineering, University of Cincinnati, June 2010 (cum laude, with honors)
Doctor of Philosophy in Biochemistry and Molecular Biology, University of California, Santa Barbara, June 2018 (expected)

PROFESSIONAL EMPLOYMENT

2007: Emerson Climate Technologies, Inc., Co-op Student, Materials Engineering Lab, Metallurgical Engineering and Services group
2008-2009: Air Force Research Laboratory, Student Trainee, Ceramics Branch, Materials and Manufacturing Directorate (AFRL/RXLN)

PUBLICATIONS

H. Li, **J. Somerson**, F. Xia, K. Plaxco; "Electrochemical DNA-based biosensors for continuous, real-time melamine detection in a flowing stream of foodstuffs", *submitted Apr 2018*

J. Somerson and K. Plaxco; "Electrochemical Aptamer-Based Sensors for Rapid Point-of-Use Monitoring of the Mycotoxin Ochratoxin A Directly in a Food Stream", *Molecules*, 2018

H. Li, P. Dauphin-Ducharme, N. Arroyo-Currás, C. Tran, P. Viera, S. Li, C. Shin, **J. Somerson**, T. Kippin, K. Plaxco; "A biomimetic surface greatly improves the in-vivo performance of electrochemical aptamer-based sensors", *Angew. Chem. Int. Ed.*, 2017

N. Arroyo-Currás, **J. Somerson**, P. Vieira, K. Ploense, T. Kippin, K. Plaxco; "Real-time measurement of small molecules in awake, ambulatory animals", *PNAS*, 2017

A. Idili, A. Amodio, M. Vidonis, **J. Feinberg-Somerson**, M. Castronovo, F. Ricci, "Folding-upon-Binding and Signal-on Electrochemical DNA sensor with High Affinity and Specificity", *Analytical Chemistry*, 2014

J. Somerson, N. Arroyo-Currás, G. Ortega, K. Ploense, H. Li, T. Kippin, K. Plaxco; "Calibration-free measurement of a specific protein directly in whole blood and in living animals", *in preparation*

J. Somerson, J. Yu, J.P. Wang and K.W. Plaxco, "An electrochemical sensor for point-of-care measurement of a malaria biomarker in small volume clinical samples", *in preparation*

PATENTS

N. Arroyo, **J. Somerson**, K. Plaxco, "Bio-electrochemical Sensor for Real-time, In Vivo Clinical Tests", UC Case 2016-135-0

AWARDS

2014-17 NIH / NCI F31, "Personalized, high-resolution pharmacokinetic measurements to improve drug dosing", Sole PI, Ruth L. Kirschstein National Research Service Award

MENTORSHIP

Visiting scientists
- Emma Bigelow, March 2014
  - Vice President, Research and Development
  - Diagnostic Biochips, Inc.
- Stefano Cinti, Ph.D., Summer 2016
  - U. Rome Tor Vergata

Visiting graduate students
- Katie Brombeck, Summer 2013, University of Kent

Postdoc training
- Hui Li, January 2015
- Netz Arroyo-Currás, February 2015

Undergraduate and first year graduate students
- Kenneth Pessino, Fall 2012 – Spring 2016,
  - undergraduate researcher
- Zoe Swank, Winter 2012 – Spring 2012,
  - undergraduate researcher
- Clayton Woodcock, Winter 2012, Ph.D. Rotation student
- Grant Gucinski, Fall 2012, Ph.D. Rotation student
- Megan Larisch, Spring 2014, Ph.D. Rotation student

Jack Kent Cooke Summer Institute: July 29 – August 4, 2012
- *A research experience for first-generation, low-income STEM students*
  - Eunice Santiago, San Joaquin Delta College
  - Edith Rodriguez, Santa Barbara City College
  - Ilda Fernandez, Napa Valley Community College
  - Ken Chow, College of San Mateo

Jack Kent Cooke Bridges and HSI-Condor Techs programs: Summer 2013
- Advise graduate students in mentoring STEM students
- Organize and facilitate professional development seminars
- Teach scientific communication skills

Writing and presentation
- Dr. Dusty Rose Miller, January – August 2015
  - Scientific writing and editing
  - Effective presentation and storytelling

FIELDS OF STUDY

Major Field: Biomolecular Science and Engineering with an emphasis in Biophysics and Bioengineering

PROFESSIONAL DEVELOPMENT AND TEACHING

Courses taught:

"The Power of the Plot: Tips and Tools for Figures and Graphs"
with Peter Allen (Marketing Director, College of Engineering)
Professional Development Seminar for graduate students and postdocs

General Chemistry Laboratory, Spring 2012
51 students in two sections

General Chemistry Laboratory, Winter 2012
41 students in two sections

Workshops:

Writing for Scientists: Transition Words for Science Writing
Teaching and Research: A Symbiotic Relationship
Getting Started: Techniques for Getting Your Writing Going
Grant Writing A: Grants, Funding Agencies, and Foundations: A-Z
Grant Writing B: Faculty Panel on Funding Programs
Grant Writing C: Story and Structure
Communicating your Science: Writing for the Public
Teaching Quantitative Concepts
Teaching Diverse Learners in Labs and Discussion Sections

Courses:

Teaching Assistant Training, University of California, Santa Barbara
Technical and Scientific Writing, University of Cincinnati

ABSTRACT

Translating electrochemical aptamer-based sensors to real-world applications

by

Jacob Somerson

By coupling the specific and selective binding of biomolecules with conformation-linked signaling and electrochemical outputs, electrochemical aptamer-based sensors (E-AB sensors) provide a unique ability to measure molecules in real-time directly in complex media. Because E-AB sensors do not require washing steps or reagent additions, they open the door for measurements *directly where they are needed* – in complex sample streams such as foodstuffs, clinical samples, and even directly within the living body. To further advance this promising technology, my work has addressed both improvements in the physical sensor and improvements in how we use the electron transfer kinetics underlying the signaling in these sensors to circumvent the drift associated with performing measurements directly in complex media. That is, using new electrode formats and new analytical signal-processing techniques, my thesis work created fully realized devices capable of measuring specific molecular targets in real time in relevant, highly complex sample streams. As examples, in my thesis I describe sensors supporting the measurement of a mycotoxin directly within the flowing sample stream of a foodstuff affected by that mycotoxin, the measurement of a malaria diagnostic protein in clinically-relevant ranges directly in a fingerprick-sized sample

of human serum, a new technique to measure a protein of interest directly in unprocessed whole blood – without pre-calibration, and new deployments of thin, surgically-implanted wire electrodes with sensors that measure, for the first time, *in vivo* blood concentrations *in real time* of a variety of small-molecule drugs as well as an arbitrary circulating protein of interest.

TABLE OF CONTENTS

I. Introduction

"The problem"

Current methods for measuring specific molecules are, by and large, cumbersome, slow laboratory-bound processes. The availability of technologies that could measure arbitrary molecules rapidly and directly at the point-of-use or, ultimately, could monitor them in real-time in a flowing sample stream could revolutionize healthcare, improve food safety, and enhance the efficiency of many industrial processes.

The case for improved molecular measurements is amply illustrated in medicine, where sufficiently sensitive and inexpensive point-of-care testing promises to transform the field by further personalizing diagnosis, monitoring and treatment of infectious disease, chronic conditions and other indicators of health status. While outcomes vary wildly depending on a dizzying array of variables present in the intersection of human biology and medical infrastructure, point-of-care testing may reduce the length of hospital stays, ameliorate emergency department crowding and reduce time to clinical intervention [1–4]. Point-of-care testing is as effective in ensuring patient medication adherence as testing at a centralized pathology laboratory, and patients report higher satisfaction and a better relationship with their physician when their physician has immediate point-of-care results [5]. These measurements to improve patient adherence tend generally to be highly cost-effective if not cost-saving, with nonadherence costing the US $100 billion in avoidable healthcare costs [6]. In the developing world, point-of-care diagnostics improve linkage to care, reducing mortality and improving patient outcomes [7–9].

A. Current approaches to clinical point-of-use measurements

Molecular measurements play a role in a wide range of applications, including clinical diagnostics, of course, but also wide manufacturing, environmental monitoring, and defense. To illustrate the gap between where current point-of-use measurement techniques are and where they aspire to be it is necessary to understand the state of the field as it exists today. To that end, I will examine the relatively well-developed market for point-of-care clinical diagnostics before discussing, in less detail, applications outside of the clinic.

To date, point-of-use medical measurement approaches (e.g., home use or point-of-care) devices range from the simple, hand-held "dipstick" lateral flow immunoassay [10] to complex benchtop devices which miniaturize and automate multiplexed chemistry assays [11]. Of course, no device is perfect for all use cases and all settings, but there are general rules developed by the World Health Organization which have become benchmarks for point-of-use devices as a class [12]. A point-of-use device must be affordable, which can mean different things to different users. Generally, point-of-care medical devices look at the cost per quality-adjusted life year, a measure of life expectancy weighted to reflect the quality of life during those years [13]. Point-of-use devices must be accessible to end users which includes physical delivery of a device to the location where it is needed, ability for any (preferably minimal) equipment to operate within the degree of infrastructure where it is needed and ability for the test to be performed and understood by the person performing it. A point-of-use device must also be a good sensor: it must be sensitive, specific, rapid and robust. Of note, a point-of-use device may be less sensitive than a typical laboratory instrument but still provide results: a moderately-sensitive clinical test that gives immediate results improves outcomes just as much as a much-more-sensitive clinical test that requires a 10-14 day waiting period between testing and action [14].

Ideally, these criteria make these devices relevant for multiple use cases along a range of infrastructure and budget levels. Nayak and coworkers describe four major medical use cases: moderate budget and a clinic infrastructure (e.g., ICUs, military base clinics), moderate budget and a field infrastructure (e.g. consumer devices, ambulance/EMS services), a constrained budget with clinic infrastructure (e.g. primary care clinics, NGO health centers) and a constrained budget with field infrastructure (e.g. global health, self testing) [15]. While the field of these devices is always expanding, I will aim to describe the major technologies driving commercially-available point-of-care devices: lateral flow immunoassays, strip technology with handheld readers, microfluidic cartridge-based devices, miniaturized flow cytometers, blood gas analyzers and miniaturized, automated clinical chemistry instruments [16].

Lateral flow immunoassays describe a broad class of qualitative (or semi-quantitative) single-use point-of-care sensors, best known as the underlying technology of the home pregnancy test [17]. These are typically presented as a strip or a card impregnated with multiple bio-recognition elements. The liquid sample of interest is applied to a pad on one end of the device and is wicked through a pad containing labeled recognition elements – typically antibodies [18], though assays have been described using nucleic acid recognition elements to measure DNA-DNA interactions [19] or nucleic acid aptamers [20]. The sample of interest and these recognition elements interact as the liquid flows through a membrane strip. The complex of the labeled recognition element and the target of interest are captured by another recognition element immobilized on a test line, giving a visible line in the presence of target [21]. Multiple test lines may be used to test for multiple targets [22] or the same target with varying affinity, giving semi-quantitative measurement [23]. These point-of-care sensors are broadly applicable to a range of markers for infections, metabolic

disorders, toxic compounds, vaccination confirmation, contamination and pregnancy [17]. However, they are single-use and semi-quantitative at best.

Handheld readers allow strip-based testing to add complexity and automation, reducing user error and enabling quantitative measurement of results. The most commonly-used (and most highly-developed) handheld meter – test strip device is the portable blood glucose sensor [24]. These sensors draw a ~1 μL volume of blood from a shallow finger-stick through a strip containing a specific enzyme that recognizes glucose, its coenzymes, an electrochemical mediator and a measurement electrode or a color-changing indicator molecule. The enzyme oxidizes glucose and electrons from the glucose are transferred to an electrochemical mediator. This molecule either delivers the electrons to an electrode for an electrochemical measurement or to a color-changing indicator for photometric measurement [25]. Handheld meters contain machinery for a simple electrochemical or photometric measurement, a timer for accurate sample measurement and internal calibration controls [26]. These systems provide simple, accurate quantitative measurements of blood glucose [27] but are of course dependent on the central sensor molecule: a naturally-occurring enzyme capable of converting blood glucose to an electrical signal. Efforts to expand this sort of detection have focused on coupling these handheld readers with microfluidic chips [28–32]. This enables the use of simple colorimetric, fluorescent and electrochemical devices to measure a readout of more-complicated chemistry to give quantitative results, though as of yet, only a few devices are FDA approved and large-scale microfluidics manufacturing is a challenge [33].

Another direction to move clinical measurement to the point of care is the miniaturized, automated instrument. Companies have commercialized automated clinical chemistry analyzers, blood gas analyzers and miniature flow cytometers to provide these technologies

to doctors' offices, resource-poor regions or areas without trained lab personnel. As a general rule, the defining characteristic of these instruments is the move towards automation of all of the analytical and sample-processing steps required and removing all steps which may be sources of operator error [34]. Because these are often designed for clinicians with little training in laboratory quality practices, these instruments often include internal quality controls [35]. Bringing these instruments out of the laboratory and closer to the patient can provide faster turn-around times which can expedite therapeutic interventions [36]. Benchtop clinical chemistry analyzers cover a broad range of clinical chemistries from simple panels of blood chemistry (e.g., enzymes, substrates, lipids, electrolytes) [37] to measurements of blood gases and coagulopathy [38] to specialized panels for specific patient presentations (e.g., point-of-care cardiac troponin sensors for patients with acute chest pain) [39]. The need to count CD4 T-cells in HIV patients drove the miniaturization of the flow cytometer into a benchtop-sized analyzer [40].

Beyond the clinic, point of use technologies provide critical information regarding food taint, environmental monitoring, workplace safety assessments, air and water quality testing are a few among the many applications for which the need for rapid, decentralized information is more pressing than the absolute accuracy of the measurement. As most food quality measurements are commercialized, proprietary technologies, published articles are much more rare than clinical devices. That said, the range of commercial devices for decentralized food monitoring include analysis of bacterial and fungal food taint, food quality deterioration, allergen content and other food contents [41].

B. Continuous monitoring

While the range of point-of-use molecular detection technologies provide valuable information at the bedside or other areas with limited infrastructure, there are no general approach to date that can provide continuous, quantitative measurement directly in a complicated sample stream (including *in vivo*) against an arbitrary target of interest. An example of a particularly promising clinical application is use in therapeutic drug monitoring. Therapeutic drug monitoring is recommended in cases of pharmacokinetic variability, drug interactions, diseases with poor prognosis or for patient populations with significant underlying immunological conditions [42], but current techniques for drug monitoring are traumatic for the patient , complicated or expensive to perform. Typical drug monitoring requires up to a dozen individual blood draws timed precisely over twenty-four hours [43] and can be expensive and time-consuming to measure [44]. Even in best circumstances, the *ex vivo* measurement necessitates that all meaningful information will not be processed until *after* dosing. Promising drugs are often not prescribed because of the difficulty of monitoring individual patients for adverse events linked to their pharmacokinetics [42]. Similar challenges exist for monitoring the outputs of food production [45] and pharmaceutical manufacturing [46]. Given the still pressing need for continuous, quantitative sensing which can work *directly* in complicated sample streams, in my thesis work I aim to translate the electrochemical aptamer-based sensor, a technology with roughly fifteen years of benchtop use, into complex sample streams, including foodstuffs, clinical media and direct *in vivo* measurements in the bloodstream of a living animal.

C. The approach

To create a synthetic sensor that is a) single step and reversible (thus ensuring ease of use and, ultimately, continuous monitoring) and b) performs well even in complex environments, my research turns to biological inspiration. That is, predicated by the argument that evolution has solved the problem of molecular sensing in complex environments (your body contains hundreds of receptors responding quantitatively to a myriad of specific small molecule and protein cues), my research program set out to engineer synthetic biomolecules to undergo similar robust measurement in complex media. To achieve this, I exploited two key elements of the chemoperception systems that nature employs: biomolecular recognition, and conformation-linked signaling.

Engineering biomolecular recognition against arbitrary targets

Biomolecular nanomachines successfully perform continuous monitoring and translation of binding events into biological response in incredibly complex intracellular environments and directly in the bloodstream. The most abundant biological recognition approach, protein recognition uses a large available chemical space (the twenty available functional groups of the twenty canonical amino acids plus the range of post-translational modifications) and millions of years of natural selection to create molecules which can sensitively recognize a target of interest with high specificity (recognizing the target over its similar analogues) and high selectivity (recognizing the target in a complex, crowded sample medium). Groups have tried to re-engineer proteins towards a new function of interest and though there have been advances in protein engineering towards adapting their specific recognition to a target of interest, we are still far from being able to generate synthetic proteins with specific

desired functions [47,48]. To mimic the biological functions of proteins in a more tractable molecule, we instead choose to engineer nucleic acids towards our desired functions.

We use a biomolecule with a similarly large sequence diversity but significantly more predictable structure in our attempts to engineer novel synthetic biological recognition elements. To exploit the sensitivity, specificity and selectivity of biological recognition, we use deoxyribonucleic acid (DNA) as a powerful bioengineering building block. Though DNA has the biological function of coding the genetic instructions of an organism, its ease of synthesis and replication, chemical and physical stability, information density and structural predictability present a range of novel applications. Synthetic DNA is cheap to produce (cents per base) [49,50] and easy to replicate, as is required by its biological role [51,52]. DNA is physically and chemically stable unless exposed to strong oxidizing agents, low pH or nucleases, enzymes specifically evolved to degrade DNA [53]. The four distinct bases making up each position of this polymer chain enable a massive amount of information density: N4 possible sequences for a chain N bases long. This massive information density combined with the structural predictability of DNA base-pairing [54] enable the synthesis of molecularly encoded shapes [55] and even functional devices [56,57]. Other groups have used the massive sequence space of DNA molecules to barcode small molecules and short peptides for simple analysis and separation of large-scale chemical library spaces [53]. We use the large sequence diversity of DNA to find specific biorecognition of a target of interest by selectively enriching a very large pool of (semi-) random DNA sequences.

Artificial selection applied to a large, randomized pool of nucleic acid sequences can create sensitive, specific and selective biological recognition between an arbitrary molecule and a specific, selected sequence known as an aptamer. Aptamers exploit the ease of

artificial DNA synthesis to create a large, random pool of DNA sequences, isolate the small fraction of sequences which bind to an arbitrary target of interest and replicate those sequences for either more stringent rounds of selection or further characterization of the selected sequence. Since Tuerk and Gold [58] and Ellington and Szostak [59] first described this method in 1990, aptamers have been reported to bind small molecule drugs, arbitrary proteins, heavy metals and full pathogen cells [60].

Conformation-linked signaling: a strategy for measurement specificity

Most biosensor approaches follow a two-step measurement strategy: a specific biomolecule binds its target followed by a second step to generate signal. For example, Enzyme-Linked ImmunoSorbent Assays (ELISAs) use highly specific antibody-antigen interactions to sensitively measure small amounts of clinical antigens, but their signal is linked to subsequent less-specific antibody recognition, and they thus require multiple washing steps to avoid false positives from nonspecific binding to the assay well [61]. Similarly, techniques like quartz crystal microbalance, surface plasmon resonance and electrochemical impedance measure use specific biochemical binding to measure small amounts of target, but their signal is linked not to the specific biochemical interaction [62–64]. Rather, their signal is linked to change in the physical properties of the supporting surface and so they require extensive antifouling and washing treatments [65]. While these techniques perform well in a clean laboratory environment, bringing these technologies to areas with limited infrastructure or even to the patient bedside frustrates their selectivity.

Biology, however, performs signal transduction directly within incredibly crowded, complex environments. Proteins transduce environmental cues into active signals reliably and repeatedly directly in circulating blood and living cells. A common strategy across

proteins is linking function directly to binding-induced conformational change. For example, the glucokinase protein catalyzes the physphorylation of glucose after being activated by a small molecule. Binding of the glucokinase activator to glucokinase stabilizes a conformational shift which properly orients the catalytic residues of the enzyme to the glucose binding pocket [66]. Similarly, G-protein coupled receptors use binding-induced conformational changes to physically transduce environmental cues from outside cells to trigger responses inside the cell [67]. To mimic this mechanism, we use structure-switching DNA sensors which directly transduce target binding into a conformational change which intrinsically changes the electronic signal from the attached electrochemical tag [68].

Electrochemical aptamer-based sensors

Electrochemical aptamer-based sensors (E-AB sensors) combine artificially engineered biological recognition with selective, conformationally-linked signaling and analytic, quantitative electrochemical measurement to enable sensitive, selective measurements directly in complex media. By synthesizing a specific aptamer sequence modified with a thiol anchor and an electrochemically-active redox tag, we create biosensor molecules which bind with near-covalent strength to a gold electrode and translate the binding of their target of interest to a quantitative change in the electrical signal from the redox tag. This approach uses the selectivity of electrochemical measurement to complement the specificity of biochemical binding; electrochemical voltammetry measures only the current at a specific, narrow electrochemical potential. The narrow measurement window minimizes the number of potential species which may interfere with the sensor signal, enabling measurements directly in complex samples which obstruct fluorescent or colorimetric biosensors. Electrochemical measurement also enables rapid, robust, repeated measurements of the same

molecule in quick succession, allowing for continuous, long-term measurement. Because these sensors can operate directly in their complex medium of interest without preprocessing or washing, this opens the door for continuous biosensing of a target of interest directly in a complex sample stream.

Previous work in our group began to demonstrate the ability of E-AB sensors and their analogues, E-DNA sensors (DNA-based electrochemical sensors which recognize complementary strands of DNA), to find their targets in dirty, somewhat complex samples. Lubin et al. demonstrated single measurements of DNA-DNA interactions directly in blood serum, urine, saliva, mud and Guinness beer [69]. Cash et al. devised a general strategy for using electrochemical DNA-based sensors to take single measurements of antibody concentrations in blood serum and White et al. created a platform to measure six specific antibodies of interest in blood serum [70,71]. Swensen et al. performed the first continuous measurement in complex media, measuring changes in cocaine concentration for just over an hour in blood serum flowing through a microfluidic device [72]. However, further challenges remained in translating these biosensors to implantation within the bloodstream of a living animal or continuous measurements in whole, unprocessed blood or even expanding the repertoire of molecular measurement directly within the medium present at the point-of-use.

In the next few chapters, I will demonstrate the translation of these electrochemical aptamer-based sensors off of the benchtop and directly into the complex environments where they can provide uniquely continuous quantitative measurements. I demonstrate the use of these sensors as measurements of food safety by measuring a mycotoxin directly in coffee and melamine directly in milk, rapid reagent-free measurements of arbitrary protein

biomarkers directly in clinical media, continuous quantitative measurements of arbitrary small-molecule drugs directly in the bloodstream of a living animal and continuous monitoring for arbitrary protein spikes directly in the blood of a living animal.

D. My contribution

Two major challenges to moving E-AB sensors from the benchtop into the point-of-use (including direct in vivo implantation) are the design of an electrode well-suited to the environmental conditions where it will be used and overcoming the nonspecific signal drift observed in particularly complex samples.

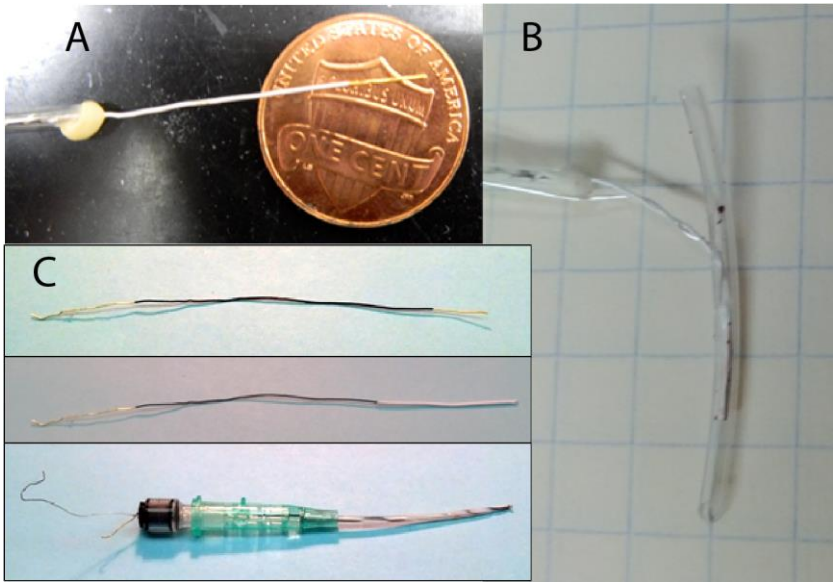

Figure 1.1. Development of an electrode for deployment directly in the jugular vein of a living rat. (**A**) Early electrode prototypes consisted of a thick gold wire to be surgically inserted directly into the jugular vein of a rat. (**B**) An early attempt to prevent venous collapse protected the wire electrode and a combination counter/reference electrode within a crude stent made from a short length of flexible tubing. (**C**) Another electrode prototype protected a gold wire electrode with a short length of microdialysis tubing and delivered both the working electrode and a combination counter/reference electrode within a standard 18 gauge catheter. A variation of this electrode (without the microdialysis tubing and catheter) is used for in vitro PDGF-BB detection in **Chapter IV**.

A substantial portion of moving a sensor from the benchtop to the point-of-use is the physical engineering of an electrode which can survive the environment where measurements take place. The development of an electrode for surgical implantation into the jugular vein of a rat proved a challenge – even with expert surgeries, early experiments were plagued with collapsing veins following surgical implantation. The development of a sensor which could be inserted with minimal invasiveness and that did not occlude bloodflow required multiple generations of electrode development. Early electrode generations, shown in **Figure 1.1**, attempted to combine a working electrode (modified with our E-AB sensor) and a counter/reference electrode (required for voltammetric measurement) in a minimal package which would ensure delivery of fresh bloodflow over the sensor surface.

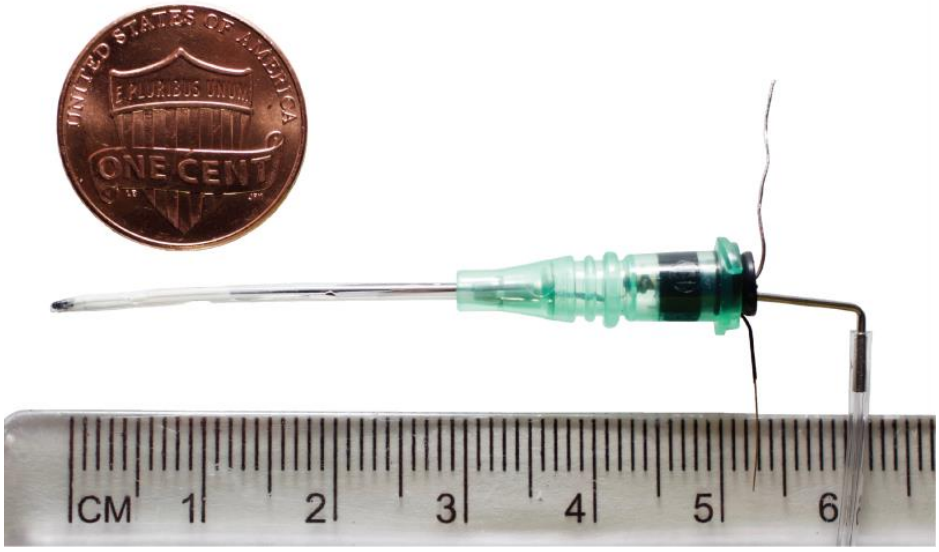

Figure 1.2. Our successful electrode design packages a microdialysis-membrane-protected gold working electrode and a counter/reference electrode within an 18 gauge catheter. Crucially, slits are cut into the catheter to encourage bloodflow over the electrode surface and a tube is inserted into the top of the catheter to allow pressure exchange following surgical implantation. (Patent application filed, UC Case 2016-135-0)

Our final electrode design, used for the *in vivo* studies in **Chapters V** and **VI**, maintains the microdialysis-membrane-protected working electrode and the small counter/reference electrode packaged in an 18 gauge surgical catheter (**Fig. 1.2**). This new design, however,

includes a mechanism to equalize pressure within the catheter following implantation and slits in the catheter to encourage bloodflow over the electrode surface. This electrode, developed from the prototypes in Fig. 1.1 with the help of Netz Arroyo-Currás, has a patent application filed under UC Case 2016-135-0.

Another large component of my work relies on using the kinetic information measured with square wave voltammetry, a kinetically-sensitive electrochemical technique. This expands on work from White et al. examining the kinetic dependence of the electric signal generated by our sensors [73]. Briefly, square wave voltammetry uses short potential pulses and differential measurement to precisely measure the faradaic current generated by oxidation and reduction of a redox-active molecule and not the capacitive charging current at the electrode surface [74]. We understand the amount of current to be related to the equilibrium probability of the redox tag interacting with the electrode surface in a manner that supports electron transfer, which is intrinsically linked to the overall flexibility of the DNA construct [75]. (Though, of course, there is not a consensus on the mechanism of electron transfer [76,77], this model proves sufficient to explain and predict the phenomena observed in sensor signal.) The binding of a target to an E-AB sensor changes the observed flexibility of the E-AB construct, which results in a measurable shift in the electron transfer kinetics between the redox tag and the electrode surface [73]. By measuring one population of molecules at different timescales, we are able to deconvolute the specific target-binding signal from the nonspecific signal drift that may occur in particularly complex clinical media.

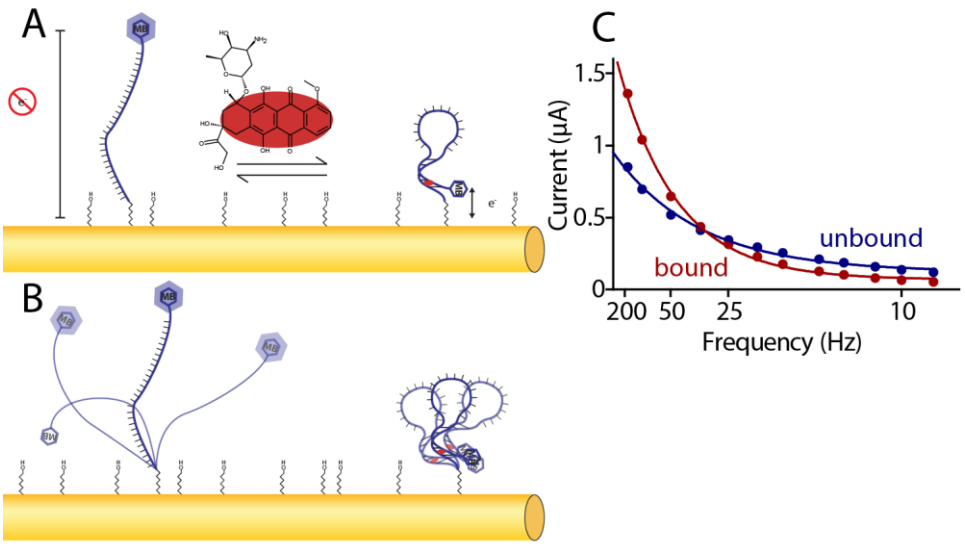

Figure 1.3. Rather than (**A**) the model assumed from FRET and fluorophore-quencher studies where target binding (red oval) changes the E-AB probe from an unbound state which does not exchange electrons with the electrode surface (left) to a bound state which does exchange electrons with the electrode surface (right), E-AB sensors are better understood as two populations with distinct kinetics (**B**). The unbound state can explore a larger conformational space, with a relatively low equilibrium probability of the redox tag (blue hexagon) exchanging electrons with the electrode surface. The bound state is more tightly constrained, holding the redox tag closer to the electrode surface and speeding up electron transfer. (**C**) Plotting peak currents against the square wave pulse width shows that binding of a target, here 3 μM of doxorubicin, increases the overall speed of electron transfer. This allows us to measure multiple regimes of sensor signal.

By modifying the timescale of our square wave measurement, we are able to explore multiple signaling regimes of the same population of molecules. **Figure 1.3** shows the kinetic model of our sensors in their unbound and bound states (**Fig. 1.3B**) and the kinetically-dependent currents observed in bound and unbound states (**Fig. 1.3C**). When measuring at higher frequencies, the faster electron transfer between the tightly-constrained bound sensor and the electrode surface dominate, so current increases upon binding. When measuring at lower frequencies, the faster electron transfer from the tightly-constrained bound sensor is depleted by the end of the pre-measurement pulse, and so the slower electron transfer from the unbound, loosely-constrained sensor molecule dominates, so

current decreases upon binding. There is also a crossover point where the electron transfer rates between the bound and unbound states are balanced, this creates a non-responsive measurement frequency insensitive to target binding.

By using measurement frequencies from multiple regimes, we can create a self-calibrating reading to separate the non-specific signal drift from the specific target-derived signal. This is described in more detail in **Chapters IV**, **V** and **VI**. Briefly, multiple parallel measurements at different frequencies are compared to create a stable sensor signal that responds only to target and rejects nonspecific drift. KDM, a technique first described by Ferguson et al. [78], finds two frequencies with similar drift and dissimilar signal response, normalizes each signal to some baseline, and subtracts the normalized signals from each other to create more stable measurement baselines. Using this technique and the electrode development earlier described, I measured target addition directly in whole unprocessed blood for this first time. This work further developed into the in vivo small molecule work described in **Chapter V**.

"Calibration-free" measurement, a technique first described by Li et al. [79], uses the ratio between a signal-on frequency and a nonresponsive frequency to reproducibly measure concentrations in complex media as long as a reliable "training set" of electrodes in similar conditions can be used to create a reliable fit in advance. Ratiometric measurement, a technique first described in my work in **Chapter VI**, adds the robustness from KDM stabilization to the advantages of calibration-free measurement by calibrating a baseline reading directly in the medium of interest before measurement begins. This new ratiometric methodology produces in vivo continuous measurements with greater stability and reproducibility than other previously employed techniques.

E. References

1. Andrews, D.; Chetty, Y.; Cooper, B. S.; Virk, M.; Glass, S. K.; Letters, A.; Kelly, P. A.; Sudhanva, M.; Jeyaratnam, D. Multiplex PCR point of care testing versus routine, laboratory-based testing in the treatment of adults with respiratory tract infections: a quasi-randomised study assessing impact on length of stay and antimicrobial use. BMC Infect. Dis. 2017, 17, 671, doi:10.1186/s12879-017-2784-z.
2. Schimke, I. Quality and timeliness in medical laboratory testing. Anal. Bioanal. Chem. 2009, 393, 1499–1504, doi:10.1007/s00216-008-2349-5.
3. Kankaanpää, M.; Raitakari, M.; Muukkonen, L.; Gustafsson, S.; Heitto, M.; Palomäki, A.; Suojanen, K.; Harjola, V.-P. Use of point-of-care testing and early assessment model reduces length of stay for ambulatory patients in an emergency department. Scand. J. Trauma. Resusc. Emerg. Med. 2016, 24, 125, doi:10.1186/s13049-016-0319-z.
4. Hsiao, A. L.; Santucci, K. A.; Dziura, J.; Baker, M. D. A Randomized Trial to Assess the Efficacy of Point-of-Care Testing in Decreasing Length of Stay in a Pediatric Emergency Department. Pediatr. Emerg. Care 2007, 23, 457–462, doi:10.1097/01.pec.0000280506.44924.de.
5. Gialamas, A.; Yelland, L. N.; Ryan, P.; Willson, K.; Laurence, C. O.; Bubner, T. K.; Tideman, P.; Beilby, J. J. Does point-of-care testing lead to the same or better adherence to medication? A randomised controlled trial: the PoCT in General Practice Trial. Med. J. Aust. 2009, 191, 487–91.
6. Simon-Tuval, T.; Neumann, P. J.; Greenberg, D. Cost-effectiveness of adherence-enhancing interventions: a systematic review. Expert Rev. Pharmacoecon. Outcomes Res. 2016, 16, 67–84, doi:10.1586/14737167.2016.1138858.
7. Hyle, E. P.; Jani, I. V.; Lehe, J.; Su, A. E.; Wood, R.; Quevedo, J.; Losina, E.; Bassett, I. V.; Pei, P. P.; Paltiel, A. D.; Resch, S.; Freedberg, K. A.; Peter, T.; Walensky, R. P. The Clinical and Economic Impact of Point-of-Care CD4 Testing in Mozambique and Other Resource-Limited Settings: A Cost-Effectiveness Analysis. PLoS Med. 2014, 11, e1001725, doi:10.1371/journal.pmed.1001725.
8. Turner, K. M. E.; Round, J.; Horner, P.; Macleod, J.; Goldenberg, S.; Deol, A.; Adams, E. J. An early evaluation of clinical and economic costs and benefits of implementing point of care NAAT tests for Chlamydia trachomatis and Neisseria gonorrhoea in genitourinary medicine clinics in England. Sex. Transm. Infect. 2014, 90, 104–111, doi:10.1136/sextrans-2013-051147.
9. Chadee, A.; Blackhouse, G.; Goeree, R. Point-of-Care Hemoglobin A1c Testing: A Budget Impact Analysis. Ont. Health Technol. Assess. Ser. 2014, 14, 1–23.
10. Walter, B.; Greenquist, A. C.; Howard, W. E. Solid-phase reagent strips for detection of therapeutic drugs in serum by substrate-labeled fluorescent immunoassay. Anal. Chem. 1983, 55, 873–8.
11. Schembri, C. T.; Ostoich, V.; Lingane, P. J.; Burd, T. L.; Buhl, S. N. Portable simultaneous multiple analyte whole-blood analyzer for point-of-care testing. Clin. Chem. 1992, 38, 1665–70.
12. Kettler, H.; White, K.; Hawkes, S. Mapping the landscape of diagnostics for sexually transmitted infections: Key findings and recommendations. Unicef/Undp/World Bank/Who 2004, 1–44.

13. Loubiere, S.; Moatti, J.-P. Economic evaluation of point-of-care diagnostic technologies for infectious diseases. Clin. Microbiol. Infect. 2010, 16, 1070–1076, doi:10.1111/j.1469-0691.2010.03280.x.
14. Vickerman, P.; Watts, C.; Alary, M.; Mabey, D.; Peeling, R. W. Sensitivity requirements for the point of care diagnosis of Chlamydia trachomatis and Neisseria gonorrhoeae in women. Sex. Transm. Infect. 2003, 79, 363–7.
15. Nayak, S.; Blumenfeld, N. R.; Laksanasopin, T.; Sia, S. K. Point-of-Care Diagnostics: Recent Developments in a Connected Age. Anal. Chem. 2017, 89, 102–123, doi:10.1021/acs.analchem.6b04630.
16. St John, A.; Price, C. P. Existing and Emerging Technologies for Point-of-Care Testing. Clin. Biochem. Rev. 2014, 35, 155–67.
17. Posthuma-Trumpie, G. A.; Korf, J.; van Amerongen, A. Lateral flow (immuno)assay: its strengths, weaknesses, opportunities and threats. A literature survey. Anal. Bioanal. Chem. 2009, 393, 569–82, doi:10.1007/s00216-008-2287-2.
18. Ngom, B.; Guo, Y.; Wang, X.; Bi, D. Development and application of lateral flow test strip technology for detection of infectious agents and chemical contaminants: a review. Anal. Bioanal. Chem. 2010, 397, 1113–1135, doi:10.1007/s00216-010-3661-4.
19. Edwards, K. A.; Baeumner, A. J. Optimization of DNA-tagged dye-encapsulating liposomes for lateral-flow assays based on sandwich hybridization. Anal. Bioanal. Chem. 2006, 386, 1335–1343, doi:10.1007/s00216-006-0705-x.
20. Xu, H.; Mao, X.; Zeng, Q.; Wang, S.; Kawde, A.-N.; Liu, G. Aptamer-Functionalized Gold Nanoparticles as Probes in a Dry-Reagent Strip Biosensor for Protein Analysis. Anal. Chem. 2009, 81, 669–675, doi:10.1021/ac8020592.
21. Bahadır, E. B.; Sezgintürk, M. K. Lateral flow assays: Principles, designs and labels. TrAC Trends Anal. Chem. 2016, 82, 286–306, doi:10.1016/j.trac.2016.06.006.
22. Oku, Y.; Kamiya, K.; Kamiya, H.; Shibahara, Y.; Ii, T.; Uesaka, Y. Development of oligonucleotide lateral-flow immunoassay for multi-parameter detection. J. Immunol. Methods 2001, 258, 73–84, doi:10.1016/S0022-1759(01)00470-7.
23. Cho, J.-H.; Paek, S.-H. Semiquantitative, bar code version of immunochromatographic assay system for human serum albumin as model analyte. Biotechnol. Bioeng. 2001, 75, 725–732, doi:10.1002/bit.10094.
24. Kricka, L. J.; Thorpe, G. H. G. Technology of Handheld Devices for Point-of-Care Testing. In Point-of-Care Testing: Needs, Opportunity, and Innovation; Price, C. P., St John, A., Kricka, L. J., Eds.; AACC Press: Washington, DC, 2010 ISBN 978-1-59425-103-0.
25. Hönes, J.; Müller, P.; Surridge, N. The Technology Behind Glucose Meters: Test Strips. Diabetes Technol. Ther. 2008, 10, S-10-S-26, doi:10.1089/dia.2008.0005.
26. Clarke, S. F.; Foster, J. R. A history of blood glucose meters and their role in self-monitoring of diabetes mellitus. Br. J. Biomed. Sci. 2012, 69, 83–93, doi:10.1080/09674845.2012.12002443.
27. Arabadjief, D.; Nichols, J. H. Assessing glucose meter accuracy. Curr. Med. Res. Opin. 2006, 22, 2167–2174, doi:10.1185/030079906X148274.
28. Kumar, S.; Kumar, S.; Ali, M. A.; Anand, P.; Agrawal, V. V.; John, R.; Maji, S.; Malhotra, B. D. Microfluidic-integrated biosensors: Prospects for point-of-care diagnostics. Biotechnol. J. 2013, 8, 1267–1279, doi:10.1002/biot.201200386.

29. Warren, A. D.; Kwong, G. A.; Wood, D. K.; Lin, K. Y.; Bhatia, S. N. Point-of-care diagnostics for noncommunicable diseases using synthetic urinary biomarkers and paper microfluidics. Proc. Natl. Acad. Sci. 2014, 111, 3671–3676, doi:10.1073/pnas.1314651111.
30. Su, W.; Gao, X.; Jiang, L.; Qin, J. Microfluidic platform towards point-of-care diagnostics in infectious diseases. J. Chromatogr. A 2015, 1377, 13–26, doi:10.1016/j.chroma.2014.12.041.
31. Watkins, N. N.; Hassan, U.; Damhorst, G.; Ni, H.; Vaid, A.; Rodriguez, W.; Bashir, R. Microfluidic CD4+ and CD8+ T Lymphocyte Counters for Point-of-Care HIV Diagnostics Using Whole Blood. Sci. Transl. Med. 2013, 5, 214ra170-214ra170, doi:10.1126/scitranslmed.3006870.
32. Laksanasopin, T.; Guo, T. W.; Nayak, S.; Sridhara, A. A.; Xie, S.; Olowookere, O. O.; Cadinu, P.; Meng, F.; Chee, N. H.; Kim, J.; Chin, C. D.; Munyazesa, E.; Mugwaneza, P.; Rai, A. J.; Mugisha, V.; Castro, A. R.; Steinmiller, D.; Linder, V.; Justman, J. E.; Nsanzimana, S.; Sia, S. K. A smartphone dongle for diagnosis of infectious diseases at the point of care. Sci. Transl. Med. 2015, 7, 273re1-273re1, doi:10.1126/scitranslmed.aaa0056.
33. Chin, C. D.; Linder, V.; Sia, S. K. Commercialization of microfluidic point-of-care diagnostic devices. Lab Chip 2012, doi:10.1039/c2lc21204h.
34. St. John, A.; Ritter, C. Benchtop Instruments for Point-of-Care Testing. In Point-of-Care Testing: Needs, Opportunity, and Innovation; Price, C. P., St John, A., Kricka, L., Eds.; AACC Press: Washington, DC, 2010; pp. 43–62 ISBN 978-1-59425-103-0.
35. Lewandrowski, K.; Gregory, K.; Macmillan, D. Assuring Quality in Point-of-Care Testing: Evolution of Technologies, Informatics, and Program Management. Arch. Pathol. Lab. Med. 2011, 135, 1405–1414, doi:10.5858/arpa.2011-0157-RA.
36. Drenck, N.-E. Point of care testing in Critical Care Medicine: the clinician's view. Clin. Chim. Acta 2001, 307, 3–7, doi:10.1016/S0009-8981(01)00448-X.
37. Price, C. P.; Koller, P. U. A multicentre study of the new Reflotron system for the measurement of urea, glucose, triacylglycerols, cholesterol, gamma-glutamyltransferase and haemoglobin. J. Clin. Chem. Clin. Biochem. 1988, 26, 233–50.
38. Wahr, J. A.; Lau, W.; Tremper, K. K.; Hallock, L.; Smith, K. Accuracy and precision of a new, portable, handheld blood gas analyzer, the IRMA. J. Clin. Monit. 1996, 12, 317–24.
39. Ho, C.; Cimon, K.; Weeks, L.; Mierzwinski-Urban, M.; Dunfield, L.; Soril, L.; Clement, F.; Jabr, M. Point-of-Care Troponin Testing in Patients With Symptoms Suggestive of Acute Coronary Syndrome: A Health Technology Assessment Economic authors: Cite as: Point-of-Care Troponin Testing in Patients With Symptoms Suggestive of Acute Coronary Syndrome. A Heal. Technol. Assess. 2016, 5.
40. Kestens, L.; Mandy, F. Thirty-five years of CD4 T-cell counting in HIV infection: From flow cytometry in the lab to point-of-care testing in the field. Cytom. Part B Clin. Cytom. 2017, 92, 437–444, doi:10.1002/cyto.b.21400.
41. Bahadır, E. B.; Sezgintürk, M. K. Applications of commercial biosensors in clinical, food, environmental, and biothreat/biowarfare analyses. Anal. Biochem. 2015, 478, 107–120, doi:10.1016/j.ab.2015.03.011.

42. Ashbee, H. R.; Barnes, R. A.; Johnson, E. M.; Richardson, M. D.; Gorton, R.; Hope, W. W. Therapeutic drug monitoring (TDM) of antifungal agents: guidelines from the British Society for Medical Mycology. J. Antimicrob. Chemother. 2014, 69, 1162–1176, doi:10.1093/jac/dkt508.
43. Eksborg, S.; Strandler, H. S.; Edsmyr, F.; Näslund, I.; Tahvanainen, P. Pharmacokinetic study of i.v. infusions of adriamycin. Eur. J. Clin. Pharmacol. 1985, 28, 205–12.
44. Huttner, A.; Harbarth, S.; Hope, W. W.; Lipman, J.; Roberts, J. A. Therapeutic drug monitoring of the β-lactam antibiotics: what is the evidence and which patients should we be using it for?: Figure 1. J. Antimicrob. Chemother. 2015, dkv201, doi:10.1093/jac/dkv201.
45. Galbán, J.; Sanz-Vicente, I.; Ortega, E.; del Barrio, M.; de Marcos, S. Reagentless fluorescent biosensors based on proteins for continuous monitoring systems. Anal. Bioanal. Chem. 2012, 402, 3039–3054, doi:10.1007/s00216-012-5715-2.
46. Myerson, A. S.; Krumme, M.; Nasr, M.; Thomas, H.; Braatz, R. D. Control Systems Engineering in Continuous Pharmaceutical Manufacturing May 20–21, 2014 Continuous Manufacturing Symposium. J. Pharm. Sci. 2015, 104, 832–839, doi:10.1002/jps.24311.
47. Till, M.; Race, P. R. Progress challenges and opportunities for the re-engineering of trans-AT polyketide synthases. Biotechnol. Lett. 2014, 36, 877–888, doi:10.1007/s10529-013-1449-2.
48. Swint-Kruse, L. Using Evolution to Guide Protein Engineering: The Devil IS in the Details. Biophys. J. 2016, 111, 10–18, doi:10.1016/j.bpj.2016.05.030.
49. Carlson, R. The changing economics of DNA synthesis. Nat. Biotechnol. 2009, 27, 1091–1094, doi:10.1038/nbt1209-1091.
50. Kosuri, S.; Church, G. M. Large-scale de novo DNA synthesis: technologies and applications. Nat. Methods 2014, 11, 499–507, doi:10.1038/nmeth.2918.
51. Lehman, I. R.; Bessman, M. J.; Simms, E. S.; Kornberg, A. Enzymatic synthesis of deoxyribonucleic acid. I. Preparation of substrates and partial purification of an enzyme from Escherichia coli. J. Biol. Chem. 1958, 233, 163–70.
52. Bessman, M. J.; Lehman, I. R.; Simms, E. S.; Kornberg, A. Enzymatic synthesis of deoxyribonucleic acid. II. General properties of the reaction. J. Biol. Chem. 1958, 233, 171–7.
53. Goodnow, R. A.; Dumelin, C. E.; Keefe, A. D. DNA-encoded chemistry: enabling the deeper sampling of chemical space. Nat. Rev. Drug Discov. 2017, 16, 131–147, doi:10.1038/nrd.2016.213.
54. Zuker, M. Mfold web server for nucleic acid folding and hybridization prediction. Nucleic Acids Res. 2003, 31, 3406–15.
55. Saccà, B.; Niemeyer, C. M. DNA Origami: The Art of Folding DNA. Angew. Chemie Int. Ed. 2012, 51, 58–66, doi:10.1002/anie.201105846.
56. Bath, J.; Turberfield, A. J. DNA nanomachines. Nat. Nanotechnol. 2007, 2, 275–284, doi:10.1038/nnano.2007.104.
57. Seeman, N. C. From genes to machines: DNA nanomechanical devices. Trends Biochem. Sci. 2005, 30, 119–25, doi:10.1016/j.tibs.2005.01.007.
58. Tuerk, C.; Gold, L. Systematic evolution of ligands by exponential enrichment: RNA ligands to bacteriophage T4 DNA polymerase. Science 1990, 249, 505–10.
59. Ellington, A. D.; Szostak, J. W. In vitro selection of RNA molecules that bind specific ligands. Nature 1990, 346, 818–822, doi:10.1038/346818a0.

60. Yüce, M.; Ullah, N.; Budak, H. Trends in aptamer selection methods and applications. Analyst 2015, 140, 5379–5399, doi:10.1039/C5AN00954E.
61. Engvall, E.; Perlmann, P. Enzyme-linked immunosorbent assay (ELISA) quantitative assay of immunoglobulin G. Immunochemistry 1971, 8, 871–874, doi:10.1016/0019-2791(71)90454-X.
62. Prakrankamanant, P. Quartz crystal microbalance biosensors: prospects for point-of-care diagnostics. J. Med. Assoc. Thai. 2014, 97 Suppl 4, S56-64.
63. Nguyen, H.; Park, J.; Kang, S.; Kim, M. Surface Plasmon Resonance: A Versatile Technique for Biosensor Applications. Sensors 2015, 15, 10481–10510, doi:10.3390/s150510481.
64. Bahadır, E. B.; Sezgintürk, M. K. A review on impedimetric biosensors. Artif. Cells, Nanomedicine, Biotechnol. 2016, 44, 248–262, doi:10.3109/21691401.2014.942456.
65. Ostuni, E.; Chapman, R. G.; Holmlin, R. E.; Takayama, S.; Whitesides, G. M. A Survey of Structure−Property Relationships of Surfaces that Resist the Adsorption of Protein. Langmuir 2001, 17, 5605–5620, doi:10.1021/la010384m.
66. Zorn, J. A.; Wells, J. A. Turning enzymes ON with small molecules. Nat. Chem. Biol. 2010, 6, 179–188, doi:10.1038/nchembio.318.
67. Rosenbaum, D. M.; Rasmussen, S. G. F.; Kobilka, B. K. The structure and function of G-protein-coupled receptors. Nature 2009, 459, 356–363, doi:10.1038/nature08144.
68. Lubin, A. A.; Plaxco, K. W. Folding-based electrochemical biosensors: the case for responsive nucleic acid architectures. Acc. Chem. Res. 2010, 43, 496–505, doi:10.1021/ar900165x.
69. Lubin, A. A.; Lai, R. Y.; Baker, B. R.; Heeger, A. J.; Plaxco, K. W. Sequence-specific, electronic detection of oligonucleotides in blood, soil, and foodstuffs with the reagentless, reusable E-DNA sensor. Anal. Chem. 2006, 78, 5671–7, doi:10.1021/ac0601819.
70. Cash, K. J.; Ricci, F.; Plaxco, K. W. An electrochemical sensor for the detection of protein-small molecule interactions directly in serum and other complex matrices. J. Am. Chem. Soc. 2009, 131, 6955–7, doi:10.1021/ja9011595.
71. White, R. J.; Kallewaard, H. M.; Hsieh, K.; Patterson, A. S.; Kasehagen, J. B.; Cash, K. J.; Uzawa, T.; Soh, H. T.; Plaxco, K. W. A Wash-free, Electrochemical Platform for the Quantitative, Multiplexed Detection of Specific Antibodies. Anal. Chem. 2011, 84, 1098–1103, doi:10.1021/ac202757c.
72. Swensen, J. S.; Xiao, Y.; Ferguson, B. S.; Lubin, A. A.; Lai, R. Y.; Heeger, A. J.; Plaxco, K. W.; Soh, H. T. Continuous, real-time monitoring of cocaine in undiluted blood serum via a microfluidic, electrochemical aptamer-based sensor. J. Am. Chem. Soc. 2009, 131, 4262–6, doi:10.1021/ja806531z.
73. White, R. J.; Plaxco, K. W. Exploiting binding-induced changes in probe flexibility for the optimization of electrochemical biosensors. Anal. Chem. 2010, 82, 73–6, doi:10.1021/ac902595f.
74. O'Dea, J. J.; Osteryoung, J.; Osteryoung, R. a. Square wave voltammetry and other pulse techniques for the determination of kinetic parameters. The reduction of zinc(II) at mercury electrodes. J. Phys. Chem. 1983, 87, 3911–3918, doi:10.1021/j100243a025.
75. Uzawa, T.; Cheng, R. R.; Cash, K. J.; Makarov, D. E.; Plaxco, K. W. The length and viscosity dependence of end-to-end collision rates in single-stranded DNA. Biophys. J. 2009, 97, 205–10, doi:10.1016/j.bpj.2009.04.036.

76. Genereux, J. C.; Barton, J. K. Mechanisms for DNA charge transport. Chem. Rev. 2010, 110, 1642–1662, doi:10.1021/cr900228f.
77. Abi, A.; Ferapontova, E. E. Unmediated by DNA Electron Transfer in Redox-Labeled DNA Duplexes End-Tethered to Gold Electrodes. J. Am. Chem. Soc. 2012, 134, 14499–14507, doi:10.1021/ja304864w.
78. Ferguson, B. S.; Hoggarth, D. a; Maliniak, D.; Ploense, K.; White, R. J.; Woodward, N.; Hsieh, K.; Bonham, A. J.; Eisenstein, M.; Kippin, T. E.; Plaxco, K. W.; Soh, H. T. Real-time, aptamer-based tracking of circulating therapeutic agents in living animals. Sci. Transl. Med. 2013, 5, 213ra165, doi:10.1126/scitranslmed.3007095.
79. Li, H.; Dauphin-Ducharme, P.; Ortega, G.; Plaxco, K. W. Calibration-Free Electrochemical Biosensors Supporting Accurate Molecular Measurements Directly in Undiluted Whole Blood. J. Am. Chem. Soc. 2017, 139, 11207–11213, doi:10.1021/jacs.7b05412.

II. Electrochemical Aptamer-Based Sensors for Rapid Point-of-Use Monitoring of the Mycotoxin Ochratoxin A Directly in a Food Stream[1]

Abstract

The ability to measure the concentration of specific small molecules continuously and in real time in complex sample streams would impact many areas of agriculture, food safety, and food production. Monitoring for mycotoxin taint in real time during food processing, for example, could improve public health. Towards this end, we describe here an inexpensive electrochemical DNA-based sensor that supports real-time monitor of the mycotoxin ochratoxin A in a flowing stream of foodstuffs.

A. Introduction

Mycotoxins, a broad class of small molecule natural products produced by molds, are toxic to humans and other vertebrates. They primarily arise in foods stored in damp conditions and outbreaks are typically reported in the developing world. For example, after a jaundice outbreak in the Eastern and Central Provinces of Kenya sickened 317 with 125 deaths a survey of maize products in the region found more than half were contaminated with mycotoxin [1]. The specific mycotoxin ochratoxin A contaminates a wide range of crops worldwide, including coffee beans, grapes and many grains used both for human consumption and animal feed. It is primarily a nephrotoxin, but animal studies also show that it has liver toxicity, immune suppression, teratogenic and carcinogenic activity [2].

[1] This chapter is published as J. Somerson and K.W. Plaxco, "Electrochemical Aptamer-Based Sensors for Rapid Point-of-Use Monitoring of the Mycotoxin Ochratoxin A Directly in a Food Stream", *Molecules* **2018**, 23(4), 912; doi:10.3390/molecules23040912 and is reproduced under creative commons open access.

Ochratoxin A contaminates a variety of crops worldwide with contaminating concentrations varying widely geographically and between crops [3]. Estimates of the tolerable human intake vary widely, as do regulatory limits of maximum acceptable concentration of ochratoxin A in human and animal foodstuffs [4]. The EU limits ochratoxin A concentrations on coffee beans to 5 μg/kg (roughly corresponding to 1 nM in brewed coffee) and ochratoxin A has been reported in concentrations as high as 1200 μg/kg (roughly corresponding to 200 nM in brewed coffee) [5,6].

The ability to rapidly detect or, better still, continuously monitor for mycotoxin contamination would significantly improve the safety of our food supply. Current state of the art in mycotoxin detection, however, depends on cumbersome laboratory-based techniques, with the most common being high-performance liquid chromatography [7]. While these techniques are sensitive and accurate, they are often inaccessible or economically challenging to deploy in the developing world[8]. An inexpensive detector to measure a mycotoxin at the point of use or the point of production would make measurement accessible to the developing world and improve the ease of measurement in the developing world. In response, we have developed an electrochemical aptamer-based biosensor (E-AB sensor) for the detection of this mycotoxin.

The ochratoxin A-detecting E-AB sensors, like all sensors in this class, employ an electrode-bound, target-recognizing DNA aptamer modified with an electroactive "redox reporter" (**Fig. 2.1**). Specific binding of the target alters the conformation of the aptamer, changing the efficiency of electron transfer between the reporter and the electrode. Interrogating this system using square wave voltammetry, an electrochemical measurement technique that is particularly sensitive to changes in transfer rates, we observe a change in measured current that is quantitatively related to the concentration of the target.

Conveniently, such measurements are rapid, taking only seconds per measurement, and rely only on inexpensive equipment ranging from thousands of dollars for a research-grade instrument to under $100 for a simple, portable potentiostat [9]. Here we report an E-AB sensor for the detection of the mycotoxin ochratoxin A directly in flowing foodstuffs without the addition of any modifying reagents, allowing for the continuous monitoring of food processing workflows.

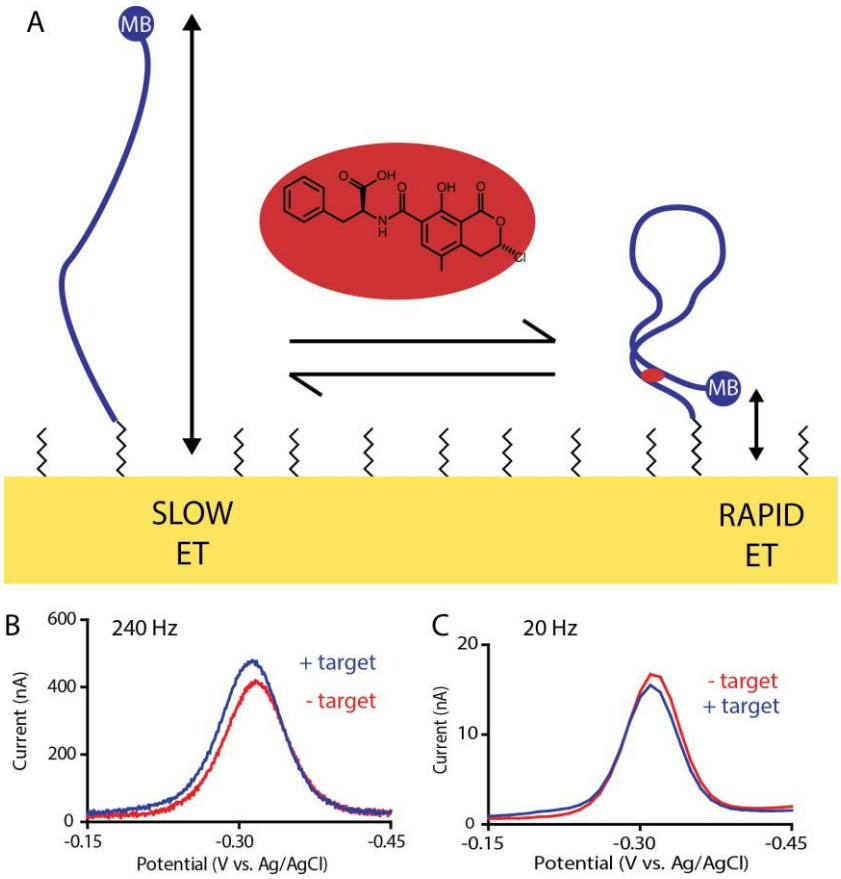

Figure 2.1. (**A**) The ochratoxin A-detecting E-AB sensor consists of an ochratoxin A-binding DNA aptamer modified attached via its 5' end to a gold electrode using a 6-carbon thiol linker (which forms part of a self-assembled monolayer) and modified on its 3' end with a methylene blue redox reporter (blue circle, "MB"). The binding of ochratoxin A (red oval) alters the aptamer's conformation, changing in turn the rate of electron transfer in a manner easily monitored using square wave voltammetry [10]. (**B**) At higher square wave frequencies square wave voltammetry is more sensitive to rapid electron transfer, and thus target addition increases the observed current. (**C**) At lower frequencies, in contrast, target addition decreases the observed current.

B. Results and Discussion

To create an ochratoxin A-detecting E-AB sensor we have employed an aptamer previously shown to bind this target with good specificity and affinity[11]. To date, several other groups have employed this aptamer for mycotoxin detection [11–14]. All of these previously reported, ochratoxin-detecting "aptasensors," however, either require reagent

additions or other processing steps, thus increasing complexity and precluding continuous, real-time monitoring, or are based on fluorescence measurements, which are cumbersome and difficult to perform in foodstuffs due to autofluoresence and often significant light absorption and scattering. E-AB sensors, in contrast, are small (millimeter-scale), are supported by inexpensive, hand-held electronics [9] and provide a reagentless, single-step approach to measurement directly in highly complex media (e.g. whole blood, cell lysates, and foodstuffs) [15–18] .

In order to support their use in E-AB sensors and many other sensing approaches an aptamer must undergo a conformational change upon target binding. Previously published works with this ochratoxin A aptamer have achieved this by adding to the sample solution a short DNA strand complementary to part of the aptamer sequence [11–14]. This creates an equilibrium between the partially double-stranded conformation (aptamer plus complement) and the free, properly folded aptamer. Because only the properly folded aptamer binds the target, target binding drives this equilibrium to the aptamer fold, coupling recognition with a large change in conformation[19,20] . The thermodynamics of this equilibrium (which is defined by the number of self-complementary bases in the complex and the stability of the aptamer fold) modulates the sensor's signal gain (relative signal change upon target binding) and its affinity, with higher gain but poorer affinity being associated with stronger hybridization to the complement. Further limiting this approach, the complement is a separate piece of DNA that is "lost" during use and must be replenished by the user before the sensor can be re-used. To overcome this limitation we instead coupled the complement to the aptamer sequence via an unstructured polythymine linker to create a single, self-complementary strand that cannot be washed away in a flowing sample stream, for example. Specifically, we created two constructs: one with the 10-base complement used in the earlier

literature and a sensor with only 5 self-complementary bases (**Fig. 2.2A**). Characterizing these constructs, however, we saw little E-AB signaling (**Fig. 2.2B**). Ironically, however, we found that the parent aptamer already produces acceptable E-AB signal gain without the addition of any complementary sequence, presumably because it undergoes a binding-induced conformational change without requiring displacement of a complement. Specifically, we observe a 12% signal increase upon addition of saturating target to this sensor when it is interrogated at a square wave frequency of 240 Hz, and a "signal-off" a 13% signal decrease when interrogated at 20 Hz (**Fig. 2.3**).

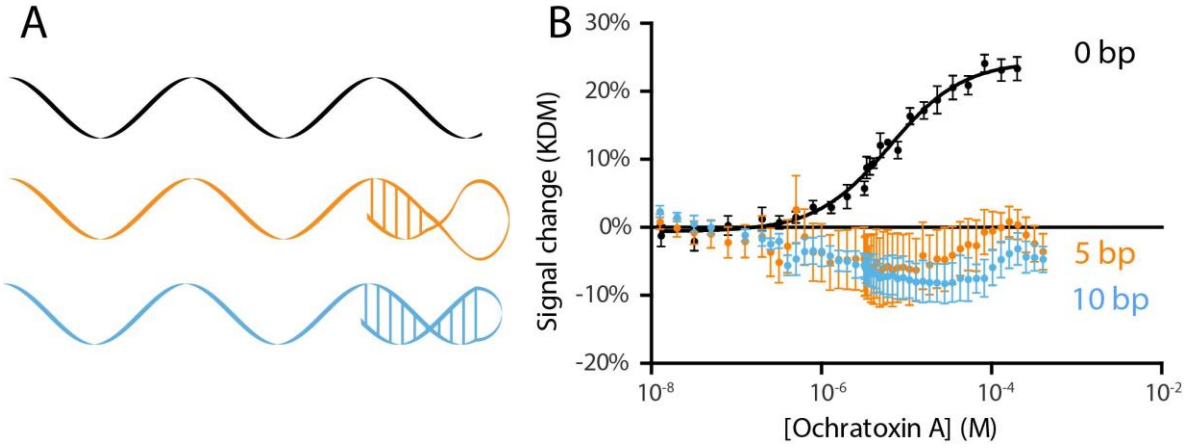

Figure 2.2. (**A**) To identify the E-AB sensor with the highest gain we explored the simplest linear aptamer sequence and two variants to which we added self-complementary tails. (**B**) Constructs with 5 and 10 self-complementary bases added to the 3' end of the aptamer (orange and light blue) do not, however, exhibit any significant change in signal upon target addition. An aptamer lacking any self-complementary tail (black), in contrast, exhibits the expected binding curve. Error bars shown are standard error of the mean for 4 (no tail) or 2 (5 bp, 10 bp tail) independently fabricated sensors.

The occurrence of both signal-on and signal-off behavior in the sensor provides an opportunity to employ Kinetic Differential Measurement (KDM), a method of improving the gain and drift stability of E-AB sensors [21]. KDM does so by measuring two regimes of the electron transfer these sensors use as their signaling mechanism: a fast, "signal-on" regime where target addition increases electrochemical signal and a slow, "signal-off" regime where

target addition decreases electrochemical signal (**Fig. 2.1**). Taking the difference between these two measurements we improve the gain of the ochratoxin A-detecting sensor to 25%. The resultant sensor binds its target with a K_D of 6.5±0.6 µM when challenged in phosphate buffered saline (**Fig. 2.3A**). It is also rapid, fully responding to the addition of 800 µM target within the few seconds it takes to perform the requisite (two per time point) square wave voltammetric scans (**Fig. 2.3B**).

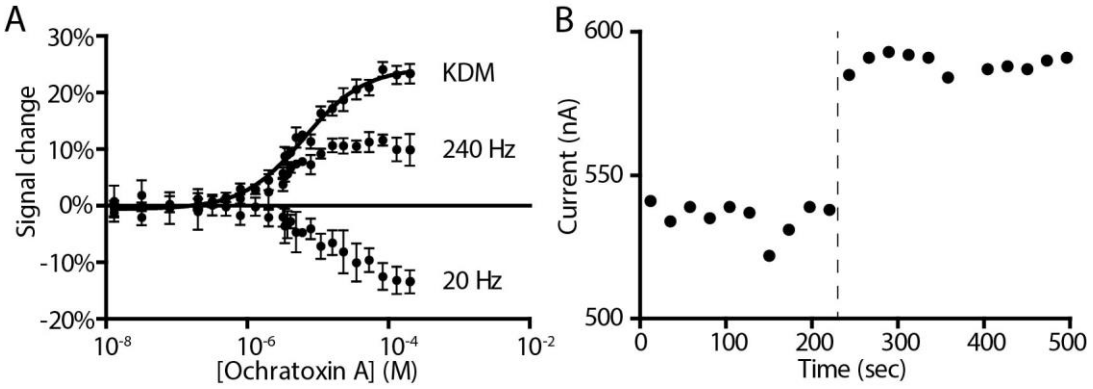

Figure 2.3. (**A**) The ochratoxin A-detecting sensor responds quantitatively to its target with a K_D of 6.5±0.6 µM in, as shown here, a simple buffer sample. Kinetic Differential Measurement (KDM), which takes the difference between measurements obtained at signal-on and signal-off square wave frequencies allows us to improve signal magnitude and self-correction for more stable signal [21]. Error bars shown for the 20 Hz and 240 Hz data are the standard deviation of 4 replicate electrodes. Error bars shown for KDM are the standard error of the mean for 4 replicate calculations. (**B**) The E-AB ochratoxin A sensor responds rapidly when challenged with target. Shown is the current of a single sensor interrogated multiple times in succession in buffer both before and after the sudden addition of saturating (800 µM) target.

To achieve real utility as a point-of-care or point-of-production sensor a device must be selective enough to measure its target directly in the unfiltered, unadulterated media of interest, and be highly specific for that target. To illustrate the utility of our sensor for the measurement food taint in relevant foodstuffs, we thus challenge it in unprocessed iced coffee and find that our sensor is selective enough to work directly in this undiluted, unadulterated commercial food product (**Fig. 2.4A**). Under these conditions it exhibits a

signal gain of 33% and a K_D of 19±2 µM. To demonstrate the value of our sensor in measuring only the target of interest, we also challenged it with five other mycotoxins and find that, as expected, our sensor responds only to the specific mycotoxin ochratoxin A (**Fig. 2.4B**).

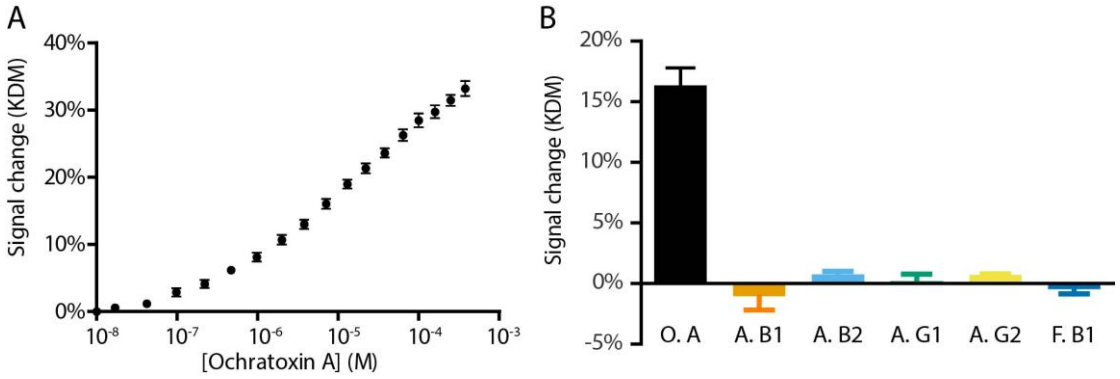

Figure 2.4. The E-AB ochratoxin sensor is selective enough to work when challenged directly in a realistically complex sample matrix, and highly specific for its target. (**A**) Shown here, for example, are data collected in flowing, undiluted coffee. Error bars shown are standard error of the mean for 6 replicate electrodes. (**B**) The E- sensor is also highly specific for its target, ochratoxin A (O. A); it does not respond to the mycotoxins, Aflatoxin B1 (A. B1), Aflatoxin B2 (A. B2), Aflatoxin G1 (A. G1), Aflatoxin G2 (A. G2) or Fumonisin B1 (F. B1). Each bar represents the KDM signal gain of sensors in buffer challenged with 10 µM of mycotoxin, error bars reflect the standard error of the mean for 3 replicate electrodes.

The resulting E-AB sensor demonstrates a sensitive, specific, rapid single-step measurement of ochratoxin A concentrations directly within a relevant foodstuff. This enables point-of-care measurements in resource-limited areas, providing a fast, simple assurance against food taint.

C. Materials and Methods

Materials.

Ochratoxin A was purchased from Enzo Life Sciences (Farmingdale, NY) and used as received without further purification. Ochratoxin A was dissolved in ethanol to a concentration of 61.9 μM (25 mg/mL) then further diluted for titration in the same media as measurements were performed. Aflatoxin B1, aflatoxin B2, aflatoxin G1, aflatoxin G2 and fumonisin B1 were purchased from Sigma Aldrich (St. Louis, MO). 20X phosphate-buffered saline (PBS) was purchased from Sigma Aldrich (St. Louis, MO), diluted to 1X concentration and pH corrected to 7.4 using sodium hydroxide and hydrochloric acid. Starbucks brand Unsweetened Iced Coffee was purchased from Ralphs supermarket (Santa Barbara, CA) and used as received. Oligonucleotides were synthesized by Biosearch Technologies (Novato, CA) and purified by dual HPLC. 6-mercapto-1-hexanol and tris(2-carboxyethyl)phosphine were purchased from Sigma Aldrich (St. Louis, MO) and used as received.

Ochratoxin A aptamer sequences.

Oligonucleotides were synthesized by Biosearch Technologies (Novato, CA) and purified by dual HPLC. All constructs had a 6-carbon thiol linker on the 5' end and a methylene blue redox tag on the 3' end. Self-complementary regions are shown underlined.

0 complementary bp

GATCG GGTGT GGGTG GCGTA AAGGG AGCAT CGGAC A

5 complementary bp

GATCG GGTGT GGGTG GCGTA AAGGG AGCAT CGGAC ATTTT TTGAT GC

10 complementary bp

GATCG GGTGT GGGTG GCGTA AAGGG AGCAT CGGAC ATTTT TTTGT CCGAT GC

Sensor preparation.

Our biosensor consists of a 2 mm diameter gold disk electrode (CH Instruments, Austin TX) coated with a mixed self-assembled monolayer of thiol-modified DNA strands and 6-mercapto-1-hexanol. Electrodes were physically polished and electrochemically cleaned as previously described [22]. DNA sequences were treated with a 1000-fold molar excess of tris(2-carboxyethyl)phosphine to reduce the 5' disulfide modification to a free thiol. Following electrochemical cleaning, electrodes were immersed in 200 nM reduced DNA in 1X PBS at room temperature for 1 h and then moved to 20 mM 6-mercapto-1-hexanol solution in 1X PBS at 4 °C overnight.

Electrochemical measurements.

Electrochemical measurements were performed at room temperature using a CHI630C potentiostat with a CHI684 multiplexer (CH Instruments, Austin, TX) and a standard-three electrode cell containing a platinum wire counter electrode and an Ag/AgCl reference electrode (both from CH Instruments, Austin, TX). Square wave voltammetry was performed at 240 Hz using a potential step of 0.004 V and at 20 Hz using a potential step of 0.001 V, both using an amplitude of 0.025 V. All experiments were conducted in a closed-loop system with a continuous flow of test media (~1 mL/s) using a circulator pump (Cole-Parmer, Vernon Hills, IL).

Acknowledgments:

This work was supported by the Institute for Collaborative Bio-technologies through Grant W911NF-09-0001 from the U.S. Army Research Office and the National Institutes of Health (Grant R01EB022015). The content of the information does not necessarily reflect the position or the policy of the Government and no official endorsement should be inferred. J.S. acknowledges support from the National Cancer Institute of the National Institute of Health (NRSA F31CA183385).

D. References

1. Nyikal, J.; Misore, A.; Nzioka, C.; Njuguna, C.; Muchiri, E.; Njau, J.; Maingi, S.; Njoroge, J.; Mutiso, J.; Onteri, J.; Langat, A.; Kilei, I. K.; Nyamongo, J.; Ogana, G.; Muture, B.; Tukei, P.; Onyango, C.; Ochieng, W.; Tetteh, C.; Likimani, S.; Nguku, P.; Galgalo, T.; Kibet, S.; Manya, A.; Dahiye, A.; Mwihia, J. (et al) Outbreak of aflatoxin poisoning - Eastern and Central Provinces, Kenya, January-July 2004. Morb. Mortal. Wkly. Rep. 2004, 53, 790–3, doi:mm5334a4 [pii].
2. Bennett, J. W.; Klich, M.; Mycotoxins, M. Mycotoxins. Clin. Microbiol. Rev. 2003, 16, 497–516, doi:10.1128/CMR.16.3.497.
3. Chen, C.; Wu, F. The need to revisit ochratoxin A risk in light of diabetes, obesity, and chronic kidney disease prevalence. Food Chem. Toxicol. 2017, 103, 79–85, doi:10.1016/j.fct.2017.03.001.
4. Bui-Klimke, T. R.; Wu, F. Ochratoxin A and Human Health Risk: A Review of the Evidence. Crit. Rev. Food Sci. Nutr. 2015, 55, 1860–1869, doi:10.1080/10408398.2012.724480.
5. Bayman, P.; Baker, J. L. Ochratoxins: A global perspective. Mycopathologia 2006, 162, 215–223, doi:10.1007/s11046-006-0055-4.
6. Studer-Rohr, I.; Dietrich, D. R.; Schlatter, J.; Schlatter, C. The occurrence of ochratoxin A in coffee. Food Chem. Toxicol. 1995, 33, 341–355, doi:10.1016/0278-6915(94)00150-M.
7. Rai, M.; Jogee, P. S.; Ingle, A. P. Emerging nanotechnology for detection of mycotoxins in food and feed. Int. J. Food Sci. Nutr. 2015, 66, 363–370, doi:10.3109/09637486.2015.1034251.
8. Hyle, E. P.; Jani, I. V.; Lehe, J.; Su, A. E.; Wood, R.; Quevedo, J.; Losina, E.; Bassett, I. V.; Pei, P. P.; Paltiel, A. D.; Resch, S.; Freedberg, K. A.; Peter, T.; Walensky, R. P. The Clinical and Economic Impact of Point-of-Care CD4 Testing in Mozambique and Other Resource-Limited Settings: A Cost-Effectiveness Analysis. PLoS Med. 2014, 11, e1001725, doi:10.1371/journal.pmed.1001725.
9. Rowe, A. A.; Bonham, A. J.; White, R. J.; Zimmer, M. P.; Yadgar, R. J.; Hobza, T. M.; Honea, J. W.; Ben-Yaacov, I.; Plaxco, K. W. CheapStat: An Open-Source, “Do-

It-Yourself" Potentiostat for Analytical and Educational Applications. PLoS One 2011, 6, e23783, doi:10.1371/journal.pone.0023783.
10. White, R. J.; Plaxco, K. W. Exploiting binding-induced changes in probe flexibility for the optimization of electrochemical biosensors. Anal. Chem. 2010, 82, 73–6, doi:10.1021/ac902595f.
11. Cruz-Aguado, J. A.; Penner, G. Determination of Ochratoxin A with a DNA Aptamer. J. Agric. Food Chem. 2008, 56, 10456–10461, doi:10.1021/jf801957h.
12. Ha, T. H. Recent advances for the detection of ochratoxin A. Toxins (Basel). 2015, 7, 5276–5300, doi:10.3390/toxins7124882.
13. Chen, J.; Fang, Z.; Liu, J.; Zeng, L. A simple and rapid biosensor for ochratoxin A based on a structure-switching signaling aptamer. Food Control 2012, 25, 555–560, doi:10.1016/j.foodcont.2011.11.039.
14. Tan, Z.; Feagin, T. A.; Heemstra, J. M. Temporal Control of Aptamer Biosensors Using Covalent Self-Caging To Shift Equilibrium. J. Am. Chem. Soc. 2016, 138, 6328–6331, doi:10.1021/jacs.6b00934.
15. Arroyo-Currás, N.; Somerson, J.; Vieira, P. A.; Ploense, K. L.; Kippin, T. E.; Plaxco, K. W. Real-time measurement of small molecules directly in awake, ambulatory animals. Proc. Natl. Acad. Sci. 2017, 114, 645–650, doi:10.1073/pnas.1613458114.
16. Cash, K. J.; Ricci, F.; Plaxco, K. W. An electrochemical sensor for the detection of protein-small molecule interactions directly in serum and other complex matrices. J. Am. Chem. Soc. 2009, 131, 6955–7, doi:10.1021/ja9011595.
17. Swensen, J. S.; Xiao, Y.; Ferguson, B. S.; Lubin, A. A.; Lai, R. Y.; Heeger, A. J.; Plaxco, K. W.; Soh, H. T. Continuous, real-time monitoring of cocaine in undiluted blood serum via a microfluidic, electrochemical aptamer-based sensor. J. Am. Chem. Soc. 2009, 131, 4262–6, doi:10.1021/ja806531z.
18. Bonham, A. J.; Hsieh, K.; Ferguson, B. S.; Vallée-Bélisle, A.; Ricci, F.; Soh, H. T.; Plaxco, K. W. Quantification of transcription factor binding in cell extracts using an electrochemical, structure-switching biosensor. J. Am. Chem. Soc. 2012, 134, 3346–3348, doi:10.1021/ja2115663.
19. Porchetta, A.; Vallée-Bélisle, A.; Plaxco, K. W.; Ricci, F. Using Distal-Site Mutations and Allosteric Inhibition To Tune, Extend, and Narrow the Useful Dynamic Range of Aptamer-Based Sensors. J. Am. Chem. Soc. 2012, 134, 20601–20604, doi:10.1021/ja310585e.
20. Vallée-Bélisle, A.; Ricci, F.; Plaxco, K. W. Thermodynamic basis for the optimization of binding-induced biomolecular switches and structure-switching biosensors. Proc. Natl. Acad. Sci. U. S. A. 2009, 106, 13802–7, doi:10.1073/pnas.0904005106.
21. Ferguson, B. S.; Hoggarth, D. a; Maliniak, D.; Ploense, K.; White, R. J.; Woodward, N.; Hsieh, K.; Bonham, A. J.; Eisenstein, M.; Kippin, T. E.; Plaxco, K. W.; Soh, H. T. Real-time, aptamer-based tracking of circulating therapeutic agents in living animals. Sci. Transl. Med. 2013, 5, 213ra165, doi:10.1126/scitranslmed.3007095.
22. Rowe, A. A.; White, R. J.; Bonham, A. J.; Plaxco, K. W. Fabrication of Electrochemical-DNA Biosensors for the Reagentless Detection of Nucleic Acids, Proteins and Small Molecules. J. Vis. Exp. 2011, doi:10.3791/2922.

III. An Electrochemical Sensor for Point-Of-Care Measurement of a Malaria Biomarker in Small Volume Clinical Samples[2]

Abstract:

The gold standard for the diagnosis of malaria, a disease that continues to affect hundreds of millions of people each year, is microscopic evaluation of a blood smear. Given that (i) this requires skilled operators and non-trivial clinical infrastructure, and that (ii) malaria predominantly strikes in resource-limited areas there remains a pressing need for improved methods of malaria diagnosis. To this end, the measurement of molecular markers of malaria appears a promising alternative means of diagnosing the disease, but to date these have been primarily deployed in "dipstick" assays. This gives only a qualitative yes-or-no answer and not quantitative information, which is linked to disease progression and severity. In response, we describe here an electrochemical DNA-based sensor that can perform the measurement of a diagnostically relevant malaria biomarker within five minutes using a finger-prick serum sample without requiring sample processing, wash steps, or operator interpretation.

A. Introduction

The World Health Organization Global Technical Strategy now aims for full elimination of the malaria parasite [1]. Despite significant recent progress, however, malaria still infects more than 200 million patients per year and kills hundreds of thousands [2]. In part this is because eradication of the disease will require diagnostic techniques that allow for rapid detection of the parasite, *Plasmodium falciparum*, in the resource-limited areas where

2 This chapter in preparation for publication as J. Somerson, J. Yu, J.P. Wang and K.W. Plaxco, "An electrochemical sensor for point-of-care measurement of a malaria biomarker in small volume clinical samples".

malaria persists. Specifically, a key element of malaria eradication will be the identification of the reservoir of asymptomatic, subcritical infections that contribute to the spread of the disease, which will require point-of-care diagnostics suitable for measuring parasite load in asymptomatic low-level infections [3]. Unfortunately, however, the current gold standard for malaria diagnosis, the examination of a blood smear by microscopy, requires a stable infrastructure and a skilled microscopist [4]. The technique is thus complex enough that it is typically only performed on acute cases; it is far too cumbersome to employ for disease surveillance

Motivated by the need for improved methods of malaria diagnosis significant effort has gone towards identifying molecular markers indicative of the infection [5]. Among the more promising of these is the histidine-rich protein 2 released by *Plasmodium falciparum* (HRP2). This 32.8 kDa, water-soluble protein correlates quantitatively to infection severity and the risk of mortality [6,7], rendering it an excellent biomarker for disease load. Moving the measurement of this protein from centralized laboratories to infected areas, however, proves challenging: while laboratory techniques exist to sensitively and specifically measure protein biomarkers, they are generally cumbersome, resource-intensive and expensive to operate. Protein measurement is further complicated by the complex clinical samples to be measured – human blood, for example, is a viscous, optically-dense fluid filled with proteins, cells, clotting factors and other potential interferents. Though recent developments in blood separation by microfluidic means [8] and clever techniques to reproduce clinical instruments in an inexpensive way such as the “paperfuge” [9] open the door for point-of-care blood separation for serum measurement, even serum remains a challenging sample matric for most biosensor approaches [10].

In contrast to most other proposed point-of-care molecular measurement technologies [11], electrochemical aptamer-based sensors (E-AB sensors) couple the specificity (recognizing a target over its similar analogues) of biomolecular recognition with the selectivity (recognizing a target in a complex, crowded sample medium) of conformation-linked, electrochemical read-outs to quantitatively measure a target of interest directly within complex media like blood serum [11]. E-AB sensors use aptamers, short nucleic acid strands selected *in vitro*, to sensitively and specifically bind their targets, rendering the approach quite general [12]. The necessary aptamer is attached by one end to an interrogating

electrode and modified with an electrochemically-reporting redox moiety at its distal end. When the aptamer changes conformation upon target binding the resultant change in the sensor's electrochemical output is quantitatively related to the concentration of the target [11]. Critically, because: i) binding-induced conformational changes are not mimicked by non-specific adsorption and ii) the electrochemical signal is limited to a narrow potential window over which there are few electrochemically-active interfering species, these sensors perform well even when challenged directly in complex media, including, for example, undiluted blood serum [13–15]. When this attribute is combined with the small size of E-AB sensors and the inexpensive electronics required to drive them [16], the platform appears well suited for point-of-care applications in resource-poor environments. Motivated by these observations we have developed here an electrochemical aptamer-based sensor capable of measuring circulating HRP2 within minutes *directly* in a small-volume serum sample at the point of care.

B. Results and Discussion

Our approach to the point-of-care diagnosis of malaria employs an E-AB sensor capable of measuring the HRP2 biomarker in a clinical sample (**Fig. 3.1**). To fabricate this we employed an aptamer previously selected to sensitively and specifically bind this target [17], which was truncated to destabilize it such that it undergoes binding-induced folding. Specifically, as the concentration of target increases, the population of target-bound aptamers increases, accelerating electron transfer (**Fig. 3.1A**) and producing a large signal increase when the sensor is interrogated using square wave voltammetry at a frequency of xxx Hz (**Fig. 3.1B**). Measuring over a range of HRP2 concentrations we observed the expected Langmuir isotherm relating signal response to target concentration (**Figs. 3.2, 3.3**). Specifically. When challenged in phosphate buffered saline the sensor exhibits a K_D of ~9000 ng/mL HRP2 and a 60% increase in electrochemical signal at saturation (**Fig. 3.2**).

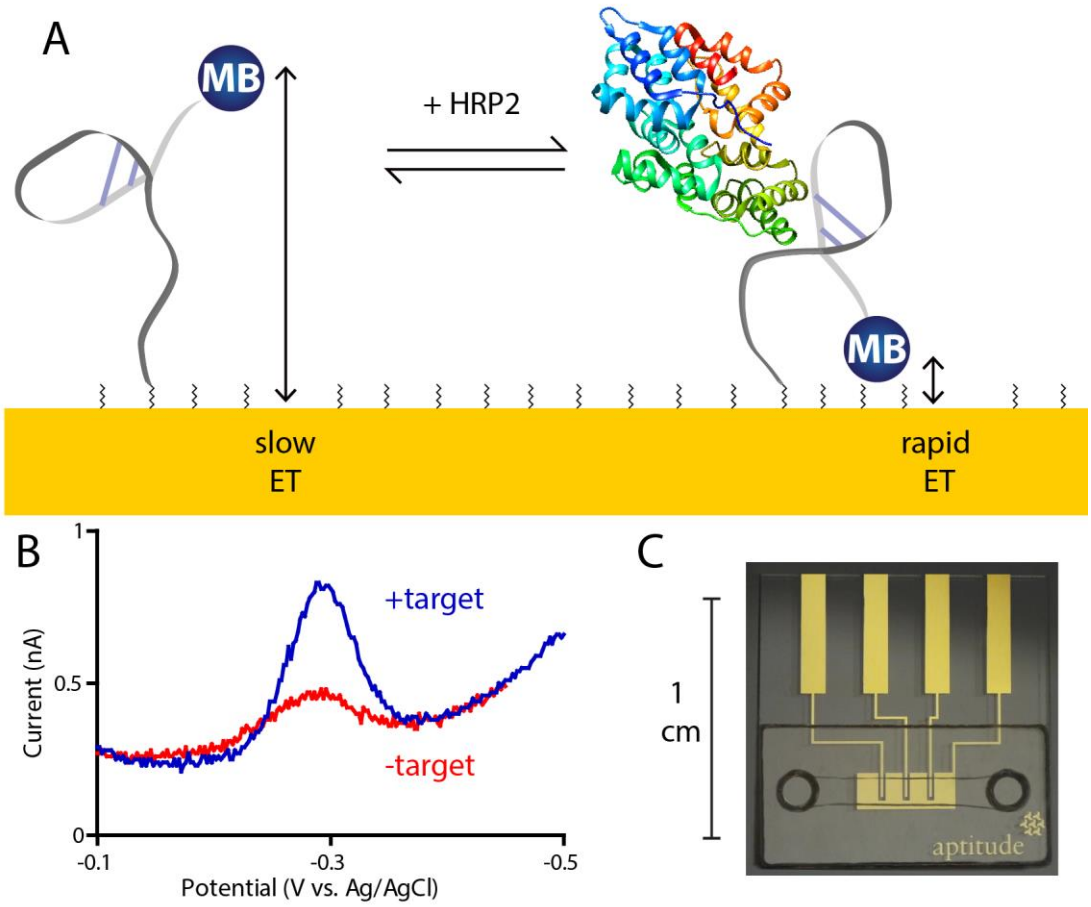

Figure 3.1. (**A**) The aptamer used in our E-AB sensor changes conformation upon binding to the HRP2 protein, which, in turn, improves the accessibility of the methylene blue electrochemical reporter to the electrode surface. This innately changes the rate of electron transfer, which is exhibited as a change in the peak current (**B**). (**C**) The versatile self-assembly of our aptamer system allows us to use a variety of electrode formats; the chip used in this work allows us to measure in <10 µL sample volumes.

To enhance signal gain and reduce sensor drift we employ Kinetic Differential Measurement (KDM) [18]. This technique takes advantage of the fact that square-wave voltammetry is extremely sensitive to changes in electron transfer rate; so much so that we can convert our sensor from being signal on (current increases upon binding) to signal off by altering the square wave frequency (**Fig. 3.2**). By taking the difference between these two normalized signals KDM increases the signal gain of our sensor. Using this approach we observe the expected Langmuir isotherm response to HRP2 with a signal change (signal gain) of ~70% at saturating target concentrations in phosphate buffered saline.

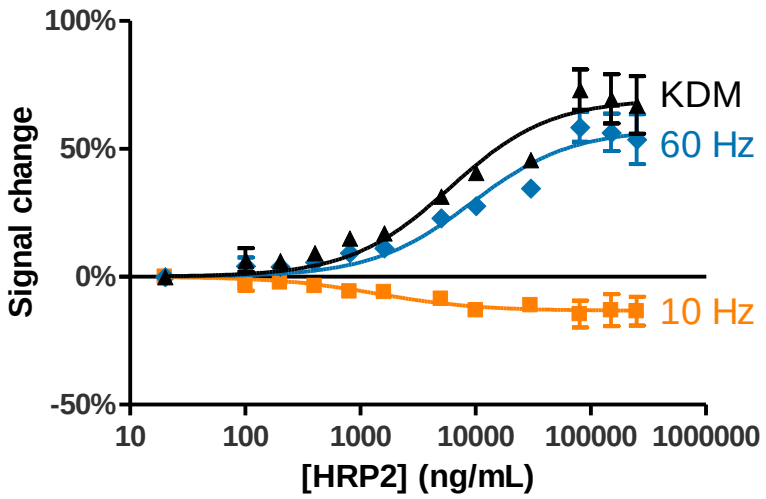

Figure 3.2: Measurement of HRP2 in flowing buffer on micro-scale electrodes in a small volume chip. Our sensors sensitively measure HRP2, a malaria diagnostic protein, in 1X PBS buffer with 1% added BSA. We use two measurement frequencies to improve signal gain and correct for *in vitro* drift from electrode fouling. 60 Hz (blue diamonds) is a "signal-on" frequency and 10 Hz (orange squares) is a "signal-off" frequency. KDM (black triangles) is the subtractive difference between these two frequencies. Error bars represent the standard deviation of two electrodes. Sample medium is 1X PBS with 1% BSA.

To achieve point-of-care clinical utility a technology must provide actionable results within the roughly twenty minute timeframe of the average outpatient doctor-patient interaction [19] and cannot require anything more cumbersome than a finger-prick blood sample. Towards this end, we have developed a sensor which can return a quantitative answer directly in a fingerprick-sized droplet of blood serum within minutes. Using our micro-electrodes in a small-volume chip (**Fig. 3.1C**) we measure in <10 µL of blood serum with no wash steps or reagent addition and we observe response with an equilibrium time constant of 1.0 ± 0.4 min^{-1} (95% confidence interval) (**Fig. 3.3**). In this low-volume device supporting rapid measurements, we observe the expected Langmuir isotherm response to HRP2 with a signal gain of ~50% at saturating target concentrations and a K_D of ~9000 ng/mL (**Fig. 3.4**), well within the clinically observed range between 1 and ~20000 ng/mL in patient serum [7].

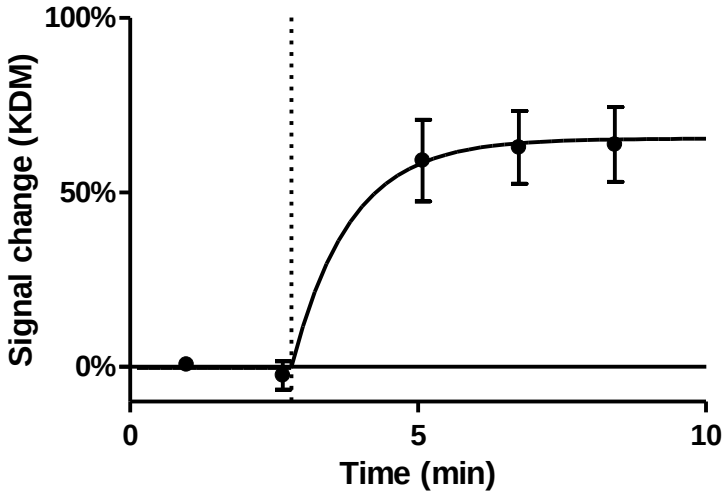

Figure 3.3. These sensors return actionable results within 5 minutes, allowing for immediate diagnosis and treatment within the same visit. Signal shown is KDM using the difference between 60 Hz and 10 Hz measurements. At the dashed line, 10000 ng/mL of HRP2 was spiked into the sample medium (1X PBS with 1% BSA). The equilibrium time constant for signal response is 1 ± 0.4 min^{-1} (95% confidence interval). Error bars shown are the standard deviation of 3 microelectrodes in a small-volume chip.

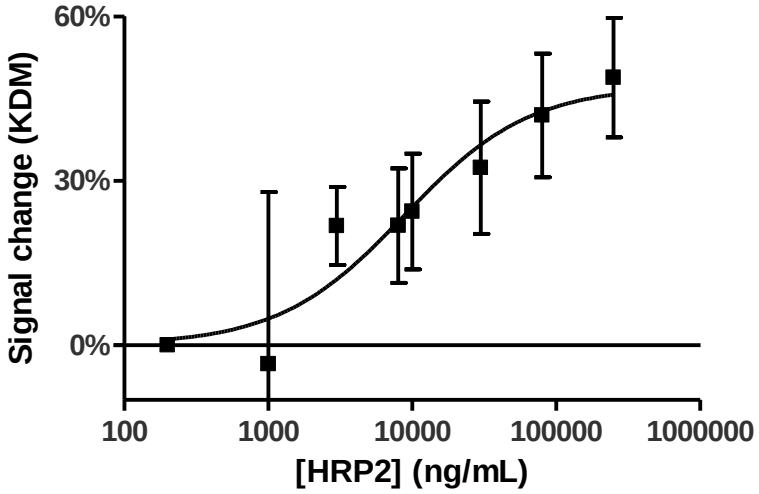

Figure 3.4. Measurement of HRP2 *in vitro* in bovine blood serum. Our sensors sensitively measure HRP2, a malaria diagnostic protein, directly in clinical samples. We use multiple measurement frequencies to improve signal gain and correct for *in vitro* drift from electrode fouling. Signal shown is KDM using the difference between 100 Hz and 40 Hz measurements. Error bars shown are the standard deviation of two microelectrodes.

Using this technology, we have demonstrated a point-of-care device for the rapid, quantitative measurement of clinically-relevant values of HRP2, a biomarker indicative of malaria infection and disease progression. This device measures directly within fingerprick volumes of patient serum samples, enabling new methodologies for truly point-of-care quantitative diagnostics.

By providing a rapid, quantitative measurement to be deployed directly at the point-of-care, we provide not just diagnostics but a new method for better monitoring disease progression and severity. These sensors can work with inexpensive electronics without the need for any centralized infrastructure or operator interpretation, allowing for patient- and community-centered surveillance and intervention. The speed of sensor response allows for the full measurement to take place during a single patient-doctor interaction, ensuring that no patient is lost to follow-up care.

C. Materials and Methods

Materials.

Recombinant *Plasmodium falciparum* Histidine-Rich Protein 2 (expressed in *E. coli*) was purchased from Fitzgerald Industries International (Acton, MA) and used as received without further purification. 20X phosphate-buffered saline (PBS) was purchased from Sigma Aldrich (St. Louis, MO), diluted to 1X concentration and pH corrected to 7.4 using sodium hydroxide and hydrochloric acid. Bovine serum was purchased from HemoStat Laboratories (Dixon, CA). Oligonucleotides were synthesized by Biosearch Technologies (Novato, CA) and purified by dual HPLC. Bovine serum albumin, 6-mercapto-1-hexanol

and tris(2-carboxyethyl)phosphine were purchased from Sigma Aldrich (St. Louis, MO) and used as received.

Microfluidic chip fabrication

The device is comprised of an electrode substrate and channel layer. The electrode substrate possesses gold electrodes which are photolithographically patterned via e-beam evaporation onto borofloat glass substrates (thickness = 500 µm) using a chrome promotor layer (Cr/Au thickness = 20/200 nm). The channel layer is comprised of a double-sided silicon-based adhesive layer (Adhesives Research) attached to a 200 µm-thick mylar substrate via one of its adhesive surfaces. A laser cutter (Trotec Speedy) is used to cut the channel pattern in the adhesive layer (channel cross section = 140 µm x 900 µm) and the fluidic vias in the mylar substrate. The device is assembled by positioning and bonding the second adhesive surface of the channel layer onto the electrode substrate. The electrodes may be functionalized with the aptamer before or after assembly.

The microfluidic chamber was coupled to a syringe pump using pipet tips manually glued onto the top layer. Experiments were performed under constant flow of 10 µL/min.

HRP-2 aptamer sequence.

The aptamer sequence used is a truncated version of a previously published aptamer [17].

5′ – 6-carbon thiol linker – AGGGG TTTGG CTTTG GGTCT GGCA –

methylene blue redox tag – 3′

Sensor preparation.

Electrodes were cleaned using repeated CV measurements in 80 mM H_2SO_4. DNA sequences were treated with a 1000-fold molar excess of tris(2-carboxyethyl)phosphine to reduce the 5' disulfide modification to a free thiol. Following electrochemical cleaning, electrodes were immersed in 200 nM reduced DNA in 1X PBS at room temperature for 1 h and then moved to 20 mM 6-mercapto-1-hexanol solution in 1X PBS at 4 °C overnight.

Electrochemical measurements.

Electrochemical measurements were performed at room temperature using a PalmSens EmStat 3 multichannel potentiostat (PalmSens BV, Houten, The Netherlands). Square wave voltammetry was performed at 10 Hz using a potential step of 0.004 V and at 40 Hz, 60 Hz and 100 Hz using a potential step of 0.001 V, all using an amplitude of 0.025 V.

D. References

1. WHO Global technical strategy for malaria 2016-2030. World Heal. Organ. 2015, 1–35, doi:ISBN: 978 92 4 156499 1.
2. Bhatt, S.; Weiss, D. J.; Cameron, E.; Bisanzio, D.; Mappin, B.; Dalrymple, U.; Battle, K. E.; Moyes, C. L.; Henry, A.; Eckhoff, P. A.; Wenger, E. A.; Briët, O.; Penny, M. A.; Smith, T. A.; Bennett, A.; Yukich, J.; Eisele, T. P.; Griffin, J. T.; Fergus, C. A.; Lynch, M.; Lindgren, F.; Cohen, J. M.; Murray, C. L. J.; Smith, D. L.; Hay, S. I.; Cibulskis, R. E.; Gething, P. W. The effect of malaria control on Plasmodium falciparum in Africa between 2000 and 2015. Nature 2015, 526, 207–11, doi:10.1038/nature15535.
3. Zimmerman, P. A.; Howes, R. E. Malaria diagnosis for malaria elimination. Curr. Opin. Infect. Dis. 2015, 28, 446–454, doi:10.1097/QCO.0000000000000191.
4. Kilian, A. H. D.; Metzger, W. G.; Mutschelknauss, E. J.; Kabagambe, G.; Langi, P.; Korte, R.; Sonnenburg, F. Von Reliability of malaria microscopy in epidemiological studies: resul... - PubMed - NCBI. 2000, 5, 3–8.
5. World Health Organization Malaria Rapid Diagnostic Test Perfomance. 2008, 1.
6. Hendriksen, I. C. E.; Mwanga-Amumpaire, J.; von Seidlein, L.; Mtove, G.; White, L. J.; Olaosebikan, R.; Lee, S. J.; Tshefu, A. K.; Woodrow, C.; Amos, B.; Karema, C.; Saiwaew, S.; Maitland, K.; Gomes, E.; Pan-Ngum, W.; Gesase, S.; Silamut, K.;

Reyburn, H.; Joseph, S.; Chotivanich, K.; Fanello, C. I.; Day, N. P. J.; White, N. J.; Dondorp, A. M. Diagnosing Severe Falciparum Malaria in Parasitaemic African Children: A Prospective Evaluation of Plasma PfHRP2 Measurement. PLoS Med. 2012, 9, doi:10.1371/journal.pmed.1001297.
7. Rubach, M. P.; Mukemba, J.; Florence, S.; John, B.; Crookston, B.; Lopansri, B. K.; Yeo, T. W.; Piera, K. A.; Alder, S. C.; Weinberg, J. B.; Anstey, N. M.; Granger, D. L.; Mwaikambo, E. D. Plasma Plasmodium falciparum histidine-rich protein-2 concentrations are associated with malaria severity and mortality in Tanzanian children. PLoS One 2012, 7, 3–7, doi:10.1371/journal.pone.0035985.
8. Browne, A. W.; Ramasamy, L.; Cripe, T. P.; Ahn, C. H. A lab-on-a-chip for rapid blood separation and quantification of hematocrit and serum analytes. Lab Chip 2011, 11, 2440, doi:10.1039/c1lc20144a.
9. Bhamla, M. S.; Benson, B.; Chai, C.; Katsikis, G.; Johri, A.; Prakash, M. Hand-powered ultralow-cost paper centrifuge. Nat. Biomed. Eng. 2017, 1, 9, doi:10.1038/s41551-016-0009.
10. Gaster, R. S.; Hall, D. A.; Nielsen, C. H.; Osterfeld, S. J.; Yu, H.; Mach, K. E.; Wilson, R. J.; Murmann, B.; Liao, J. C.; Gambhir, S. S.; Wang, S. X. Matrix-insensitive protein assays push the limits of biosensors in medicine. Nat. Med. 2009, 15, 1327–1332, doi:10.1038/nm.2032.
11. Lubin, A. A.; Plaxco, K. W. Folding-based electrochemical biosensors: the case for responsive nucleic acid architectures. Acc. Chem. Res. 2010, 43, 496–505, doi:10.1021/ar900165x.
12. Wilson, D. S.; Szostak, J. W. In vitro selection of functional nucleic acids. Annu. Rev. Biochem. 1999, 68, 611–47, doi:10.1146/annurev.biochem.68.1.611.
13. Somerson, J.; Plaxco, K. Electrochemical Aptamer-Based Sensors for Rapid Point-of-Use Monitoring of the Mycotoxin Ochratoxin A Directly in a Food Stream. Molecules 2018, 23, 912, doi:10.3390/molecules23040912.
14. Lubin, A. A.; Lai, R. Y.; Baker, B. R.; Heeger, A. J.; Plaxco, K. W. Sequence-specific, electronic detection of oligonucleotides in blood, soil, and foodstuffs with the reagentless, reusable E-DNA sensor. Anal. Chem. 2006, 78, 5671–7, doi:10.1021/ac0601819.
15. Swensen, J. S.; Xiao, Y.; Ferguson, B. S.; Lubin, A. A.; Lai, R. Y.; Heeger, A. J.; Plaxco, K. W.; Soh, H. T. Continuous, real-time monitoring of cocaine in undiluted blood serum via a microfluidic, electrochemical aptamer-based sensor. J. Am. Chem. Soc. 2009, 131, 4262–6, doi:10.1021/ja806531z.
16. Rowe, A. A.; Bonham, A. J.; White, R. J.; Zimmer, M. P.; Yadgar, R. J.; Hobza, T. M.; Honea, J. W.; Ben-Yaacov, I.; Plaxco, K. W. CheapStat: An Open-Source, "Do-It-Yourself" Potentiostat for Analytical and Educational Applications. PLoS One 2011, 6, e23783, doi:10.1371/journal.pone.0023783.
17. Wang, J.; Yu, J.; Yang, Q.; McDermott, J.; Scott, A.; Vukovich, M.; Lagrois, R.; Gong, Q.; Greenleaf, W.; Eisenstein, M.; Ferguson, B. S.; Soh, H. T. Multiparameter Particle Display (MPPD): A Quantitative Screening Method for the Discovery of Highly Specific Aptamers. Angew. Chemie - Int. Ed. 2017, 56, 744–747, doi:10.1002/anie.201608880.
18. Ferguson, B. S.; Hoggarth, D. a; Maliniak, D.; Ploense, K.; White, R. J.; Woodward, N.; Hsieh, K.; Bonham, A. J.; Eisenstein, M.; Kippin, T. E.; Plaxco, K. W.; Soh, H. T. Real-time, aptamer-based tracking of circulating therapeutic agents in living animals. Sci. Transl. Med. 2013, 5, 213ra165, doi:10.1126/scitranslmed.3007095.

19. Abbo, E. D.; Zhang, Q.; Zelder, M.; Huang, E. S. The Increasing Number of Clinical Items Addressed During the Time of Adult Primary Care Visits. J. Gen. Intern. Med. 2008, 23, 2058–2065, doi:10.1007/s11606-008-0805-8.

IV. Single-step, Calibration-Free Measurement of a Specific Protein Directly in Whole Blood[3]

Abstract:

Methods for the detection of diagnostically-relevant proteins are limited to either multi-step, laboratory-based procedures, such as ELISAs, or point-of-care tests, such as lateral-flow "dipsticks," that merely confirm absence or presence of the protein without quantifying its level. Here, however, we demonstrate here the application of electrochemical aptamer-based (E-AB) sensors to the rapid, single-step, calibration-free measurement of human platelet-derived growth factor (PDGF) directly in undiluted whole blood samples.

A. Introduction

The point-of-care measurement of diagnostically relevant molecules has the potential to improve clinical outcomes and reduce healthcare costs. In the developing world, for example, point-of-care testing is a critical substitute for laboratory testing as these resource-limited regions often lack the infrastructure necessary to maintain and utilize a network of centralized clinical laboratories[1,2]. Even in the relatively advantaged developed world, point-of-care tests augment centralized laboratory testing by speeding diagnosis, accelerating the initiation of treatment and reducing the need for follow-up visits, which in turn improve outcomes and lower costs[3–5]. To this end, recent decades have seen the development of a number of point-of-care molecular diagnostics, including, for example, lateral flow "dip

[3] This chapter in preparation for publication (with Chapter VI) as **J. Somerson**, N. Arroyo-Currás, G. Ortega, K. Ploense, H. Li, T. Kippin and K.W. Plaxco, "Nanomolar *in vivo* and calibration-free *in vitro* measurement of a circulating protein"**.**

sticks," which have revolutionized the detection of pregnancy, infectious diseases, and drug abuse both at the point of care and in home use[6]. Dipstick tests, however, are qualitative, generally rendering them suitable only for the detection of health states that are binary (e.g., pregnant or not, using a drug or not), leaving an unmet need for point-of-care molecular detection platforms that are, in contrast, quantitative. Rather than reporting the mere absence or presence of a target, such measurements can be used to monitor the specific level of a given marker, providing valuable information on disease state and progression[7–9].

To achieve practicality at the point of care, a technology must be simple (single-step, wash-free and reagent-free), rapid (providing an answer within the 15 min of a typical provider/patient interaction), and low overhead (inexpensive, small)[10]. Our approach to achieving these ends is based on electrochemical, aptamer-based (E-AB) sensors, a reagentless, single-step sensing platform that couples the specificity of biomolecular recognition with the convenience and selectivity of electrochemical measurements (**Fig. 4.1A**). E-AB sensors are comprised of a DNA aptamer artificially selected to bind the specific target of interest that is modified with an electrochemical reporter and attached (via thiol-on-gold monolayer formation) to an interrogating electrode. Upon binding its specific molecular target the aptamer changes conformation, which, in turn, changes accessibility of the electrochemical reporter to the electrode surface and generates a measurable change in faradaic current quantitatively related to the concentration of target present. By thus coupling the selectivity of biomolecular recognition with the specificity of binding-induced conformational changes and the quantitative value of electrochemical measurements, E-AB sensors are able to measure their target directly even in complex clinical media, such as undiluted blood serum[11–14] without the need for reagent additions, washing or any other

processing steps. Critically, the equipment required for this measurement is easily miniaturized and brought directly to the point of care, even in resource-limited settings. Multiple groups, for example, have described construction of laptop- or smartphone-powered potentiostats supporting such sensors at a cost of <$100[15–18].

Despite the many attributes that speak to the potential utility of E-AB sensors as a point-of-care molecular diagnostic, the platform still suffers from two significant limitations that have hindered the deployment of many (if not all) prior efforts to achieve practical point-of-care molecular measurements. First, while E-AB sensors are selective enough to work in undiluted blood serum[11,12,19], they tend to drift when deployed in undiluted whole blood[20–22], thus they have historically required the conversion of blood into serum prior to analysis. And although such conversion is relatively straightforward[23], it requires a degree of infrastructure ill-suited for use at the bedside or in the developing world[24]. Second, the raw, absolute output signal produced by E-AB sensors varies significantly from sensor-to-sensor due to variation in their fabrication, a problem that continues to bedevil quantitative biosensor approaches[25–28]. Historically, we have solved this problem by calibrating each individual sensor against a standard of known (or known to be zero) target concentration[29,30]. Here, however, we demonstrate the ability of the E-AB platform to achieve reproducible, single-step measurements[31] of a specific protein target *in vitro* in unprocessed whole blood without the need for calibrating each individual sensor.

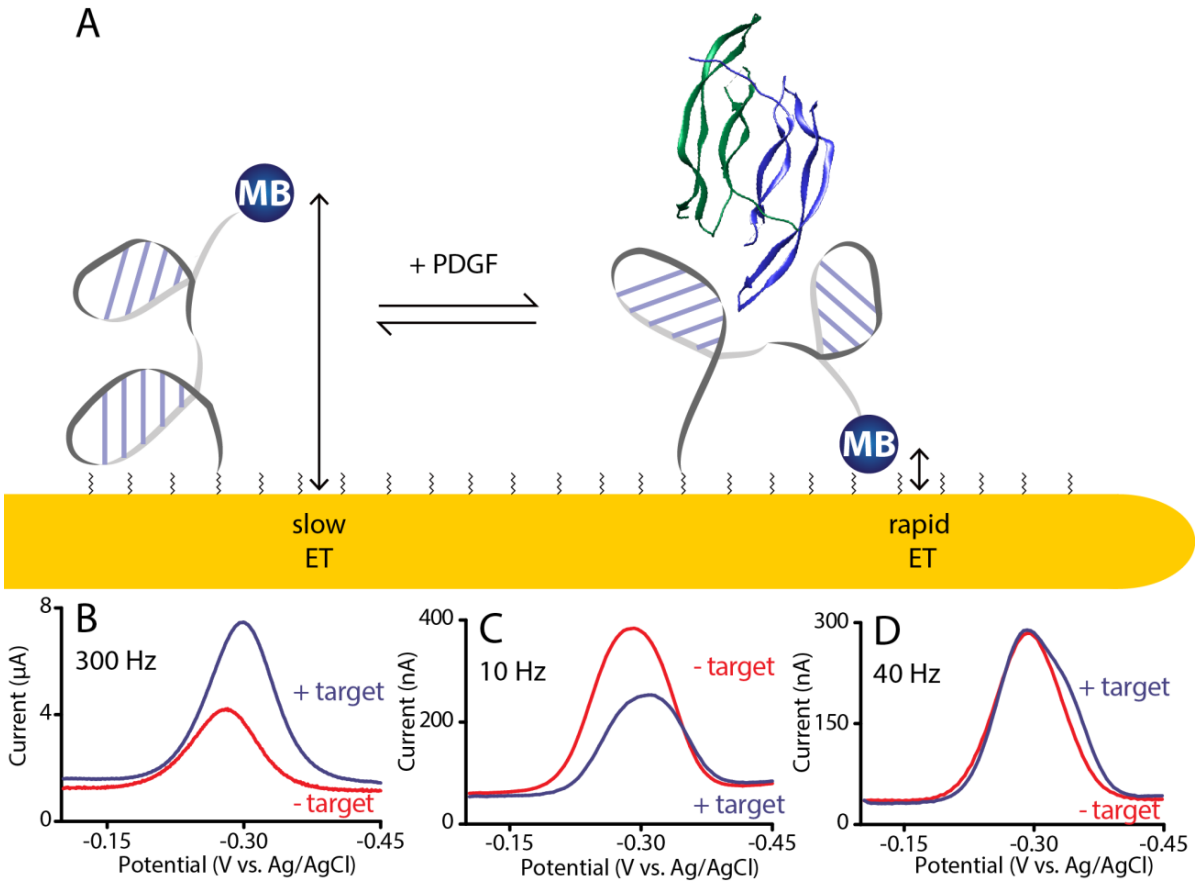

Figure 4.1. (**A**) The binding of the BB isoform of human platelet-derived growth factor (PDGF) to the aptamer in our sensor changes its conformation, which, in turn, renders the methylene blue redox reporter more accessible to the electrode surface. This change in accessibility results in a corresponding change in electron transfer rate, which is "read out" as a change in peak current when the sensor is interrogated using square wave voltammetry. (**B**) At high square-wave frequencies target binding increases the peak current (the "signal-on" regime)[32]. (**C**) At low square wave frequencies (here, 10 Hz), in contrast, target binding is associated with a reduction in peak current. (**D**) Given this, there exists an intermediate frequency (here, 40 Hz) at which the peak current is insensitive to the presence or absence of target[31].

B. Results

As our protein-detecting sensor we have been exploring an E-AB sensor supporting the detection of the BB isoform of human platelet derived growth factor (PDGF)[12]. This sensor consists of a DNA aptamer binding to PDGF and modified with a thiol linker group

on its 5' end and a redox active methylene blue reporter on its 3' end (**Fig. 4.1A**). As noted above, the binding of the aptamer to its target alters the rate of electron transfer from the attached methylene blue, producing an easily measured change in signal when the sensor is interrogated via square-wave voltammetry (**Fig. 4.1 B-D**). The magnitude –and even the sign– of the resultant signal gain is a strong function of square wave frequency[32] At higher square wave frequencies (here > 40 Hz), which are more sensitive to rapid electron transfer, the peak current increases upon target binding ("signal-on", **Fig 4.1B**). At lower square wave frequencies (< 40 Hz), the slow electron transfer of the unbound state dominates and the peak current decreases upon binding ("signal-off", **Fig 4.1C**). Given these behaviors, there necessarily also exists an intermediate frequency (here, 40 Hz) at which the peak current is insensitive to the presence or absence of target (**Fig 4.1D**), which, as described below, forms the basis of our calibration-free measurement approach..

As is typical of such sensors, the raw current output by our PDGF-detecting E-AB sensor, *i*, varies significantly from sensor to sensor (**Fig. 4.2**), likely due to differences in the total surface area of the electrode and thus the total number and packing density of redox reporters that are exchanging electrons with the electrode. We have historically circumvented this problem via calibration using a target-free "blank." That is, using the current measured in a blank, i_0, we calculate "relative signal gain," $(i - i_0)/i_0$, which, in contrast to absolute E-AB current, is highly reproducible from sensor to sensor[14]. Such calibration has proven sufficient for many applications, for example continuous monitoring of an exogenous target[11] or benchtop applications with blank samples readily available[33]. When coupled with drift correction algorithms, this calibrated approach even supports direct measurements *in vivo* in the veins of live animals[20,21]. But the need for

calibration increases the complexity of a point-of-care diagnostic, motivating us to pursue "calibration-free" measurements that can accurately quantify the concentration of a given molecular analyte irrespective of sensor-to-sensor fabrication variation or blood-induced drift[31,34].

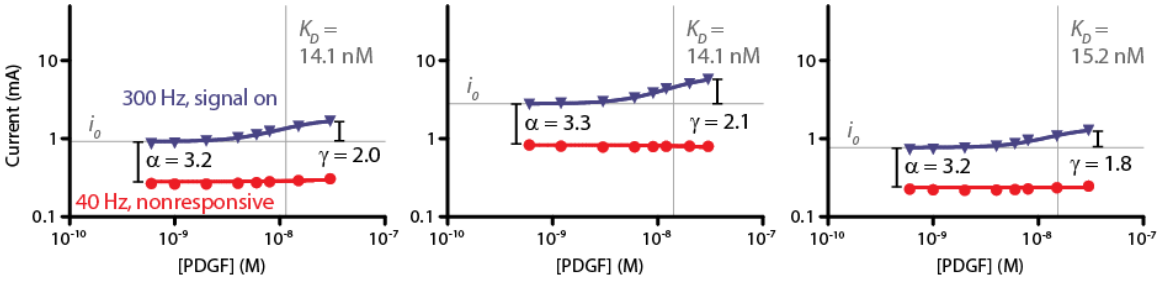

Figure 4.2. Due to variations in electrode surface area and aptamer packing density (and thus the total number of redox-reporters) the raw currents obtained from E-AB sensors vary significantly from sensor to sensor; shown in blue are the signal-on responses of three independently hand-fabricated, PDGF-detecting E-AB sensors. Historically we have corrected this variation by performing a calibration measurement in a target-free reference sample to determine i_0, the current seen in the absence of target. Using this in conjunction with the signal gain, γ, and dissociation constant, K_D, both of which are constant for all sensors in a given class[31], we can accurately determine target concentrations[14]. To avoid the need for this calibration, however, here we use measurement of the current observed at a square-wave frequency at which the sensor does not respond to target (i_{NR}, red) in place of the calibration-derived measurement of i_0. Specifically, i_0 is related to i_{NR} via a proportionality constant, α, that is constant for all sensors employing this aptamer. Given this relationship, we can determine i_0 from measurements of i_{NR} performed in the sample of unknown concentration itself rather than in a known calibration standard.

To enable calibration-free measurement we exploit the above-mentioned square-wave-frequency dependence of E-AB signaling to generate a signal that can be used to correct for sensor-to-sensor variation without the need for separate calibration in a sample of known target concentration for each individual sensor. Specifically, because the sensor is signal-on at higher square wave frequencies and signal-off at lower frequencies there exists an intermediate frequency at which the sensor does not respond to the presence or absence of target (**Fig. 4.1D**). Provided that there is some constant ratio, α, between the current observed at this non-responsive frequency, i_{NR}, and the current that would be seen at the

signal-on frequency in a target free sample, i_0, measurement of i_{NR} *in the actual sample* can be used in place of a separate measurement in a calibration standard. As is required for this approach to work, the ratio of current measured at the non-responsive frequency (40 Hz for this sensor) to the "blank" current at the signal-on frequency (here we employ 300 Hz) is constant from sensor to sensor (**Fig. 4.2**). Using this ratio, the sensor's known (and also constant) signal gain, γ, and the known (and, again, also constant) dissociation constant, K_D, of the aptamer we can then estimate target concentration from measurements of i, and i_{NR} taken in the sample itself (rather than a calibration blank) from:

$$[Target] = K_D \frac{{}^{i}/_{i_{NR}} - \alpha}{\gamma\alpha - {}^{i}/_{i_{NR}}} \quad (1)$$

To determine the appropriate values of α, γ and K_D for this class of E-AB sensors we globally fit data derived from a training set of 6 individual sensors titrated with PDGF directly in whole blood (**Fig. S4.1**), thus setting the stage for calibration free measurements of this protein target. A global fit of this training set produces a K_D of 10.9 ± 6 nM, an α of 3.0 ± 0.1, and a γ of 1.1 ± 0.2 for this PDGF-detecting sensor (**Fig. S4.2**).

To test our approach, we prepared a new set of electrodes (not included in the training set used to define α, γ and K_D) and used them to monitor titrations of known quantities of PDGF in unprocessed whole blood. Using this approach, the estimated PDGF concentrations we derive are in good agreement with the concentration of protein added to a sample *even when the sample is undiluted whole blood* (**Fig. 4.3**). That is, there is an order of magnitude concentration range over which almost all measured points are within 50% of their known concentrations and more than half of the calculated values are within 20% of the known concentration. As a basis for comparison: the FDA recommends that home glucose meters, a

fully mature, commercialized technology, may have measurements within 15% of actual glucose values[35]. Thus, while there is room for improvement as this technology matures, we find this initial level of accuracy encouraging. Likewise speaking to its point-of-care relevance, this "calibration-free" technique does not require blank measurements, reagent additions or other wash steps, and thus the speed of these measurements relies only on the equilibration time of the sensor (<10 minutes, **Fig. S4.3**) and the time to take two subsequent electrochemical measurements in the same sample (seconds).

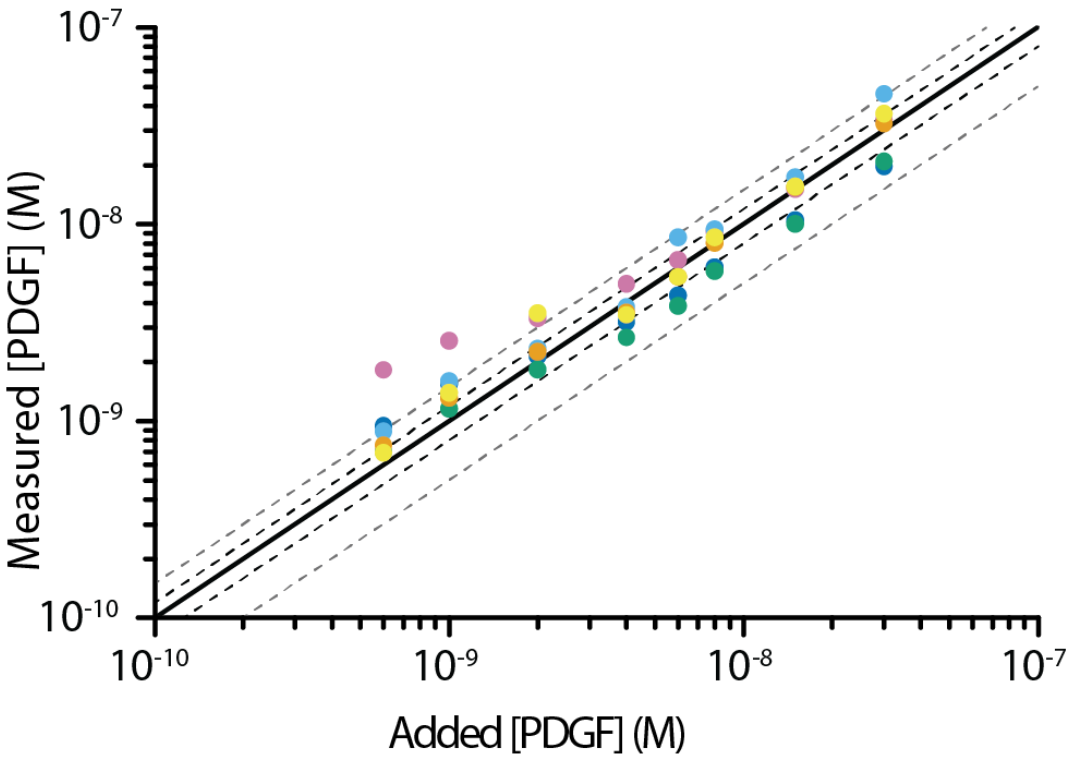

Figure 4.3. Using our calibration-free approach we find good agreement between calculated protein concentrations (circles) and the known amount of protein added to each unprocessed blood sample (dark line). Dashed lines represent 50% (black) and 20% (gray) variance. Each measured concentration is calculated without calibration to any other point, and each color point represents a different, independently hand-fabricated sensor.

Here we demonstrate the calibration-free, rapid, single-step measurement of a specific protein directly in whole, unprocessed blood using a convenient, single-step platform

seemingly well suited for point-of-care applications. This approach expands the utility of this point-of-care clinical technology to enable quantitative, single-step measurement of protein biomarkers of disease, endogenous levels of protein biomarkers and metabolites, and protein markers of disease progression. As this technique is limited only by the development of suitable aptamers, this method should be broadly applicable to any protein target of interest, especially as aptamer selection techniques continue to improve.

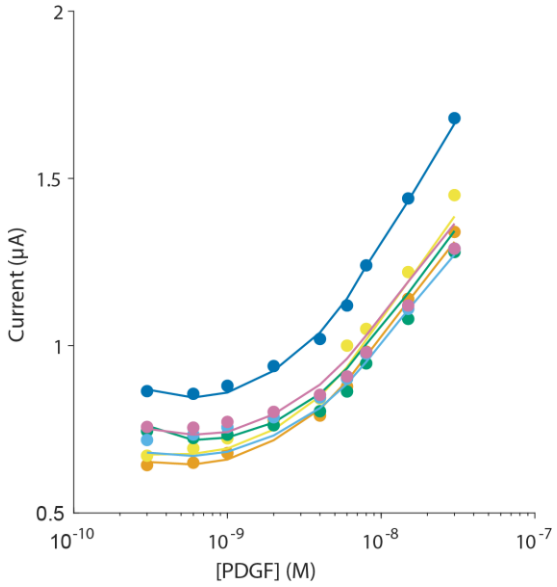

Figure S4.1. Global fitting of the outputs of PDGF-detecting sensors in undiluted whole blood. We globally fit the output of a training set of six sensors to Eq. 4 to define K_D, α, and γ for this type of sensor under the conditions employed (whole blood, room temperature). The solid lines illustrate how well the globally fit parameters describe the output of each individual sensor. Each color line corresponds to the fit for the electrode with the same color points, though the fits overlap.

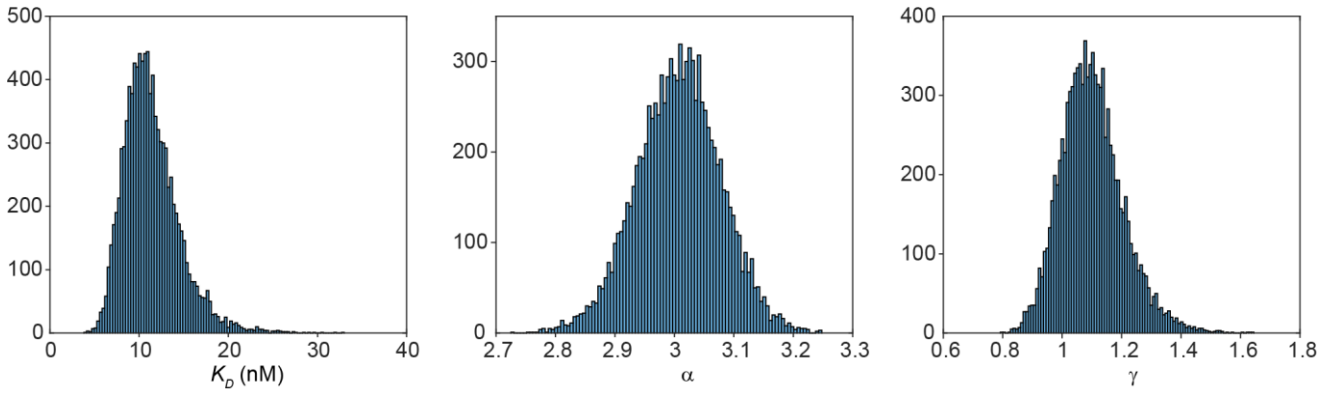

Figure S4.2. Optimized parameters obtained via global fitting. The squared errors in the fittings (**Fig. S4.1**) were propagated by Monte-Carlo analysis (10,000 steps) in order to provide a distribution of the variability in the calculated parameters K_D, α and γ.

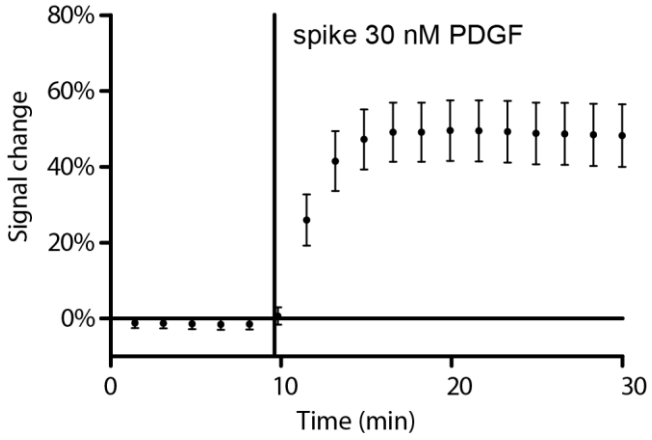

Figure S4.3. Rapid response of sensors to target. Following addition of target into flowing buffer, sensor signal is within error of the equilibrium value within 10 minutes. Shown are the mean of six electrodes with error bars representing the standard deviation.

C. Materials and Methods

Materials.

Human recombinant Platelet-derived Growth Factor-BB (expressed in *E. coli*) was purchased from Prospec-Tany Technogene Ltd. (Ness Ziona, Israel) and used as received without further purification. PDGF-BB was dissolved in water to a concentration of 10.3 µM (250 µg/mL) then further diluted for titration in the same media as measurements were

performed. 20X phosphate-buffered saline (PBS) was purchased from Sigma Aldrich (St. Louis, MO), diluted to 1X concentration and pH corrected to 7.4 using sodium hydroxide and hydrochloric acid. Whole bovine blood and bovine plasma were purchased from HemoStat Laboratories (Dixon, CA). Blood was shipped with 3 IU/mL sodium heparin and used within a week of receipt. Gold wire was purchased from A-M Systems (Sequim, WA). Heat-shrink PTFE was purchased from Zeus Labs (Branchburg Township, CA). Oligonucleotides were synthesized by Biosearch Technologies (Novato, CA) and purified by dual HPLC. 6-mercapto-1-hexanol and tris(2-carboxyethyl)phosphine were purchased from Sigma Aldrich (St. Louis, MO) and used as received.

PDGF-BB aptamer sequence.

5’ – 6-carbon thiol linker – CAGGC TACGG CACGT AGAGC ATCAC CATGA TCCTG – methylene blue redox tag – 3’

Sensor preparation.

Our biosensor consists of a 200 µm diameter gold wire covered with heat-shrinkable PTFE insulation. A window of bare gold was then coated with a mixed self-assembled monolayer of thiol-modified DNA strands and 6-mercapto-1-hexanol. Electrodes were electrochemically roughened and cleaned as previously described[21]. DNA sequences were treated with a 1000-fold molar excess of tris(2-carboxyethyl)phosphine to reduce the 5’ disulfide modification to a free thiol. Following electrochemical cleaning, electrodes were immersed in 200 nM reduced DNA in 1X PBS at room temperature for 1 h and then moved to 20 mM 6-mercapto-1-hexanol solution in 1X PBS at 4 °C overnight.

Electrochemical measurements.

Electrochemical measurements were performed at room temperature using a CHI630C potentiostat with a CHI684 multiplexer (CH Instruments, Austin, TX) and a standard-three electrode cell containing a platinum wire counter electrode and an Ag/AgCl reference electrode (both from CH Instruments, Austin, TX). Square wave voltammetry was performed at 300 Hz using a potential step of 0.001 V, 10 Hz using a potential step of 0.004 V and at 40 Hz using a potential step of 0.001 V, all using an amplitude of 0.025 V. All experiments were conducted in a closed-loop system with a continuous flow of test media (~1 mL/s) using a circulator pump (Cole-Parmer, Vernon Hills, IL).

D. References

1. Zwerling, A.; Dowdy, D. Economic evaluations of point of care testing strategies for active tuberculosis. Expert Rev. Pharmacoecon. Outcomes Res. 2013, 13, 313–325, doi:10.1586/erp.13.27.
2. Hyle, E. P.; Jani, I. V.; Lehe, J.; Su, A. E.; Wood, R.; Quevedo, J.; Losina, E.; Bassett, I. V.; Pei, P. P.; Paltiel, A. D.; Resch, S.; Freedberg, K. A.; Peter, T.; Walensky, R. P. The Clinical and Economic Impact of Point-of-Care CD4 Testing in Mozambique and Other Resource-Limited Settings: A Cost-Effectiveness Analysis. PLoS Med. 2014, 11, e1001725, doi:10.1371/journal.pmed.1001725.
3. Oliver, P.; Buno, A.; Alvarez-Sala, R.; Fernandez-Calle, P.; Alcaide, M. J.; Casitas, R.; Garcia-Quero, C.; Madero, R.; Gomez-Rioja, R.; Iturzaeta, J. M. Clinical, operational and economic outcomes of point-of-care blood gas analysis in COPD patients. Clin. Biochem. 2015, 48, 412–418, doi:10.1016/j.clinbiochem.2014.12.020.
4. Chadee, A.; Blackhouse, G.; Goeree, R. Point-of-Care Hemoglobin A1c Testing: A Budget Impact Analysis. Ont. Health Technol. Assess. Ser. 2014, 14, 1–23.
5. Turner, K. M. E.; Round, J.; Horner, P.; Macleod, J.; Goldenberg, S.; Deol, A.; Adams, E. J. An early evaluation of clinical and economic costs and benefits of implementing point of care NAAT tests for Chlamydia trachomatis and Neisseria gonorrhoea in genitourinary medicine clinics in England. Sex. Transm. Infect. 2014, 90, 104–111, doi:10.1136/sextrans-2013-051147.
6. Posthuma-Trumpie, G. A.; Korf, J.; van Amerongen, A. Lateral flow (immuno)assay: its strengths, weaknesses, opportunities and threats. A literature survey. Anal. Bioanal. Chem. 2009, 393, 569–82, doi:10.1007/s00216-008-2287-2.
7. Nemiroski, A.; Christodouleas, D. C.; Hennek, J. W.; Kumar, A. A.; Maxwell, E. J.; Fernández-Abedul, M. T.; Whitesides, G. M. Universal mobile electrochemical detector designed for use in resource-limited applications. Proc. Natl. Acad. Sci. U. S. A. 2014, 111, 11984–9, doi:10.1073/pnas.1405679111.

8. Krisp, C.; Randall, S. A.; McKay, M. J.; Molloy, M. P. Towards clinical applications of selected reaction monitoring for plasma protein biomarker studies. Proteomics - Clin. Appl. 2012, 6, 42–59, doi:10.1002/prca.201100062.
9. Chin, C. D.; Laksanasopin, T.; Cheung, Y. K.; Steinmiller, D.; Linder, V.; Parsa, H.; Wang, J.; Moore, H.; Rouse, R.; Umviligihozo, G.; Karita, E.; Mwambarangwe, L.; Braunstein, S. L.; van de Wijgert, J.; Sahabo, R.; Justman, J. E.; El-Sadr, W.; Sia, S. K. Microfluidics-based diagnostics of infectious diseases in the developing world. Nat. Med. 2011, 17, 1015–1019, doi:10.1038/nm.2408.
10. Mabey, D.; Peeling, R. W.; Ustianowski, A.; Perkins, M. D. Diagnostics for the developing world. Nat. Rev. Microbiol. 2004, 2, 231–40, doi:10.1038/nrmicro841.
11. Swensen, J. S.; Xiao, Y.; Ferguson, B. S.; Lubin, A. A.; Lai, R. Y.; Heeger, A. J.; Plaxco, K. W.; Soh, H. T. Continuous, real-time monitoring of cocaine in undiluted blood serum via a microfluidic, electrochemical aptamer-based sensor. J. Am. Chem. Soc. 2009, 131, 4262–6, doi:10.1021/ja806531z.
12. Lai, R. Y.; Plaxco, K. W.; Heeger, A. J. Aptamer-Based Electrochemical Detection of Picomolar Platelet-Derived Growth Factor Directly in Blood Serum. Anal. Chem. 2007, 79, 229–233, doi:10.1021/ac061592s.
13. Cash, K. J.; Ricci, F.; Plaxco, K. W. An electrochemical sensor for the detection of protein-small molecule interactions directly in serum and other complex matrices. J. Am. Chem. Soc. 2009, 131, 6955–7, doi:10.1021/ja9011595.
14. Lubin, A. A.; Plaxco, K. W. Folding-based electrochemical biosensors: the case for responsive nucleic acid architectures. Acc. Chem. Res. 2010, 43, 496–505, doi:10.1021/ar900165x.
15. Dryden, M. D. M.; Wheeler, A. R. DStat: A Versatile, Open-Source Potentiostat for Electroanalysis and Integration. PLoS One 2015, 10, e0140349, doi:10.1371/journal.pone.0140349.
16. Sun, A.; Wambach, T.; Venkatesh, A. G.; Hall, D. A. A low-cost smartphone-based electrochemical biosensor for point-of-care diagnostics. In 2014 IEEE Biomedical Circuits and Systems Conference (BioCAS) Proceedings; IEEE, 2014; Vol. 10, pp. 312–315.
17. Nemiroski, A.; Christodouleas, D. C.; Hennek, J. W.; Kumar, A. A.; Maxwell, E. J.; Fernandez-Abedul, M. T.; Whitesides, G. M. Universal mobile electrochemical detector designed for use in resource-limited applications. Proc. Natl. Acad. Sci. 2014, 111, 11984–11989, doi:10.1073/pnas.1405679111.
18. Rowe, A. A.; Bonham, A. J.; White, R. J.; Zimmer, M. P.; Yadgar, R. J.; Hobza, T. M.; Honea, J. W.; Ben-Yaacov, I.; Plaxco, K. W. CheapStat: An Open-Source, "Do-It-Yourself" Potentiostat for Analytical and Educational Applications. PLoS One 2011, 6, e23783, doi:10.1371/journal.pone.0023783.
19. Rowe, A. A.; Miller, E. A.; Plaxco, K. W. Reagentless Measurement of Aminoglycoside Antibiotics in Blood Serum via an Electrochemical, Ribonucleic Acid Aptamer-Based Biosensor. Anal. Chem. 2010, 82, 7090–7095, doi:10.1021/ac101491d.
20. Ferguson, B. S.; Hoggarth, D. a; Maliniak, D.; Ploense, K.; White, R. J.; Woodward, N.; Hsieh, K.; Bonham, A. J.; Eisenstein, M.; Kippin, T. E.; Plaxco, K. W.; Soh, H. T. Real-time, aptamer-based tracking of circulating therapeutic agents in living animals. Sci. Transl. Med. 2013, 5, 213ra165, doi:10.1126/scitranslmed.3007095.

21. Arroyo-Currás, N.; Somerson, J.; Vieira, P. A.; Ploense, K. L.; Kippin, T. E.; Plaxco, K. W. Real-time measurement of small molecules directly in awake, ambulatory animals. Proc. Natl. Acad. Sci. 2017, 114, 645–650, doi:10.1073/pnas.1613458114.
22. Li, H.; Arroyo-Currás, N.; Kang, D.; Ricci, F.; Plaxco, K. W. Dual-Reporter Drift Correction To Enhance the Performance of Electrochemical Aptamer-Based Sensors in Whole Blood. J. Am. Chem. Soc. 2016, 138, 15809–15812, doi:10.1021/jacs.6b08671.
23. Tuck, M. K.; Chan, D. W.; Chia, D.; Godwin, A. K.; Grizzle, W. E.; Krueger, K. E.; Rom, W.; Sanda, M.; Sorbara, L.; Stass, S.; Wang, W.; Brenner, D. E. Standard Operating Procedures for Serum and Plasma Collection: Early Detection Research Network Consensus Statement Standard Operating Procedure Integration Working Group. J. Proteome Res. 2009, 8, 113–117, doi:10.1021/pr800545q.
24. Urdea, M.; Penny, L. A.; Olmsted, S. S.; Giovanni, M. Y.; Kaspar, P.; Shepherd, A.; Wilson, P.; Dahl, C. A.; Buchsbaum, S.; Moeller, G.; Hay Burgess, D. C. Requirements for high impact diagnostics in the developing world. Nature 2006, 444 Suppl, 73–9, doi:10.1038/nature05448.
25. Chen, J.-Q.; Heldman, M. R.; Herrmann, M. A.; Kedei, N.; Woo, W.; Blumberg, P. M.; Goldsmith, P. K. Absolute quantitation of endogenous proteins with precision and accuracy using a capillary Western system. Anal. Biochem. 2013, 442, 97–103, doi:10.1016/j.ab.2013.07.022.
26. Leligdowicz, A.; Conroy, A. L.; Hawkes, M.; Zhong, K.; Lebovic, G.; Matthay, M. A.; Kain, K. C. Validation of two multiplex platforms to quantify circulating markers of inflammation and endothelial injury in severe infection. PLoS One 2017, 12, doi:10.1371/journal.pone.0175130.
27. Stenken, J. A.; Poschenrieder, A. J. Bioanalytical chemistry of cytokines--a review. Anal. Chim. Acta 2015, 853, 95–115, doi:10.1016/j.aca.2014.10.009.
28. Ellington, A. A.; Kullo, I. J.; Bailey, K. R.; Klee, G. G. Antibody-based protein multiplex platforms: technical and operational challenges. Clin. Chem. 2010, 56, 186–93, doi:10.1373/clinchem.2009.127514.
29. Bonham, A. J.; Hsieh, K.; Ferguson, B. S.; Vallée-Bélisle, A.; Ricci, F.; Soh, H. T.; Plaxco, K. W. Quantification of transcription factor binding in cell extracts using an electrochemical, structure-switching biosensor. J. Am. Chem. Soc. 2012, 134, 3346–3348, doi:10.1021/ja2115663.
30. Rowe, A. A.; White, R. J.; Bonham, A. J.; Plaxco, K. W. Fabrication of Electrochemical-DNA Biosensors for the Reagentless Detection of Nucleic Acids, Proteins and Small Molecules. J. Vis. Exp. 2011, doi:10.3791/2922.
31. Li, H.; Dauphin-Ducharme, P.; Ortega, G.; Plaxco, K. W. Calibration-Free Electrochemical Biosensors Supporting Accurate Molecular Measurements Directly in Undiluted Whole Blood. J. Am. Chem. Soc. 2017, 139, 11207–11213, doi:10.1021/jacs.7b05412.
32. White, R. J.; Plaxco, K. W. Exploiting binding-induced changes in probe flexibility for the optimization of electrochemical biosensors. Anal. Chem. 2010, 82, 73–6, doi:10.1021/ac902595f.
33. Lubin, A. A.; Lai, R. Y.; Baker, B. R.; Heeger, A. J.; Plaxco, K. W. Sequence-specific, electronic detection of oligonucleotides in blood, soil, and foodstuffs with the reagentless, reusable E-DNA sensor. Anal. Chem. 2006, 78, 5671–7, doi:10.1021/ac0601819.

34. Arroyo-Currás, N.; Dauphin-Ducharme, P.; Ortega, G.; Ploense, K. L.; Kippin, T. E.; Plaxco, K. W. Subsecond-Resolved Molecular Measurements in the Living Body Using Chronoamperometrically Interrogated Aptamer-Based Sensors. ACS Sensors 2017, acssensors.7b00787, doi:10.1021/acssensors.7b00787.
35. FDA, Self-Monitoring Blood Glucose Test Systems for Over-the-Counter Use. 2016.

V. Real-Time Measurement of Small Molecules Directly in Awake, Ambulatory Animals[4]

Abstract:

The development of a technology capable of tracking the levels of drugs, metabolites, and biomarkers in the body continuously and in real-time would advance our understanding of health and our ability to detect and treat disease. It would, for example, enable therapies guided by high-resolution, patient-specific pharmacokinetics (including feedback-controlled drug delivery), opening new dimensions in personalized medicine. In response, we demonstrate here the ability of electrochemical aptamer-based (E-AB) sensors to support continuous, real-time, multi-hour measurements when emplaced directly in the circulatory systems of living animals. Specifically, we have used E-AB sensors to perform the multi-hour, real-time measurement of four drugs in the bloodstream of even awake, ambulatory rats, achieving precise molecular measurements at clinically relevant detection limits and high (3 s) temporal resolution, attributes suggesting the approach could provide an important new window into the study of physiology and pharmacokinetics.

Significance

The ability to monitor arbitrary molecules directly in living subjects as they undergo their daily routines remains one of the "holy grails" of bioanalytical chemistry. Such a technology would, for example, vastly improve our knowledge of physiology, pharmacokinetics, and

[4] This chapter adapted from Arroyo-Currás, N.; **Somerson, J.**; Vieira, P. A.; Ploense, K. L.; Kippin, T. E.; Plaxco, K. W. Real-time measurement of small molecules directly in awake, ambulatory animals. *Proc. Natl. Acad. Sci.* **2017**, *114*, 645–650, doi:10.1073/pnas.1613458114, reprinted with permission.

toxicology by allowing the high-precision measurement of drugs, metabolites and biomarkers under realistic physiological conditions. Such a technology would also provide an unparalleled, real-time window into health status (e.g., monitoring kidney or endocrine function by measuring creatinine or hormones) and would facilitate "therapeutic drug monitoring," in which dosing is personalized to the accurately measured metabolism of each individual patient. Finally, the ability to measure molecules in the body continuously and in real time would provide unprecedented new routes by which drugs with dangerously narrow therapeutic windows or complex optimal dosing regimens could be safely and efficiently administered.

A. Introduction

The availability of versatile and convenient sensors supporting the continuous, real-time measurement of specific molecules directly in the body could prove transformative in research and in medicine. In the short term, for example, such an advance would allow the in vivo concentrations of drugs, metabolites, hormones, and other biomarkers to be measured with high precision in subjects as they undergo their normal daily routine, improving our knowledge of physiology, pharmacokinetics, and toxicology. On longer timescales, such an advance would facilitate "therapeutic drug monitoring," in which dosing is personalized using a patient's directly measured (rather than crudely and indirectly estimated) metabolism. By permitting the continuous monitoring of biomarkers (e.g., creatinine and hormones), such a technology would likewise provide a new and highly detailed window into health status (e.g., kidney or endocrine function). Finally, the real-time measurement of specific molecules in the body would advance drug delivery (1). Such a technology, for

example, could easily support feedback-controlled dosing, in which the delivery of drugs is adjusted in real time based on their concentration in the body or on the body's molecular-level response to treatment. This real-time, feedback-controlled drug delivery would provide new routes by which drugs with dangerously narrow therapeutic windows or complex optimal dosing regimens can be administered safely and efficiently.

Although technologies already exist for the continuous or near-continuous measurement of a small number of metabolites [e.g., glucose (2) and lactate (3)] and neurotransmitters [e.g., dopamine (4, 5), serotonin (6), glutamate (7), and acetylcholine (8)] in vivo, these approaches all rely on the specific chemical reactivities of their targets (e.g., the redox chemistry of the analyte or its ability to be oxidized by a specific enzyme). Because of their dependence on reactivity, these technologies are not generalizable to the detection of many other physiologically or clinically important molecules, and there remains an open, critical need for strategies that support the continuous detection of specific molecules in the body irrespective of their reactivity. Unfortunately, however, serious technical hurdles stand in the way of realizing this goal (9, 10). First, to support continuous measurements, a sensor cannot rely on batch processing, such as wash or separation steps. Second, to support in vivo measurements, a sensor cannot use exogenously added reagents and must remain stable against prolonged exposure to blood or interstitial fluids in vivo. To date, the vast majority of molecular detection strategies have failed to meet one or both of these critical challenges. Chromatography, mass spectrometry, and immunochemistry, for example, are complex, multistep batch processes requiring wash steps, separation steps, and/or sequential reagent additions, hindering their ability to perform continuous measurements. Conversely, whereas biosensors based on surface plasmon resonance (SPR), quartz crystal microbalances (QCM), field-effect transistors (FET), and microcantilevers all support continuous, real-time

operation, each fails when challenged in blood (much less in vivo) due to their inability to discriminate between the specific binding of their target and the nonspecific adsorption of proteins and cells (11–14). Here, in contrast, we demonstrate the ability of electrochemical aptamer-based (E-AB) sensors, a sensing platform adaptable to the detection of any of a wide range of molecular targets irrespective of their chemical reactivity, to support continuous, real-time measurements directly within the body.

The generality of E-AB sensors stems from the versatile recognition and signal-transduction properties of aptamers, nucleic acids selected for their ability to bind specific molecular targets (15). Created using well-established in vitro selection methods (16, 17), aptamers can be generated that bind a wide range of analytes (18) and can be rationally reengineered such that they undergo a large-scale conformational change upon binding these analytes (19) over arbitrarily broad (20, 21) or narrow (20, 22) concentration windows. E-AB sensors use this conformational change to generate an easily measurable electrochemical signal without the need for the target to undergo a chemical transformation (23). To achieve this signal transduction, the aptamer's binding-induced conformational change is used to alter the efficiency with which a covalently attached redox reporter (here methylene blue) approaches an underlying electrode, producing a target-concentration-dependent change in current when the sensor is interrogated using square wave voltammetry (24) (**Fig. 5.1A** and **Fig. S5.1**). As required to support continuous in vivo measurements, E-AB signaling is not reliant on batch processes, such as wash steps, or on the addition of exogenous reagents. Furthermore, because E-AB signaling is generated by a specific, binding-induced conformational change—and not adsorption of the target to the sensor surface (which is the case for SPR, QCM, FETs, and microcantilevers)—the platform is relatively insensitive to fouling. Previous studies, for example, have shown that E-AB sensors perform well when

challenged for hours in flowing, undiluted blood serum (25), rendering them one of the most fouling resistant single-step biosensor platforms reported to date.

Despite their unprecedented ability to perform continuous monitoring in undiluted blood serum, first-generation E-AB sensors nevertheless foul when challenged in undiluted whole blood, precluding their use directly in vivo. In response, we previously developed a microfluidic approach to preventing fouling by blood cells that supports continuous ex vivo measurements of drug levels in blood continuously drawn by catheter from anesthetized animals (26). In that work, we constructed a microfluidic device using two stacked laminar flows: a bottom flow of blood continuously drawn via a jugular catheter from the animal and draining into a waste chamber, and a flow of buffer stacked on top of this first layer and in permanent contact with the relevant E-AB sensor. The buffer sheath acts as a continuous-flow diffusion filter, allowing for rapid diffusion of small-molecule targets to the sensor while preventing the approach of (much more slowly diffusing) blood cells. Using this device, we have measured the serum levels of multiple drugs for up to 4 h. The approach, however, is nevertheless not without potentially significant limitations. Being ex vivo, for example, the device suffers from a time lag (the time required for blood to leave the body and enter the device), requires continuous blood draws (the buffer-diluted blood must be discarded), and can only be used to measure molecules in blood because other bodily fluids cannot easily and continuously be withdrawn. The device is also complex, requiring a pump and buffer and waste reserves. Finally, due to the necessity of generating laminar flow, the device is sensitive to mechanical shock and thus likely not robust enough to be deployed in awake, freely moving animals. Here, in contrast, we have adapted E-AB sensors to the important problem of performing continuous, real-time, multihour measurements of specific molecules directly within the bodies of awake, freely moving animals.

B. Results and Discussion

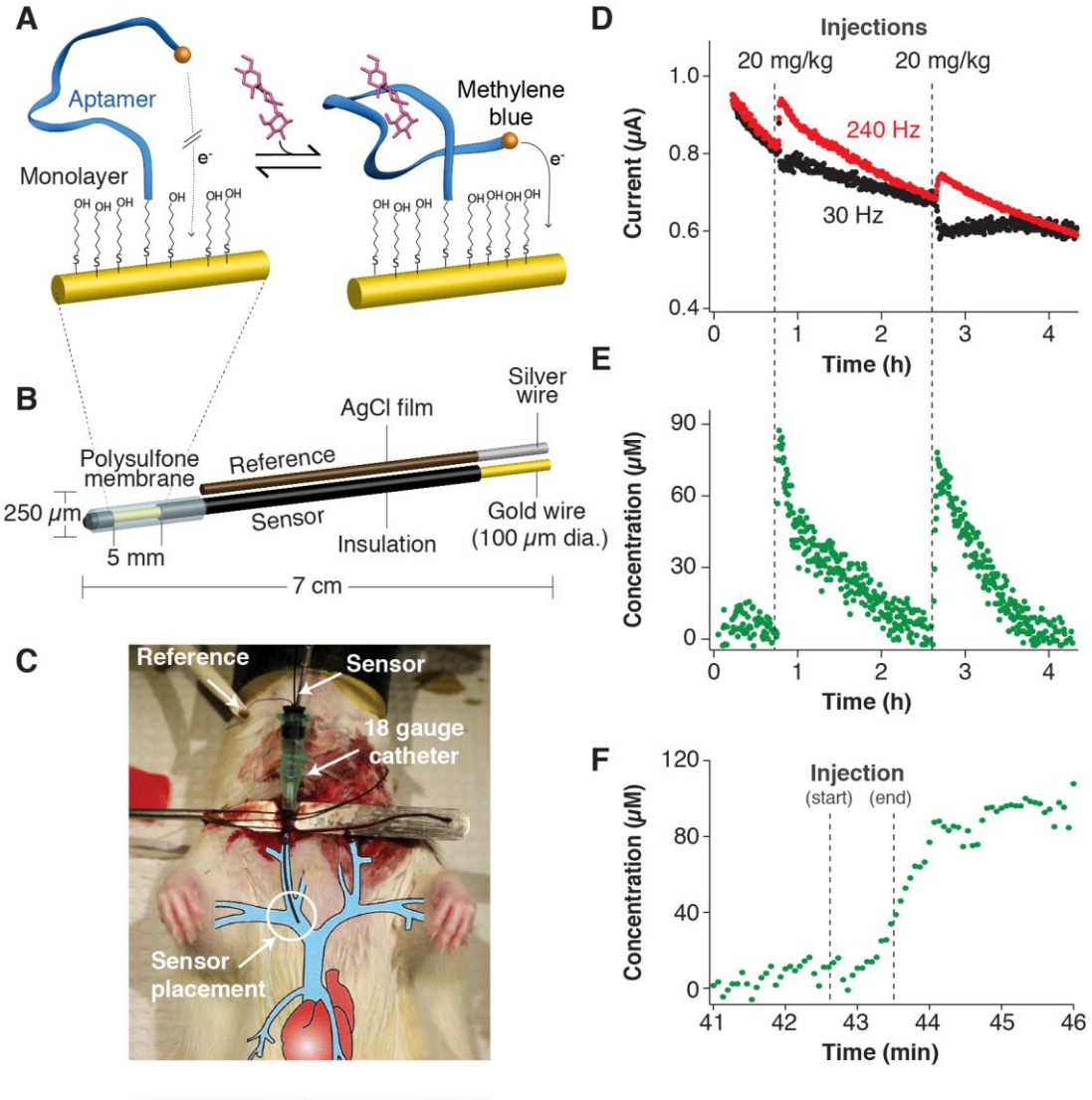

Figure 5.1. Real-time, continuous measurement of specific drugs directly in the living body. (**A**) The E-AB sensing platform, in which the binding-induced folding of an electrode-bound, redox-reporter-modified aptamer leads to a change in electron transfer easily detected using square wave voltammetry. (**B**) A microporous (0.2 μm) polysulfone membrane protects the sensor from fouling by blood cells. (**C**) The resultant device is small enough to emplace in one of the external jugulars of a rat using an 18-gauge catheter (the cartoon overlay illustrates sensor location). (**D**) To correct the drift seen in vivo, we record data at two square wave frequencies (here 30 and 240 Hz; optimal values depend on the aptamer used). At one frequency, the sensor's voltammetric signal increases upon target binding, whereas at the other, it is reduced; taking the difference between the two eliminates drift and enhances signal-to-noise (26). (**E**) Using drift-corrected E-AB sensors, we have monitored the in vivo concentrations of multiple drugs continuously and in real-time over the course of

many hours in measurements that achieve clinically relevant precision and few-second time resolution. Shown here, for example, is the measurement of the antibiotic tobramycin in the blood of an anesthetized rat after two serial injections into the opposite external jugular. (**F**) At 3 s per measurement, the time resolution of these measurements is sufficient to monitor both the injection itself and the subsequent distribution of the drug within the circulatory system and reflects an orders of magnitude improvement over the resolution of traditional pharmacokinetic methods (45).

We have taken a two-pronged approach to circumventing the challenging conditions associated with deploying sensors directly within the bodies of living animals. To reduce fouling, we encase our sensors in biocompatible (27) polysulfone membranes (**Fig. 5.1B**), the 0.2-μm pores of which prevent blood cells from approaching the sensor surface while simultaneously allowing for the rapid transport of target molecules. Using these membranes, we achieve stable E-AB baselines in flowing, undiluted whole blood in vitro over many hours (**Fig S5.1**). Even membrane-protected E-AB sensors, however, exhibit significant baseline drift when emplaced in the veins of live animals (**Fig. 5.1D**). To circumvent this drift, we use a correction scheme termed "Kinetic Differential Measurements" (KDM). Drift correction methods have historically used a physically separate reference that, although unresponsive to the targeted input, nevertheless yields an identical response to background that can be subtracted from the sensor output (28). KDM instead employs a single aptamer in both roles, thus obviating the need to fabricate a matched sensor-reference pair (26). To achieve this stand-alone performance, KDM exploits the square wave frequency dependence of E-AB signaling. Specifically, electron transfer is more rapid from the folded, target-bound aptamer than it is from the unfolded, target-free aptamer. This kinetic difference results in a binding-induced increase in current when we perform square-wave voltammetry at high frequencies and a binding-induced decrease in signal at low frequencies (**Fig. S5.2**) (19).

Conveniently, these two outputs drift in concert, and thus taking their difference effectively corrects baseline drift (**Fig. 5.1D**).

Drift-corrected, membrane-protected E-AB sensors readily support the continuous, seconds-resolved real-time measurement of specific molecules in the blood of living animals (**Fig. 5.1 E and F**). To demonstrate this ability, we first emplaced E-AB sensors for the detection of the cancer chemotherapeutic doxorubicin (DOX) (29, 30) in the external jugular vein of anesthetized Sprague–Dawley rats (**Fig. 5.1C**). Using this approach, we achieve nanomolar precision in the measurement of clinically relevant plasma drug levels following five sequential injections over 5 h of continuous monitoring (**Fig. 5.2A**). The resulting plot of concentration versus time presents consecutive spikes corresponding to each of the injections performed, with maximum DOX concentrations (C max) of ∼600 nM and the effective clearance of 90% of the drug from the circulatory system within 50 min, values in close accord with prior reports (31).

Because E-AB signaling is independent of the chemical reactivity of the target, E-AB sensors can be switched to the detection of new, chemically unrelated molecules via the simple expedient of replacing their aptamer recognition element. To demonstrate this modularity, we fabricated sensors using an aptamer recognizing the aminoglycoside antibiotics (32, 33). Using these sensors, we first followed monotonically increasing i.v. doses of kanamycin spanning the therapeutic ranges used in humans (34) (10–30 mg/kg) and animals (35) (25–30 mg/kg). The sensor responded rapidly to each injection, measuring maximum concentrations between 34 and 400 μM depending on the delivered dose (**Fig. 5.2B**). The 200 μM maximum concentration observed after a 10 mg/kg dose was in agreement with peak plasma concentrations determined previously (using cumbersome, poorly time-resolved ex vivo radioimmunoassays) after similar doses were injected into

multiple animal species (36). The sensor can likewise monitor in real time the in vivo concentrations of the aminoglycosides gentamycin (**Fig. 5.2C**) and tobramycin (**Fig. 5.2D** and **Fig. S5.3**) following either i.m. or i.v. injections, applications in which it once again achieves excellent precision and time resolution.

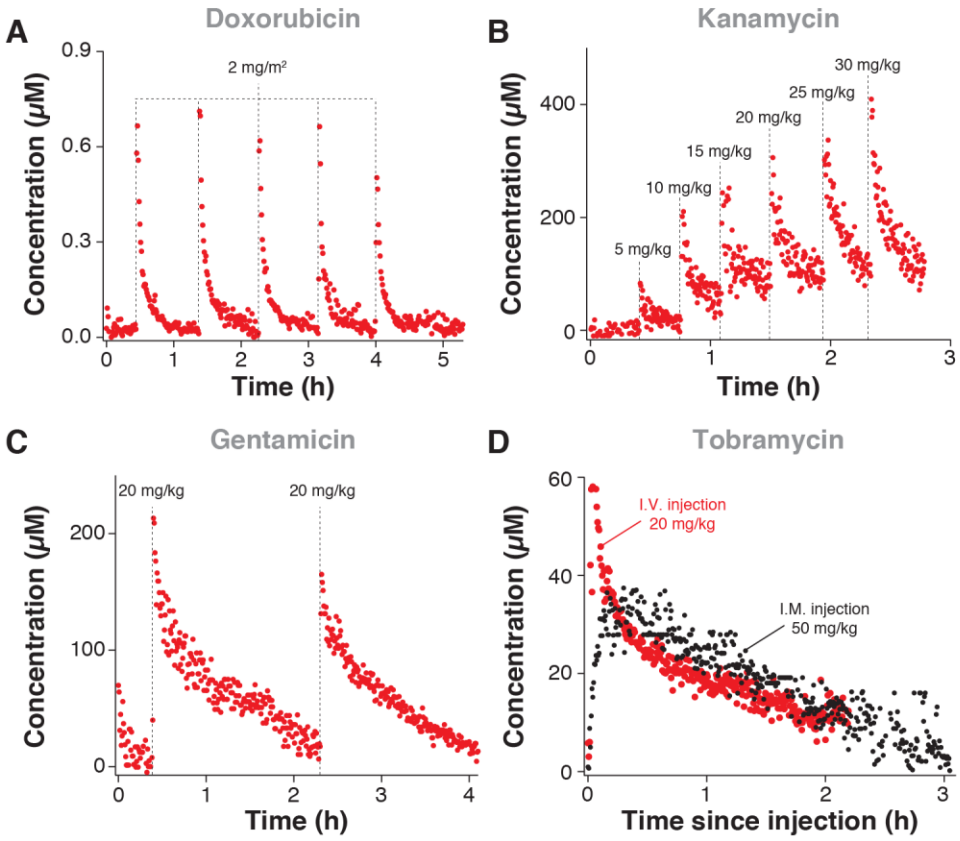

Figure 5.2. Continuous molecular measurements in vivo. We have successfully measured multiple drugs using E-AB sensors emplaced in the jugulars of anesthetized rats. (**A**) Shown here are five i.v. injections of 2 mg/m 2 of the cancer chemotherapeutic DOX, a dose more than 25 times lower than typical human doses (46). (**B**–**D**) To illustrate the generality of the approach, we have also used an aminoglycoside-detecting E-AB sensor to monitor in vivo levels of the antibiotics kanamycin, gentamicin, and tobramycin at the indicated doses. The kanamycin doses used here span the 10–30 mg/kg therapeutic range used in humans (34). For gentamicin, we focus here on two sequential i.v. injections of the drug, separated by a 2-h interval. For tobramycin, we present an overlay of data collected after sequential i.m. (thigh) and i.v. (the external jugular opposite the sensor) injections carried out in a single rat.

The ability to perform the continuous measurement of specific molecules in the body opens the door to many potentially transformative applications in the study of physiology and pharmacokinetics. For example, the few-second time resolution of E-AB sensors (**Fig. 5.1F**), which reflects orders of magnitude improvement over the time resolution of traditional pharmacokinetic methods, is sufficient to measure the kinetics with which drugs distribute following i.v. injection (**Fig. 5.3** and **Fig. S5.4**), a pharmacokinetic phase that has rarely if ever been previously measured (e.g., refs. 37–39). Indeed, the precision of E-AB measurements is sufficient not only to robustly identify animal-to-animal pharmacokinetic variability, but even variability within a single animal over the course of a few hours. To explore this ability, we monitored the pharmacokinetics of tobramycin following sequential 20 mg/kg i.v. injections conducted 2 h apart in each of three rats. Fitting the resultant data to a two-compartment model, we easily observe statistically significant inter- and even intraanimal variability (**Fig. 5.4**). The distribution phase (α phase) of this drug, for example, is defined largely by blood and body volume and thus, although the distribution differs between animals, it differs much less as a function of time within individual animals. The elimination kinetics of tobramycin (β phase), in contrast, not only vary significantly between animals but also exhibit variations within a single individual over the course of a few hours that are easily measurable using our approach (**Table 5.1**). For example, although the kinetics of the α phase remain relatively constant for a given animal, the β phase invariably slows with time. This change presumably occurs because, whereas drug absorption (captured by the α phase) is defined by body volume, which remains fixed, the elimination of tobramycin (captured in the β phase) is predominantly via excretion from the kidneys (40, 41), the function of which likely changes due to alterations in the animal's blood pressure (42) and/or hydration after several hours under anesthesia.

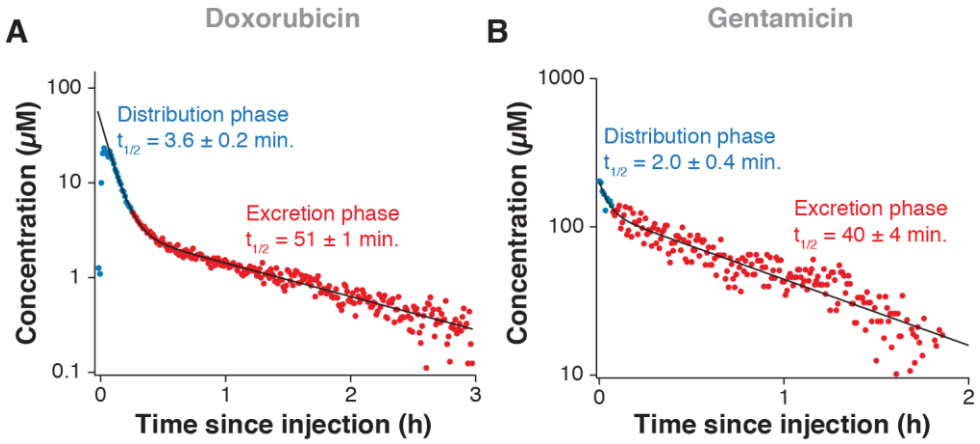

Figure 5.3. 3. High-precision pharmacokinetics. Shown are high-resolution pharmacokinetic profiles for the drugs DOX (**A**) and gentamicin (**B**) upon i.v. injection of 50 mg/m 2 and 20 mg/kg doses, respectively. As is easily seen, the resolution of in vivo E-AB sensors is sufficient not only to define the slower β phases of these drugs (red dots) but also to define their much more rapid α phases (blue dots) with excellent statistical significance. These measurements constitute a precise determination of the i.v. distribution phase of a small-molecule drug.

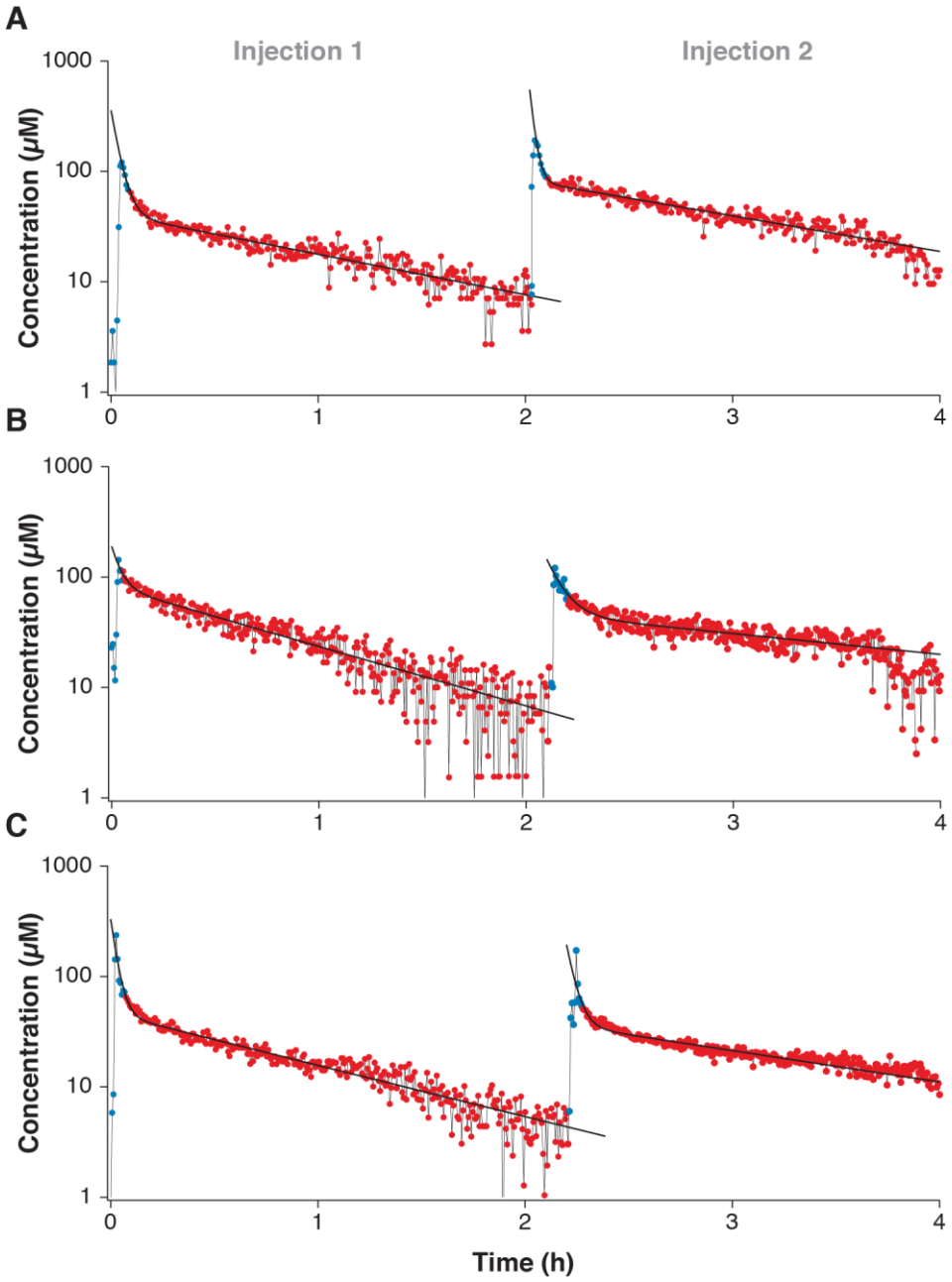

Figure 5.4. The measurement of inter- and intraanimal pharmacokinetic variability. The precision of E-AB measurements is sufficient to measure not only interanimal pharmacokinetic variability but also variability within an individual animal over time. Shown are the pharmacokinetic profiles of the drug tobramycin following two sequential 20 mg/kg i.v. injections in three different rats (**A**, **B**, and **C**). These high-precision measurements reveal a decrease in the rate of drug elimination kinetics (β phase) in the second injection with respect to the first in all three animals, an effect that presumably arises due to changes in the animal's blood pressure and/or hydration after several hours under anesthesia. The bold black lines represent the mathematical fit of each injection dataset to a two-compartment pharmacokinetic model.

Rat no.	Injection no.	A,* µM	α, min	B, µM	β, min	$C_{max,}$ † µM	AUC, µmol·min·L^{-1}	Cl_T, mL·min^{-1}
1	1	255 ± 82	2.2 ± 0.4	71 ± 2	51 ± 3	328 ± 82	117 ± 58	129 ± 64
1	2	267 ± 56	1.6 ± 0.3	80 ± 4	57 ± 4	347 ± 56	168 ± 61	90 ± 32
2	1	113 ± 38	1.6 ± 0.4	82 ± 2	32 ± 1	195 ± 38	73 ± 39	201 ± 100
2	2	109 ± 22	2.7 ± 0.6	50 ± 2	71 ± 7	159 ± 22	41 ± 15	370 ± 139
3	1	284 ± 34	1.2 ± 0.1	46 ± 2	38 ± 3	330 ± 34	237 ± 49	63 ± 13
3	2	138 ± 32	1.7 ± 0.1	35 ± 2	67 ± 3	173 ± 32	82 ± 28	186 ± 63

Table 5.1. Pharmacokinetic parameters corresponding to repeated i.v. injections of tobramycin in three Sprague-Dawley rats.
Confidence ranges reflect 95% confidence intervals.
*A, α, B and β are derived from the fit to a two compartment model: [target] = $Ae^{-t/\alpha} + Be^{-t/\beta}$, where α and β are the half-lives for distribution and elimination, respectively.
† C_{max}, AUC (area under the curve), ClT (drug clearance), and their associated confidence intervals propagated from the kinetic parameters A, α, B and β.

The ability of E-AB sensors to reject false signals arising from background interferents is excellent; none of the many endogenous metabolites and hormones in rat blood activates the sensor, as evidenced by their performance in vivo. The platform's ability to distinguish between structurally similar molecules, in contrast, can be problematic due to the sometimes [although not always (43, 44)] limited specificity of aptamers because, of course, the sensor cannot be more specific than the aptamer from which it is constructed. E-AB specificity is nevertheless sufficient for many research and clinical applications. For example, although the aminoglycoside-binding aptamer recognizes multiple members of this closely related family of drugs (**Fig. 5.2 B–D**), coadministration of more than one of these highly toxic drugs is clinically contraindicated, and thus the inability to distinguish between them is of little medical relevance. The therapeutic action of DOX is driven by its ability to bind DNA, and thus the aminoglycoside sensor also exhibits cross-reactivity to this drug (**Fig. S5.5A**). Here too, however, the coadministration of the two is so rare as to limit the clinical impact of this effect. The DOX-detecting sensor, in contrast, exhibits no significant cross-reactivity with the aminoglycosides (**Fig. S5.5B**), nor does it exhibit significant cross-reactivity with

other chemotherapeutics that are commonly coadministered with DOX in clinical applications (26).

In addition to studies, as those above, performed on anesthetized animals, the simplicity, physical robustness, and small size of E-AB sensors also renders it possible to perform measurements on awake, ambulatory animals. To illustrate this ability, we surgically implanted permanent catheters in the jugular veins of rats and allowed the animals to recover from this surgery for 2 wk before using the catheter to insert a flexible E-AB sensor under light anesthesia. The sensor connects to its supporting electronics via flexible wire leads that allow the awake animals to move largely unimpeded (**Fig. 5.5A**). Aminoglycoside sensors used under these conditions support run times of up to half a day as the animal feeds, drinks, and explores its environment (**Fig. 5.5 B** and **C**), producing pharmacokinetic data that avoid potentially confounding factors associated with measurements based on (repeated) blood draws, which require anesthetized or otherwise immobilized (and thus stressed) animals.

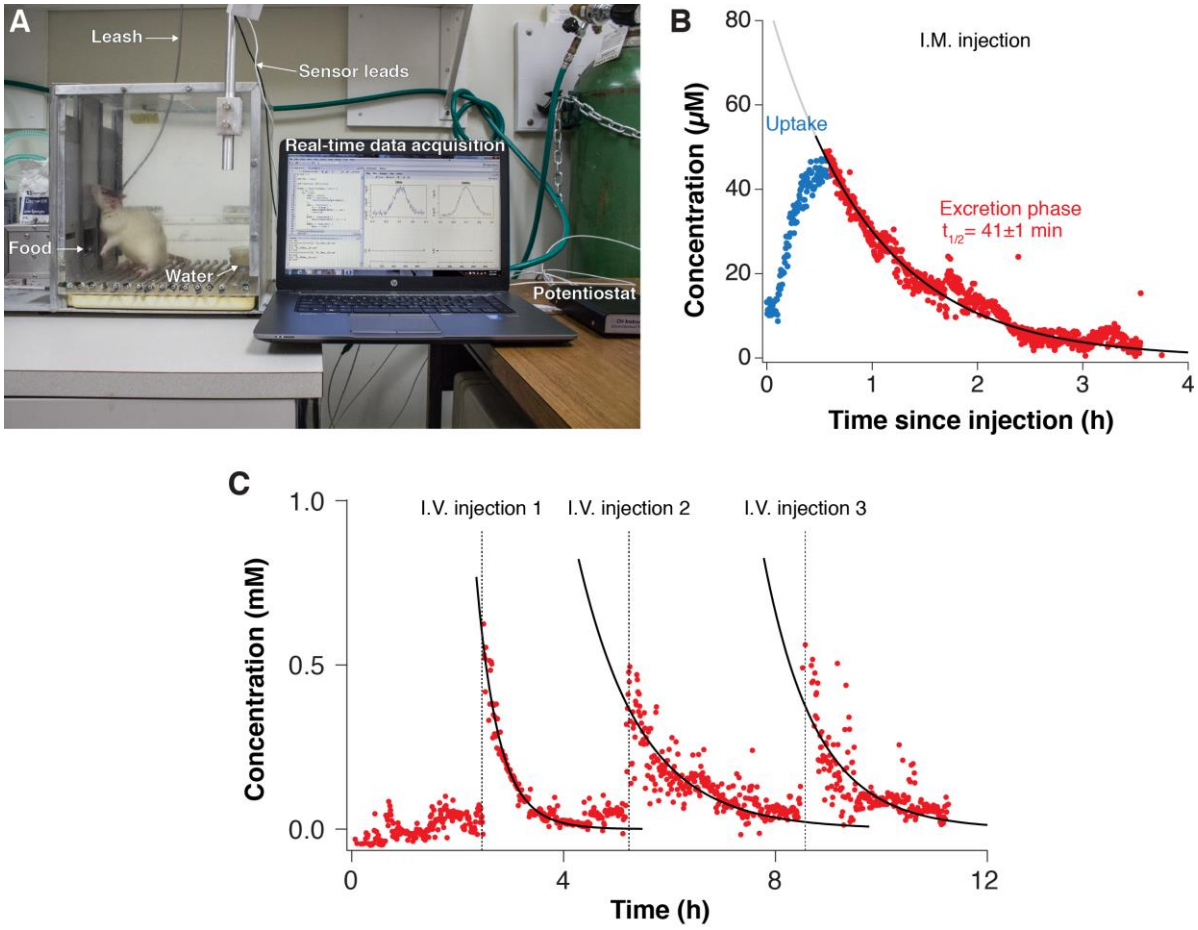

Figure 5.5. Continuous, in vivo molecular measurements on awake, ambulatory animals. (**A**) The small size and physical robustness of E-AB sensors renders it possible to use them in animals as they eat, drink, and explore their cage. This robustness, in turn, enables the measurement of specific molecules in the blood of animals as they undertake their normal daily routine, conditions perhaps more relevant to human health than those traditionally used for the collection of metabolic and pharmacokinetic data. Shown are blood levels of the drug tobramycin after a 25 mg/kg i.m. injection (thigh) (**B**) or sequential 40 mg/kg i.v. (jugular vein) injections (**C**) in awake, freely moving animals.

Here, we demonstrate the ability of E-AB sensors to track specific small molecules continuously and in real time in awake, ambulatory animals, a capability that could provide an important tool for understanding physiology and pharmacology. By allowing arbitrary molecules (limited only by the availability of an aptamer of appropriate specificity and affinity) to be monitored with high resolution in animals undergoing their normal daily routine, for example, the ability to perform such measurements could improve our

knowledge of metabolism, pharmacokinetics, and toxicology. The few-second time resolution of our approach likewise suggests that it could improve our understanding of rapidly fluctuating physiological events, such as uptake and distribution pharmacokinetics, hormone and neurotransmitter release, and the movement of drugs and metabolites across the blood–brain barrier and within the central nervous system. Finally, the ability to perform the measurement of specific molecules in the body in real time could enhance the efficiency and accuracy with which drugs are dosed, in applications ranging from personalized, patient-specific pharmacokinetic measurements as a means of precisely tailoring dosing to long-term feedback-controlled drug delivery in which the dosage of a drug is varied in real time in response to minute-to-minute changes in a patient's physiological status. In short, the technology demonstrated here could enhance not only our understanding of health but also our ability to detect, monitor, and treat disease.

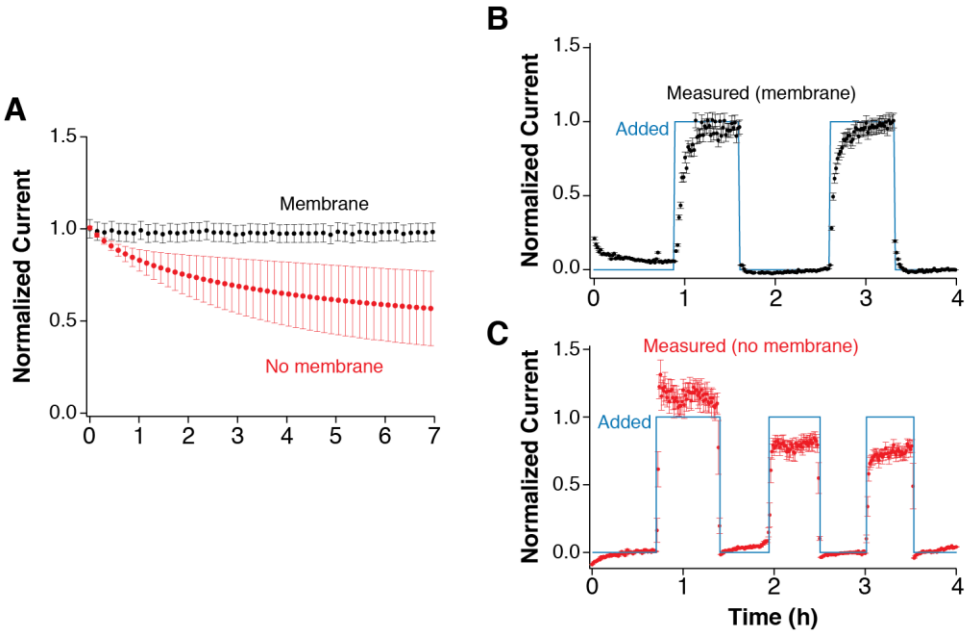

Figure S5.1. Continuous measurements in flowing whole blood *in vitro*. (A) This plot shows a comparison of baseline drift between the membrane-modified platform described in this work (no current change in 6 h) and conventional aminoglycoside E-AB sensors (40% current loss in 6 h). Normalized currents correspond to peak currents from square-wave voltammograms divided by the peak current of the first voltammogram. (**B**) Membrane-protected, KDM-corrected sensors respond identically to two identical injections of 1 mM kanamycin without loss in signal after even hours in flowing whole blood, illustrating the extent to which KDM-corrected sensors remain accurate even under these challenging conditions. Note that the sensor response time is slower in these *in vitro* experiments than in our *in vivo* experiments, likely due to the much slower flow velocities found in this artificial circulatory system than in the actual circulatory system of the rat. (**C**) Membrane-free sensors, in contrast exhibit significant signal decay due to cellular fouling. Errors correspond to the standard deviation observed across 3 independently fabricated sensors.

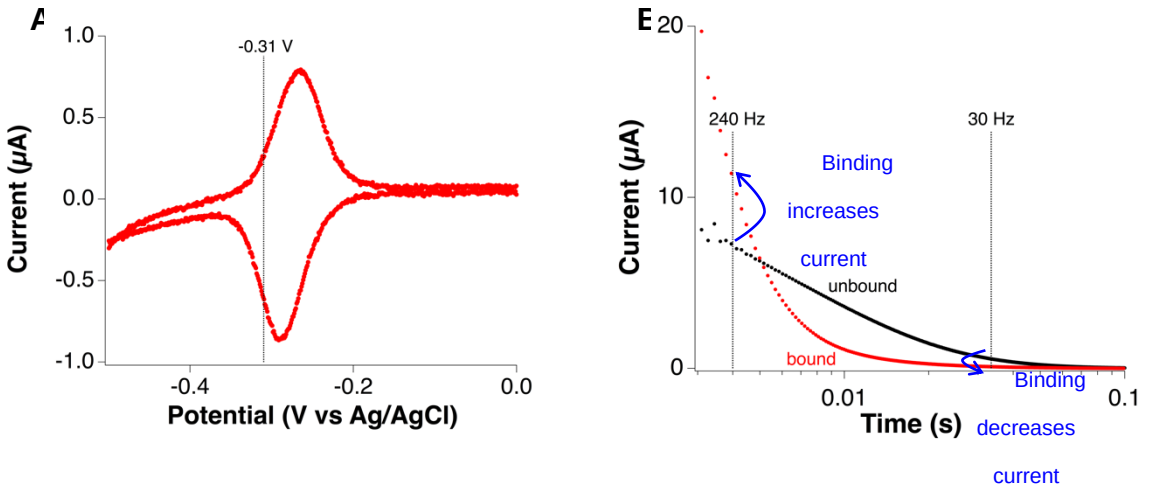

Figure S5.2. Kinetic Differential Measurements exploit the difference in current decay rates between the bound and unbound state of the aptamer. (**A**) Shown is a cyclic voltammogram recorded at 100 mV s^{-1} (negative current for reduction) from an aminoglycoside-detecting E-AB sensor. This voltammogram presents the voltage limits where no current is passing through the working electrode (0.0 V) and where the reduction of methylene blue can be carried out at constant potential (for example, -0.31 V). (**B**) Stepping the potential of this same sensor from 0.0 V to -0.31 V produces chronoamperometric measurements that can be used to illustrate the KDM method. Here, the current-time curves were recorded in the absence and presence of target (1 mM tobramycin), with a sampling rate of one point per millisecond. Because the rates of current decay are different for the two states (i.e., the target-bound aptamer transfers electrons more rapidly than the target-free state), sampling the current 33 ms after the jump (corresponding to a square-wave frequency of 30 Hz) produces a *de*crease in signaling current upon target binding. In contrast, sampling 4.2 ms after the pulse (corresponding to a square wave frequency of 240 Hz) produces a current *increase*.

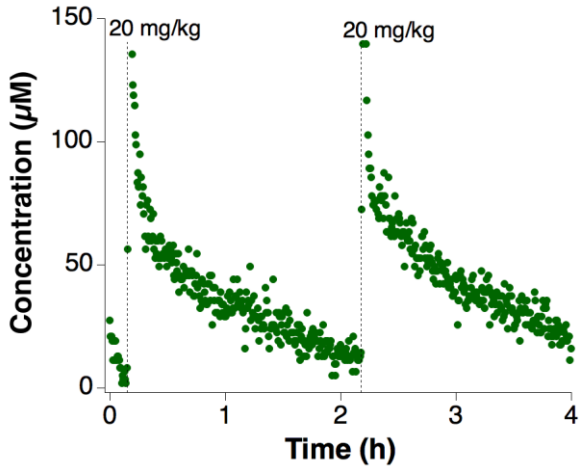

Figure S5.3. Continuous measurement of the antibiotic tobramycin in the bloodstream of an anesthetized rat. Shown are data collected on a living rat given two sequential 20 mg/kg intravenous injections of the drug.

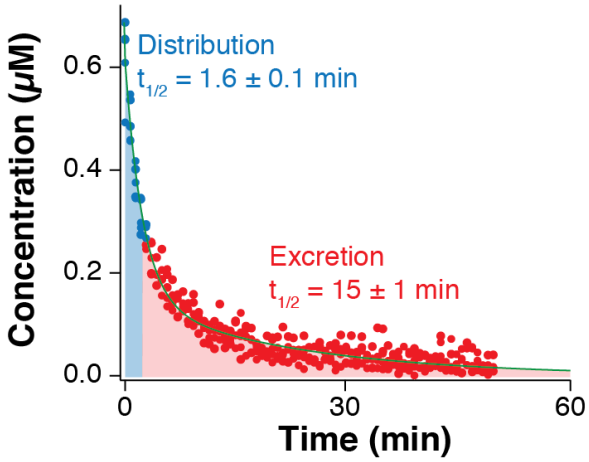

Figure S5.4. Pharmacokinetics of doxorubicin *in vivo*. Shown is an average of five 2 mg/m^2 injections of doxorubicin measured in the jugular vein of a single rat (from **Fig. 5.2A**). The indicated fit is to a two-compartment pharmacokinetic model.

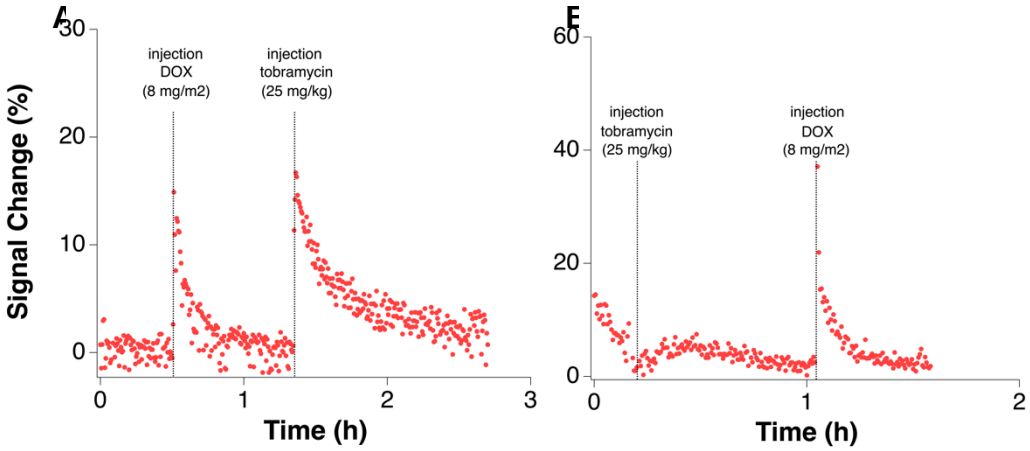

Figure S5.5. Cross-reactivity studies of E-AB sensors deployed in living rats. The specificity of E-AB sensors cannot be greater than that of the aptamers from which they are constructed, and the specificity of aptamers targeting small molecules is sometimes limited. Here we show the response of (**A**) an aminoglycoside-sensing E-AB sensor and (**B**) a DOX-sensing E-AB sensor emplaced in the right jugular veins of rats to serial intravenous injections of 8 mg/m^2 DOX and of 25 mg/kg tobramycin, respectively.

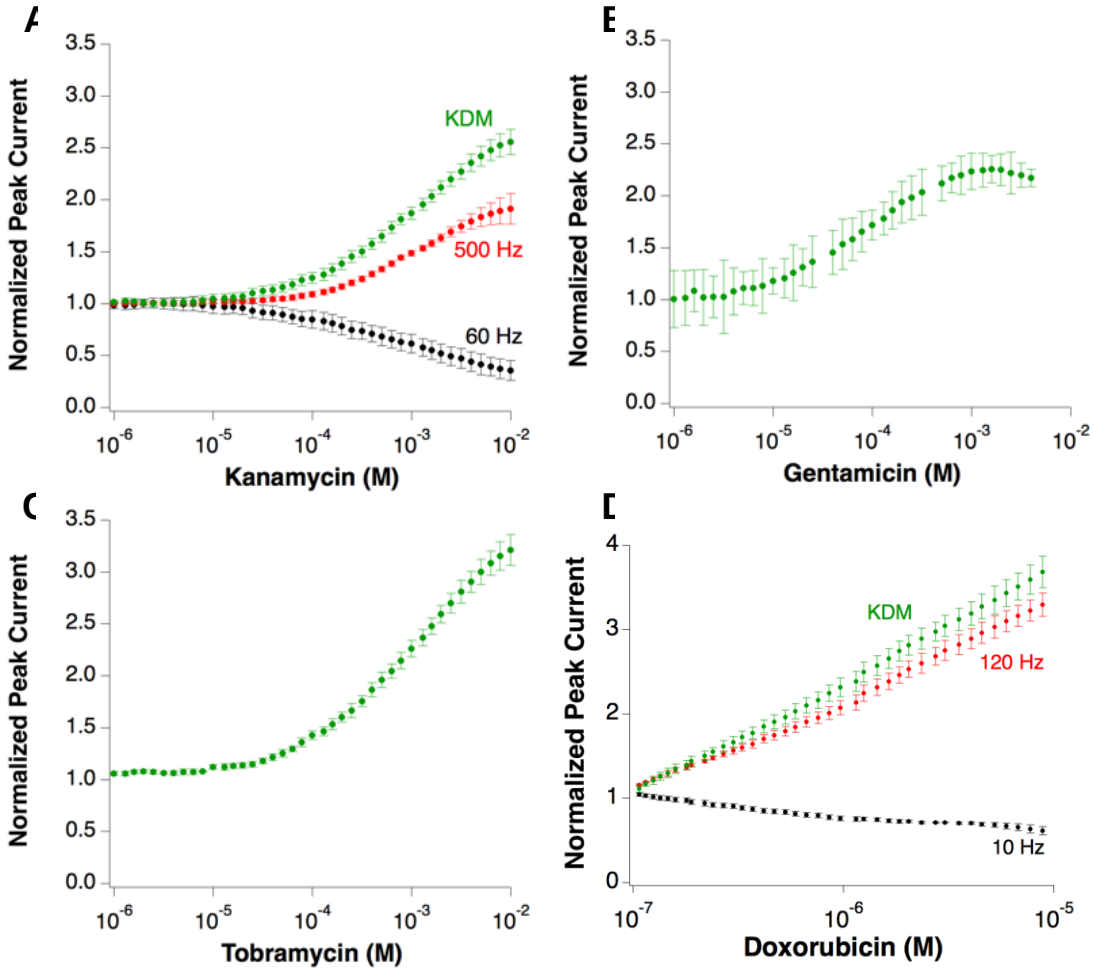

Figure S5.6. Titration curves for aminoglycoside- and doxorubicin-detecting E-AB sensors in flowing whole blood *in vitro*. (**A**) To illustrate the use of KDM with aminoglycoside-detecting sensors we show titration curves for kanamycin (K_d = 800 µM) recorded at 60 Hz and 500 Hz and the KDM-corrected curve that is the difference between the two. (**B, C**) KDM-corrected curves are shown here for gentamicin (K_d = 700 µM) and tobramycin (K_d = 790 µM). (**D**) To illustrate the use of KDM with doxorubicin-specific sensors (K_d = 5 µM) we present titration curves for doxorubicin recorded at 10 Hz and 120 Hz and the KDM-corrected curve that is the difference between the two. In the case of doxorubicin, data was normalized versus a point recorded in the absence of target, hence the small offset observed in the y-axis. Errors correspond to the standard deviations observed across three independently fabricated and tested sensors.

C. Materials and Methods

Chemicals and Materials

Sodium hydroxide, sulfuric acid, tris(hydroxymethyl)aminomethane (Tris), ethylenediaminetetraacetic acid (EDTA), sodium hydrogen phosphate, sodium chloride, potassium chloride, and potassium dihydrogen phosphate were ordered from Fisher Scientific (Waltham, MA). 6-Mercapto-1-hexanol and tris(2-carboxyethyl)phosphine were ordered from Sigma Aldrich (St. Louis, MO). Tobramycin sulfate, gentamycin sulfate, and kanamycin monosulfate were ordered in USP grade from Gold BioTechnology, Inc (St. Louis, MO). Doxorubicin hydrochloride was ordered from LC Laboratories (Woburn, MA). A 1X stock solution of phosphate buffered saline (PBS) was prepared by mixing 8 g of sodium chloride, 0.2 g of potassium chloride, 1.44 g of sodium hydrogen phosphate, and 0.24 g of potassium hydrogen phosphate in 800 mL of distilled water. The pH of this solution was adjusted to 7.4 using hydrochloric acid and the volume was adjusted to 1 L. A 1X stock solution of Tris-EDTA buffer was prepared by mixing 1 ml of 1 M Tris-HCl (pH 8.0) with 0.2 ml EDTA (0.5 M), adjusting the final volume to 100 mL. All chemicals were used as received. Heparinized human and bovine blood for flowing *in vitro* measurements were purchased from Hemostat Laboratories (Dixon, CA).

The E-AB sensors employed here were adapted from previous work.[29,32,33] To fabricate them we ordered the relevant methylene-blue-and-thiol-modified DNA constructs from Biosearch Technologies. The 5' end of each is modified with a thiol on a 6-carbon linker and the 3' end is modified with carboxy-modified methylene blue attached to the DNA via the formation of an amide bond to a primary amine on a 7-carbon linker (Table 1). The length of the surface tethering carbon linker represents a compromise between the two main criteria for electrochemical biosensor applications: stability and electron-transfer efficiency. We selected a 6-carbon linker because it exhibits good stability and improved signaling relative to that seen, for example, when using 11-carbon linkers.[47] The modified DNAs were purified through dual HPLC by the supplier and used as received. Upon receipt each construct was dissolved to 200 μM in 1X Tris-EDTA buffer and frozen at -20 °C in individual aliquots until use.

Table S5.1. DNA aptamer sequences used in this work.

Aptamer	**Sequence**
Doxorubicin	5' – HS- $(CH_2)_6$ – ACCATCTGTGTAAGGGGTAAGGGGTGGT – $(CH_2)_7$ –NH– Methylene Blue – 3'
Aminoglycoside	5' – HS- $(CH_2)_6$ – GGGACTTGGTTTAGGTAATGAGTCCC – $(CH_2)_7$ –NH– Methylene Blue – 3'

Catheters (18G) and 1 mL syringes were purchased from Becton Dickinson (Franklin Lakes, NJ). Silver wire (200 µm diameter) was purchased from Alfa Aesar (Ward Hill, MA); to employ this as a reference electrode it was immersed in bleach overnight to form a silver chloride film. Gold-plated tungsten wire (100 µm diameter) was purchased from GoodFellow (Huntingdon, England). Insulated pure gold and silver wires (100 µm diameter) were purchased from A-M systems. Polyethersulfone membranes (P/N: C02-E20U-05-N) were purchased as MicroKros Filter Modules from Spectrum Laboratories (Rancho Dominguez, CA). The filter modules were cut open and the hollow membranes were extracted from them. Heat-shrink polytetrafluoroethylene insulation (PTFE, HS Sub-Lite-Wall, 0.02, 0.005, 0.003±0.001 in, black-opaque, Lot # 17747112-3) to use on gold-plated tungsten wires was purchased from ZEUS (Branchburg Township, CA).

Sensor Fabrication

Segments of either gold-plated tungsten wire (anesthetized animals) or more malleable pure gold wire (awake animals) 7 cm in length were cut to make sensors. These wires were then insulated by applying heat to shrinkable tubing around the body of the wires, as depicted in **Fig. 5.1B**. The sensor window (i.e., the region without insulation) was approximately 5-8 mm in length. To increase surface area of these working electrodes (to obtain larger peak currents) the sensor surface was roughened electrochemically via immersion in 0.5 M sulfuric acid followed by jumping between $E_{initial}$ = 0.0 V to E_{high} = 2.0 V vs Ag/AgCl, back and forth, for 100,000 pulses. Each pulse was of 2 ms duration with no "quiet time."

To fabricate sensors an aliquot of the appropriate DNA construct was thawed and then reduced for 1 h at room temperature with a 1000-fold molar excess of tris(2-carboxyethyl)phosphine. A freshly roughened gold electrode was then rinsed in di-ionized water before being immersed in a solution of the appropriate reduced DNA construct at 200-500 nM in PBS for 1 h at room temperature. Following this the sensor was inserted into hollow polysulfone fibers 1.5 cm in length and 200 µm in diameter. The membranes were mechanically attached to the sensors by wrapping the edges with parafilm™. After attaching the membranes, the sensors were immersed overnight at 4°C for 12 h in 20 mM 6-mercapto-1-hexanol in PBS to coat the remaining gold surface and remove nonspecifically adsorbed DNA. After this the sensors were rinsed with di-ionized water and stored in PBS.

Electrochemical Methods and Data Processing

For all sensing experiments, the sensors were interrogated using square wave voltammetry from 0.0 V to -0.5 V vs. Ag/AgCl, using an amplitude of 50 mV, potential step sizes of 1-5 mV, and varying frequencies from 10 Hz to 500 Hz. The files corresponding to each voltammogram were recorded in serial order using macros in CH Instruments software. The post-experiment analysis of results was carried out using a script coded in Igor Pro 7 (SI Appendix, p.13).

All *in vitro* measurements were performed using a three-electrode setup and with a CH Instruments electrochemical workstation (Austin, TX, Model 660D) using commercial Ag/AgCl reference electrodes filled with saturated KCl solution and platinum counter electrodes.

All *in vivo* measurements were performed using a two-electrode setup in which the reference and counter electrodes were a silver wire coated with a silver chloride film as described above. The measurements carried out *in vivo* were recorded using a handheld potentiostat from CH Instruments (Model 1242 B).

In vitro Experiments

To measure aptamer affinity and correlate signal gain to target concentration, sensors were interrogated by square-wave voltammetry first in flowing PBS and next in flowing heparinized human or bovine blood with increasing concentrations of the corresponding target. These experiments were carried out in a closed flow system intended to mimic the type of blood transport found in veins. Blood flow was achieved using a magnetic gear pump (Benchtop Analog Drive, 0.261 mL/rev) from Cole Parmer (Vernon Hills, IL), setting flow rates to 1-4 mL min^{-1} as measured by a flow meter. To construct the binding curves (titrations of aptamer with target), stock solutions of each target molecule were prepared fresh prior to measurements in PBS buffer or blood, respectively. Examples of typical binding curves are provided (**Fig. S5.6)**.

In vivo Experiments

Animals. Adult male Sprague-Dawley rats (300-500 g; Charles River Laboratories, Wilmington, MA, USA) were pair housed in a temperature and humidity controlled vivarium on a 12-h light-dark cycle and provided *ad libitum* access to food and water. All animal procedures were consistent with the guidelines of the NIH *Guide for Care and Use of Laboratory Animals* and approved by the Institutional Animal Care and Use Committee of the University of California Santa Barbara.

Surgery. For the anesthetized preparation, rats were anesthetized using isoflurane gas inhalation (2.5%) and monitored throughout the experiment using a pulse oximeter (Nonin Medical, Plymouth, MN) to measure heart rate and %SpO2 to insure depth of anesthesia. After exposing both ventral jugular veins, a simple catheter made from a SILASTIC tube (Dow Corning, Midland, MI, USA) fitted with a steel cannula (Plastics One, Roanoke, VA, USA) was implanted into the left jugular vein. 0.1-0.3 mL of heparin (1000U/mL, SAGENT Pharmaceuticals, Schaumburg, IL, USA) were immediately infused through the catheter to prevent blood clotting. The sensor was inserted into the right jugular vein and secured in place with surgical suture. Following drug infusions (see below), animals were euthanized by overdose on isoflurane.

For the awake preparation, rats were anesthetized (as above) and then mounted on a stereotaxic apparatus (David Kopf Instruments, Tujunga, CA, USA) with a gas anesthesia head holder to maintain anesthesia. After a subcutaneous injection of an analgesic (1mg/kg Flunixiject, Henry Schein Animal Health, Dublin, OH, USA), a midline incision was made along the dorsal surface of the scalp and a second incision was made on the ventral portion of the neck above the jugular vein. Using a similar catheter construction described above, we implanted the catheter tube into the right jugular vein and sutured it in place before sealing the wound with skin glue. The surface of the skull was then exposed and 4 screws were drilled into the bone to provide a platform for the cannula to be cemented to the head. Dental cement was applied to the skull surface while the cannula was held in place using the stereotaxic arm. After the cement had set, the catheter was flushed with antibiotics (1 mg/kg

gentamicin Henry Schein Inc., Dublin, OH, USA and 1 mg/kg cefazolin, WG CriticalCare, Paramus, NJ, USA) and the animal was monitored for postoperative recovery before being returned to the vivarium colony. Daily monitoring of weight and condition of recovery followed for 4 days in which the animal was treated with analgesic (as above) and observed for signs of distress/wound inflammation. No further procedures were carried out on these animals for a minimum of one week.

Measurements. A 30 min sensor baseline was established before the first drug infusion. For anesthetized animals a 3 mL syringe filled with the target drug was connected to the sensor-free catheter (placed in the jugular opposite that in which the sensor is emplaced) and placed in a motorized syringe pump (KDS 200, KD Scientific Inc., Holliston, MA, USA). After establishing a stable baseline, the target drug was infused through this catheter at a rate of 0.2 mL/min. Target drugs included kanamycin (0.1 M solution; homemade), gentamicin (10 mg/mL, Henry Schein Inc., Dublin, OH, USA), tobramycin (0.1 M solution; homemade), and doxorubicin (1.0 mM, homemade). After drug infusion, recordings were taken for up to 2 h before the next infusion. The real-time plotting and analysis of voltammetric data were carried out with the help of a script written in R Studio.

For the awake preparation, a pre-catheterized animal was first briefly anesthetized (as above). The sensor was threaded down the catheter and tightly attached to it via a homemade plastic joint. The joint protects the sensor from being accidentally pulled out by the animal while exploring his surroundings. Once implanted, the E-AB sensor was affixed to a leash in an operant chamber (Med Associates Inc., Fairfield, VT, USA). The animal was then allowed to recover from anesthesia and explore the chamber while recordings proceeded as described above. Following the baseline recording, the target drug was introduced via either an intramuscular injection (thigh) or via an intravenous injection given through the same catheter used to emplace the sensor.

Acknowledgments

These studies were supported by a grant from the W. M. Keck Foundation, and by the Institute for Collaborative Biotechnologies through grant W911NF-09-0001 from the U.S. Army Research Office. The content of the information does not necessarily reflect the position or the policy of the Government, and no official endorsement should be inferred. J.S. is supported by the National Cancer Institute of the National Institutes of Health (NRSA F31CA183385). N.A.C. is supported by the Otis Williams Postdoctoral Fellowship of the Santa Barbara Foundation. The authors thank Yanxian Lin for the code used in real-time data tracking, and Dr. Martin Kurnik for providing the cartoon of a DNA strand used in Figure 5.1A.

D. References

1. Thakur MD, et al. (2013) Modelling vemurafenib resistance in melanoma reveals a strategy to forestall drug resistance. *Nature* 494(7436):251–255.
2. Renard E (2008) Implantable continuous glucose sensors. *Curr Diab Rev* 4(3):169-74.

3. Ward WK, House JL, Birck J, Anderson EM, Jansen LB (2004) A wire-based dual-analyte sensor for glucose and lactate: in vitro and in vivo evaluation. *Diabetes Technol The* 6(3):389–401.

4. Kraft JC, Osterhaus GL, Ortiz AN, Garris PA, Johnson MA (2009) In vivo dopamine release and uptake impairments in rats treated with 3-nitropropionic acid. Neuroscience. 161, 940–949.

5. Chergui K, Suaud-Chagny MF, Gonon F (1994) Nonlinear relationship between impulse flow, dopamine release and dopamine elimination in the rat brainin vivo. *Neuroscience*. 62(3), 641–645.

6. Zhang J, et al. (2013) In vivo monitoring of serotonin in the striatum of freely moving rats with one minute temporal resolution by online microdialysis–capillary high-performance liquid chromatography at elevated temperature and pressure. *Anal Chem* 85(20):9889–9897.

7. Wassum KM, et al. (2012) Transient extracellular glutamate events in the basolateral amygdala track reward-seeking actions. *J Neurosci* 32(8):2734–2746.

8. Sarter M, Kim Y (2015) Interpreting chemical neurotransmission in vivo: techniques, time scales, and theories. *ACS Chem Neurosci* 6(1):8–10

9. Gaster RS, et al (2009) Matrix-insensitive protein assays push the limits of biosensors in medicine. *Nat Med* 15(11):1327–1332

10. Plaxco KW, Soh HT (2011) Switch based biosensors: a new approach towards real-time, in vivo molecular detection. *Trends Biotechnol* 29(1):1–5.

[1]1. Couture M, Zhao SS, Masson J-F (2013) Modern surface plasmon resonance for bioanalytics and biophysics. *Phys Chem Chem Phys* 15(27):11190–11216.

[1]2. Thompson M, Sheikh S, Blaszykowski C (2014) A perspective on the application of biosensor and lab- on-a-chip technologies to biomarker detection in biological fluids. *Austin J Nanomed Nanotechnol* 2(1):1009.

13. Vaisocherová H, Brynda E, Homola J (2015) Functionalizable low-fouling coatings for label-free biosensing in complex biological media: advances and applications. *Anal Bioanal Chem* 407(14):3927–3953.

[1]4. Breault-Turcot J, Masson J-F (2015) Microdialysis SPR: diffusion-gated sensing in blood. *Chem Sci* 6(7):4247–4254.

15. Xiao Y, Lubin AA, Heeger AJ, Plaxco KW (2005) Label-free electronic detection of thrombin in blood serum by using an aptamer-based sensor. *Angew Chem* 117(34):5592-5595.

16. Wilson DS, Szostak JW (1999) In Vitro Selection of Functional Nucleic Acids. *Annu. Rev. Biochem.* 68, 611–647.

17. Gotrik MR, Feagin TA, Csordas AT, Nakamoto MA, Soh HT (2016) Advancements in Aptamer Discovery Technologies. *Acc. Chem. Res.* 49 (9), 1903–1910.

18. Hermann T, Patel DJ (2000) Adaptive recognition by nucleic acid aptamers. *Science* 287(5454):820–825.

19. White RJ, Plaxco KW (2010) Exploiting binding-induced changes in probe flexibility for the optimization of electrochemical biosensors. *Anal Chem* 82(1):73–76.

20. Porchetta A, Vallée-Bélisle A, Plaxco KW, Ricci F (2012) Using distal site mutations and allosteric inhibition to tune, extend and narrow the useful dynamic range of aptamer-based sensors. *J. Am. Chem. Soc.*, 134(51), 20601-20604.

21. Schoukroun-Barnes LR, Glaser EP, White RJ (2015) Heterogeneous Electrochemical Aptamer-Based Sensor Surfaces for Controlled Sensor Response. *Langmuir* 31(23):6563–6569.

22. Simon A, Vallée-Bélisle A, Ricci F, Plaxco KW (2014) Intrinsic disorder as a generalizable strategy for the rational design of highly responsive, allosterically cooperative receptors. *Proc. Nat. Acad. Sci. USA*, 111(42), 15048–15053.

23. Baker BR, et al. (2006) An Electronic, Aptamer-Based Small-Molecule Sensor for the Rapid, Label-Free Detection of Cocaine in Adulterated Samples and Biological Fluids. *J Am Chem Soc* 128(10):3138–3139.

24. Bard AJ, Faulkner LR (2001) Chapter 7. Electrochemical Methods: Fundamentals and Applications, 2nd Ed., (Wiley, New York).

25. Swensen JS, et al. (2009) Continuous, real-time monitoring of cocaine in undiluted blood serum via a microfluidic, electrochemical aptamer-based sensor. *J Am Chem Soc* 131(12):4262–4266.

26. Ferguson BS, et al. (2013) Real-time, aptamer-based tracking of circulating therapeutic agents in living animals. *Science Transl Med* 5(213):213ra165–213ra165.

27. Dahe GJ, et al. (2011) In vivo evaluation of the biocompatibility of surface modified hemodialysis polysulfone hollow fibers in rat. *PLoS ONE* 6(10):e25236.

28. Lavigne JJ, Anslyn EV (2001) Sensing a paradigm shift in the field of molecular recognition: from selective to differential receptors. *Angew Chem Int Edit* 40(17):3118–3130.

29. Wochner A, et al. (2008) A DNA aptamer with high affinity and specificity for therapeutic anthracyclines. *Anal Biochem* 373(1):34–42.

30. Tacar O, Sriamornsak P, Dass CR (2013) Doxorubicin: an update on anticancer molecular action, toxicity and novel drug delivery systems. *J Pharm Pharmacol* 65(2):157–170.

31. Ahmed S, et al. (2009) Selective determination of doxorubicin and doxorubicinol in rat plasma by HPLC with photosensitization reaction followed by chemiluminescence detection. *Talanta* 78(1):94–100.

32. Rowe AA, Miller EA, Plaxco KW (2010) Reagentless measurement of aminoglycoside antibiotics in blood serum via an electrochemical, ribonucleic acid aptamer-based biosensor. *Anal Chem* 82(17):7090–7095.

33. Wang Y, Rando RR (1995) Specific binding of aminoglycoside antibiotics to RNA. *Chem Biol* 2(5):281–290.

34. Centers for Disease Control and Prevention (CDC) (2003) Treatment of tuberculosis. *MMWR Morb Mortal Wkly Rep* 52(RR-11):27-28.

35. Boothe DB The Merck Veterinary Manual, Aminoglycosides (2015), (http://www.merckvetmanual.com/mvm/pharmacology/antibacterial_agents/aminoglycosides.html). [the easiest access to this source is by Internet].

36. Lashev LD, Pashov DA, Marinkov TN (1992) Interspecies differences in the pharmacokinetics of kanamycin and apramycin. *Vet Res Comm* 16(4):293–300.

37. Reinhard M. K., et al. (1994) Effects of polyaspartic acid on pharmacokinetics of tobramycin in two strains of rat. *Antimicrob Agents Chemother*. 38(1): 79–82.

38. Lin L, et al. (1994) Temporal changes of pharmacokinetics, nephrotoxicity, and subcellular distribution of tobramycin in rats. *Antimicrob Agents Chemother* 38(1):54–60.

39. Marre R, Tarara N, Louton T, Sack K (1980) Age-dependent nephrotoxicity and the pharmacokinetics of gentamicin in rats. *Eur J Pediatr*. 133, 25–29.

40. Matsuzaki M, et al. (1975) Studies on the toxicity of amikacin (BB-K 8). II. Chronic toxicity in rats. *Jpn J Antibiot* 28(4):435–457.

41. Matsumoto H, Ochiai K, Nakajima A, Matsuzaki M (1982) Absorption, excretion and distribution of amikacin following drip intravenous infusion, one shot intravenous injection and intramuscular administration of amikacin in dogs, rabbits and rats. *Jpn J Antibiot* 35(8):2034–2046

42. Kato K, Wakai J, Ozawa K, Sekiguchi M, Katahira K (2016) Different sensitivity to the suppressive effects of isoflurane anesthesia on cardiorespiratory function in SHR/Izm, WKY/Izm, and Crl:CD(SD) rats. *Exp Anim*

43. Álvarez-Martos I, Ferapontova EE (2016) Electrochemical Label-Free Aptasensor for Specific Analysis of Dopamine in Serum in the Presence of Structurally Related Neurotransmitters. *Anal. Chem*. 88(7), 3608–3616.

44. Ferapontova EE, Olsen EM, Gothelf KV (2008) An RNA Aptamer-Based Electrochemical Biosensor for Detection of Theophylline in Serum. *J. Am. Chem. Soc.* 130(13), 4256–4258.

45. Hansen DK, Davies MI, Lunte SM, Lunte CE (1999) Pharmacokinetic and Metabolism Studies Using Microdialysis Sampling. *J Pharm Sci*. 88(1), 14–27.

46. Hensley ML, et al. (1999) American Society of Clinical Oncology: Clinical Practice Guidelines for the Use of Chemotherapy and Radiotherapy Protectants. *JCO* 17(10):3333–3355.

47. Lai RY, Seferos DS, Heeger AJ, Bazan GC, Plaxco KW (2006) Comparison of the Signaling and Stability of Electrochemical DNA Sensors Fabricated from 6- or 11-Carbon Self-Assembled Monolayers. *Langmuir*. 22(25): 10796–10800.

VI. A "Clinical Watchdog" for Physiological Proteins: Real-Time *in vivo* Assurance of Subcritical Growth Factor Serum Levels[5]

Abstract:

Hundreds of protein biomarkers and many "biological" (protein therapeutics) are FDA approved for the diagnosis, monitoring and treatment of disease. Present techniques to monitor the levels of these circulating proteins are cumbersome, laboratory-based techniques, which only measure a *single timepoint* during therapy. In contrast, we describe here an implantable electrochemical aptamer-based sensor for the continuous, *in vivo* measurement of circulating platelet-derived growth factor. We use the remarkably stable interaction between the sensor and target to assess and optimize signal stability directly in the blood stream of a living rat.

A. Introduction

The number of disease-diagnostic protein "biomarkers" continues to grow, with a survey of FDA approvals for protein-based assays through 2008 alone finding more than 200 unique protein targets circulating in plasma or serum [1]. A few of the examples discovered to date reporting on heart failure, rheumatic disease, cancers and overactive immune responses [1]. Even the routine analysis of these biomarkers, however, remains challenging as existing methods for the detection of specific proteins are limited to analyzing individual blood draws (i.e., single timepoint "snapshots") most often via laboratory-based technologies that require hours-to-days to return actionable information to healthcare providers [2]. In

[5] This chapter in preparation for publication (with Chapter IV) as **J. Somerson**, N. Arroyo-Currás, G. Ortega, K. Ploense, H. Li, T. Kippin and K.W. Plaxco, "Nanomolar *in vivo* and calibration-free *in vitro* measurement of a circulating protein"**.**

contrast, were a technology available that could support the high-frequency measurement of such biomarkers in real-time and in situ in the living body it would be possible to continuously monitor many critical health states.

Real-time protein monitoring can provide a valuable tool for diagnosing diseases, observing disease progression and response to therapy and monitoring when spikes in circulating proteins might indicate dangerous events. For example, a massive upregulation of proinflammatory cytokines in response to an immune event (a “cytokine storm”) can cause harmful and even fatal inflammation [7–9]. An acute myocardial infarction is often accompanied by a large increases in plasma levels of the cardiac troponins; elevation of circulating cardiac troponin above the 99th percentile is sufficient for diagnosis of acute myocardial infarction [10]. Circulating proteins also provide diagnostic and prognostic information in the diagnosis and treatment of multiple cancers [3–6]. Current approaches to measuring such markers, however, are all single-time-point laboratory-based assays or qualitative, point-of-care dipsticks. The availability of a technology that, in contrast, provides real-time quantitative information regarding the levels of these biomarkers could provide valuable rapid diagnostic feedback and could even serve to provide timely, early warning alerts upon diagnostically relevant concentration spikes.

Motivated by the value to be added by platforms capable of continuously monitoring the levels of specific biomarkers in situ in the body, we aim to expand the in vivo success of electrochemical aptamer-based sensors to the larger challenge of in vivo protein measurement. Electrochemical aptamer-based sensors (E-AB sensors) couple the specificity of precise biological recognition with the quantitative and selective readout of electrochemical measurement. These sensors use aptamers, short nucleic acid strands selected in vitro to sensitively and specifically bind an arbitrary target of interest [11]. E-AB

sensors bind these aptamers to an electrode surface and append an electrochemically-active tag distal from the electrode. Binding of the target to the aptamer changes the conformation of the sensor molecule, creating a quantitative change in electrode signal linked to the concentration of target present [12]. Critically, because the electrochemical signal is limited to a narrow potential window, there are very few electrochemically-active interfering species, enabling the deployment of these sensors into complex media, such as blood serum [13,14], and even in vivo into living systems [15] where they continue to provide quantitative, continuous measurement of an analyte of choice. For example, we have previously used E-AB sensors to perform the real-time monitoring of several small molecule drugs in situ in the bodies of awake, freely-moving rats [15]. Here, we use the previously-described E-AB sensor against the BB isoform of the human platelet-derived growth factor [16]. This sensor consists of an aptamer against this protein bound through a thiol linker on its 5' end to an electrode surface and displaying a methylene blue electrochemical tag on its 3' end (**Fig. 6.1**). Using this sensor, here we describe the first use of an E-AB sensor to monitor rising levels of a protein biomarker directly in the bloodstream of a living animal.

Monitoring protein targets in-vivo provides new challenges relative to our past work with the E-AB platform, which, for in-vivo studies, had focused entirely on the detection of small-molecule drugs. First, the concentrations of typical protein biomarkers in blood are much lower than the clinically relevant concentrations of small molecule drugs – tens of nanomolar as opposed to the tens-to-hundreds of micromolar [15]. Protein targets can also confound anti-fouling techniques, which rely on interfering with the approach of blood proteins to the electrode surfaces. Previous work with E-AB sensors either in vivo or immediately ex vivo have used microdialysis membranes [15] and buffer diffusion layers [17] to help to reduce the drift associated with fouling of the electrode surfaces. For this

study, it is essential to allow protein to diffuse to the sensor surface and so this proves a more rigorous study of in vivo sensor stability. An additional challenge for protein-detecting sensors is the extremely slow off-rates associated with dissociation of these targets from their aptamer receptors. The PDGF sensor, for example, which is the test bed I employed in these studies, exhibits stable signal for hours even after the protein target is completely removed from the measured solution (**Fig. 6.2**). While this is a challenge for real-time measurement, we can still find great value as a clinical sensor and as a way to improve our sensor platform. Specifically many biomarker targets cause concern when their levels rapidly rise, as in the example of cytokine storms [8]. While real-time knowledge of absolute serum concentration would be of value, the understanding that a spike in protein concentration has happened or continues to occur provides the most important diagnostic information.

Beyond the clinical utility of an implantable device to continuously monitor for protein concentration spikes, this tightly-binding sensor can also provide valuable information towards improving the E-AB sensor platform. Specifically , this signal stability proves an excellent opportunity to examine the noise observed within in vivo measurements and deconvolute the noise inherent to our sensor system from the physical noise exhibited in the metabolism of the target. Because we know that this signal should remain stable for hours after a spike in protein concentration, we can use this system to more rigorously compare the stability and reproducibility of multiple drift-correction strategies. In this work, we compare two previously-described drift-correction strategies and describe for the first time a new drift-correction strategy that uses the inherent biomolecular kinetics of our sensor molecule to create self-correcting signals.

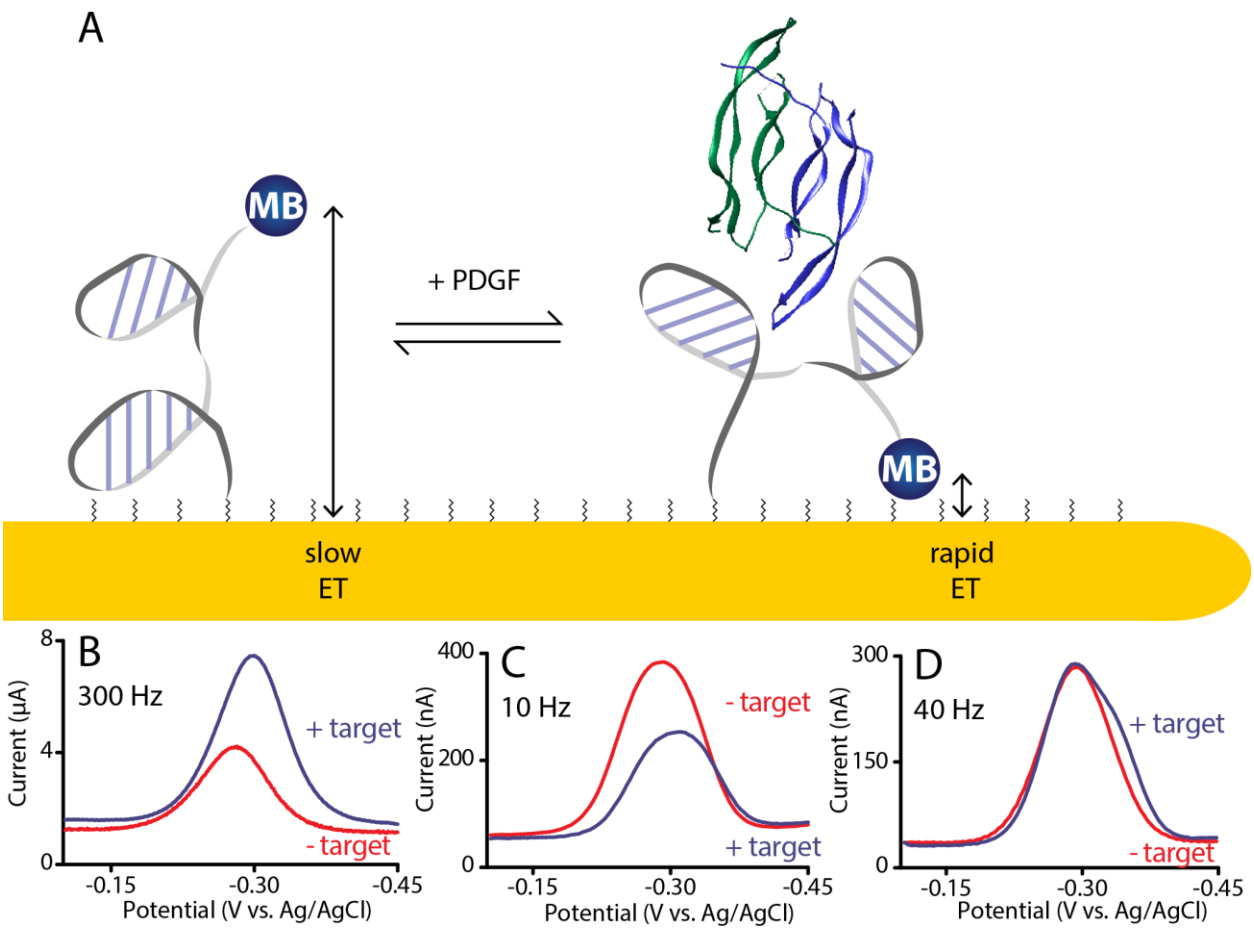

Figure 6.1. (**A**) Binding of the protein target to an electrochemical aptamer-based (E-AB) sensor alters the conformation of the electrode-bound aptamer, changing the accessibility of an attached methylene blue redox reporter (blue circle). This, in turn, results in a change in electron transfer kinetics. Monitoring electron transfer kinetics using square wave voltammetry, we see a quantitative change in peak current in response to target binding. By changing the frequency of the square wave measurement (i.e., changing the timescale of the measurement) we can obtain either (**B**) "signal-on" responses (here at high frequencies), in which peak current increases in the presence of target, (**C**) "signal-off" response (here at low frequencies, in which the peak current decreases in the presence of target, or (**D**) nonresponsive behavior (at intermediate frequencies), in which the peak current does not change in the presence of target. Using these alternative behaviors we have developed a number of means of providing drift correction to the E-AB platform.

B. Results and Discussion

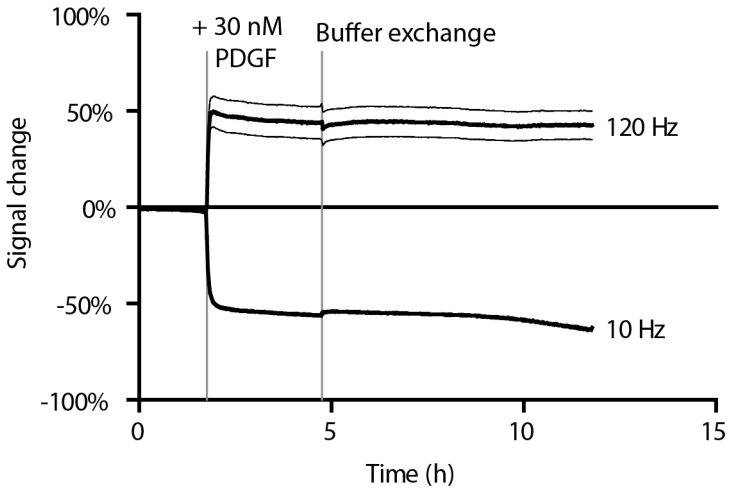

Figure 6.2. The PDGF E-AB sensor rapidly responds to increasing target concentration (first gray line). In contrast, its re-equilibration after the removal of target (second gray line) is very slow. Shown are the average signal change (dark trace) and standard error (light trace) for seven replicate electrodes in flowing buffer. The standard error for the 10 Hz measurement is obscured by the data.

We used the stability of the PDGF sensor signal to compare two previously-reported methods of drift correction and one new technique. The first, kinetic differential measurement (KDM), was first described by Ferguson et al. [17]. The second, calibration-free measurement, was first described by Li et al. [18]. And the third, ratiometric measurement, is describe d here for the first time. Each of these techniques relies on exploiting the kinetic sensitivity of square wave measurements to obtain "signal-on" measurements and either "signal-off" or nonresponsive measurements from the same population of bound sensor molecules [19]. We compare the relative stability of each of these calculations directly in vivo in the same animals (**Fig. 6.5**) and the reproducibility of these measurements between three rats given the same injected dosage (**Fig. 6.6**).

Kinetic differential measurement relies on subtractive drift correction (**Fig. 6.3**). That is, this approach employs a pair frequencies that differ in signal gain upon target binding but

drift in unison. Here I have employed a signal-on frequency (300 Hz) and a nonresponsive frequency (40 Hz), which both drift in concert when the sensor is deployed in vivo in the jugular of a live rat (**Fig. 6.3A**). KDM calculations, rather than using the raw measured electrochemical currents, normalize measured current to an observed baseline and use this normalized, proportional signal change (**Fig. 6.3B**). KDM takes the difference between these normalized responses to reduce signal drift (**Fig. 6.3C**). Using the standard Langmuir isotherm relationship between KDM-corrected signal and protein concentration allows for the calculation of protein concentrations (**Fig. 6.3D**).

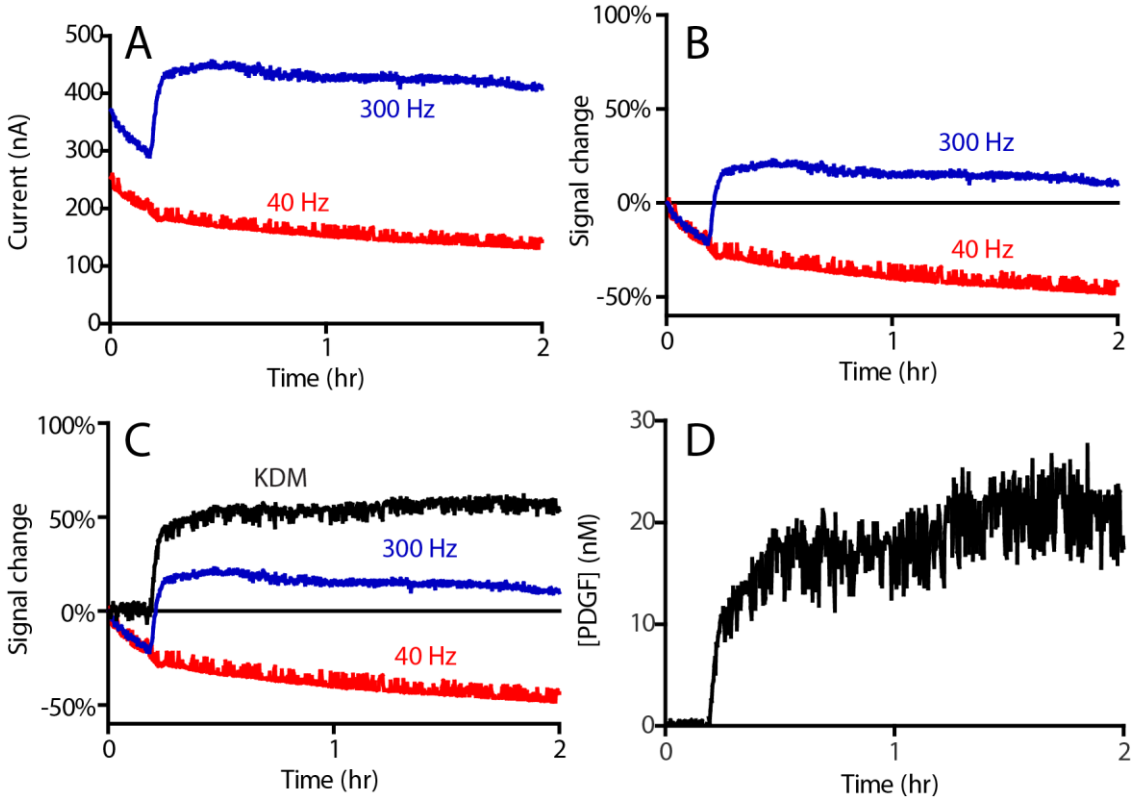

Figure 6.3. KDM uses subtractive correction to correct signal drift. (**A**) The raw *in vivo* current drifts, but signal persists. We use 300 Hz as a signal-on frequency and 40 Hz as a nonresponsive frequency. (**B**) KDM normalizes each of these frequencies to "signal change" – the proportion of the current to initial current. (**C**) Subtracting these two frequencies that drift in concert creates a flatter, more stable signal (KDM). (**D**) We use the previously measured relationship between KDM signal change and protein concentration to calculate the *in vivo* concentration of PDGF.

In contrast to KDM, which is a differential measurement, ratiometric and calibration-free measurements use the *ratios* of signaling currents to reduce drift (**Fig. 6.4**). Calibration-free measurement, explained in more detail in **Chapter IV**, uses a training set of sensors to find a global fit for three constants: the ratio between the signal-on current in the absence of target and the nonresponsive current (α), the ratio between the saturated signal-on current and the signal-on current in the absence of target (γ) and the standard binding constant K_D (**Fig. 6.4C**). Calibration-free measurement uses the relationship between the measured currents and these previously obtained constants to calculate protein concentrations (**Fig. 6.4D**). Ratiometric measurement calculates the concentration similarly, but with the new understanding that α, the ratio between the signal-on current in the absence of target and the nonresponsive current, varies from one in-vivo placement to the next. Ratiometric measurement uses similar ratiometric calculations of the raw observed currents (**Fig. 6.4B**) but instead of using a previously calculated baseline current ratio (α), ratiometric measurement uses the observed ratio between the initial currents *at the time of measurement* to create a more realistic baseline. Using this ratio instead of the pre-determined ratio provides accurate *in-vivo* concentrations (**Fig. 6.4D**).

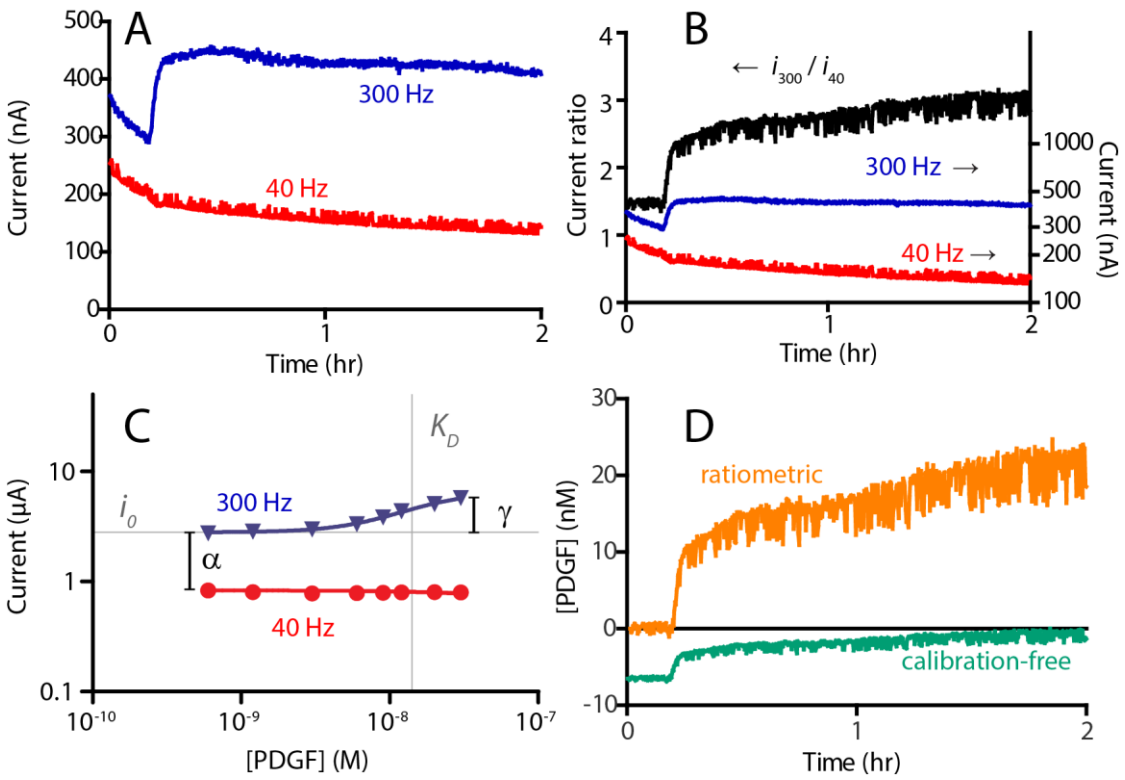

Figure 6.4. Calibration-free and ratiometric measurements are calculated from the ratio of signals obtained at a signal-on frequency (here 300 Hz) and a nonresponsive frequency (here 40 Hz). (**A**) Raw currents exhibit signal drift over the course of an *in vivo* experiment. (**B**) The ratio between these two currents (black) corrects some of the exhibited drifts. (**C**) The previously measured relationship between the signal-on and nonresponsive frequency and the concentration of PDGF produce constants α, the ratio between baseline signal-on current and nonresponsive current, γ, the ratio between baseline signal-on current and saturated signal-on current and K_D, the binding constant of these sensors. (**D**) Calibration-free measurements (green) use the constants measured previously to calculate an expected concentration from these *in vivo* measurements. Ratiometric measurements (orange) use the gain (γ) and the binding constant (K_D) to calculate an observed concentration but use the observed ratio between the measurement frequencies as a baseline rather than the previously measured constants.

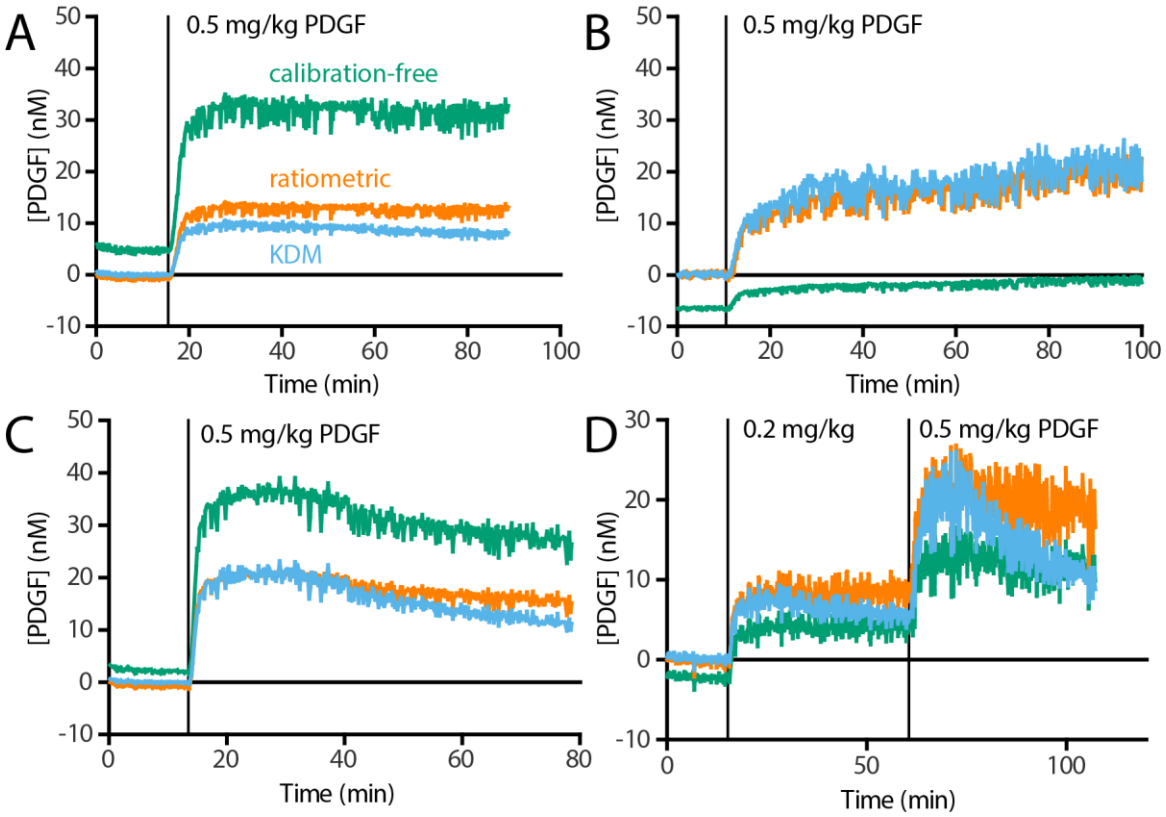

Figure 6.5. Spiking in-vivo PDGF levels are easily identified. Shown are data from four different rats, three rats (**A-C**) have one intravenous injection of 0.5 mg/kg PDGF and one rat (**D**) has two injections – one injection of 0.2 mg/kg PDGF followed by another of 0.5 mg/kg PDGF, showing our ability to measure increasing doses. Three different calculated concentrations from the same sensor are shown: KDM-calculated concentrations (light blue), calibration-free-calculated concentrations (green) and ratiometric-calculated concentrations (orange).

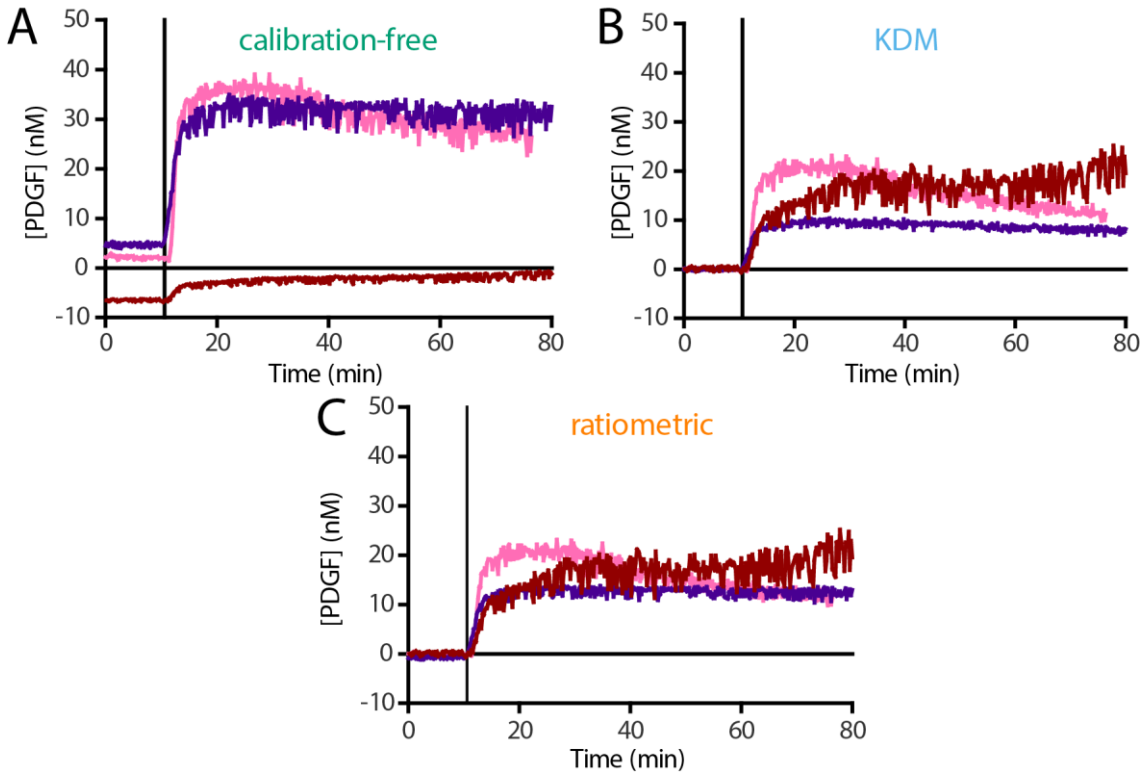

Figure 6.6. When comparing rat-to-rat *in vivo* measurement variation by calculation technique, we find reasonable agreement between KDM-calculated measurements and ratiometric-calculated measurements. Each color represents an individual rat, all are given the same dose of PDGF (0.5 mg/kg intravenous injection). The ratiometric-calculated concentrations seem to be the most stable of the three techniques.

When comparing these three measurement techniques, we find the most stable and reproducible signal using ratiometric data processing (**Fig. 6.6C**). While calibration-free measurements still have significant utility for *ex vivo* measurements, the vasculature of a living animal seems to be too variable to use the same constants for each animal (**Fig. 6.6A**). KDM measurements prove to be fairly stable and reproducible (**Fig. 6.6B**), though they are not as stable or reproducible as ratiometric measurements. KDM measurements also prove more variable towards higher concentrations, where a smaller current variation results in a large variation in measured concentrations (**Fig. 6.5D**).

In this work, we show sensitive, continuous measurement of a protein target directly in the bloodstream of living animals for the first time (**Fig. 6.5**), even observing a quantitative difference between injections of different doses in the same animal (**Fig. 6.5D**). We quantitatively measure *nanomolar* blood concentrations, making these the most sensitive E-AB *in vivo* measurements to date.

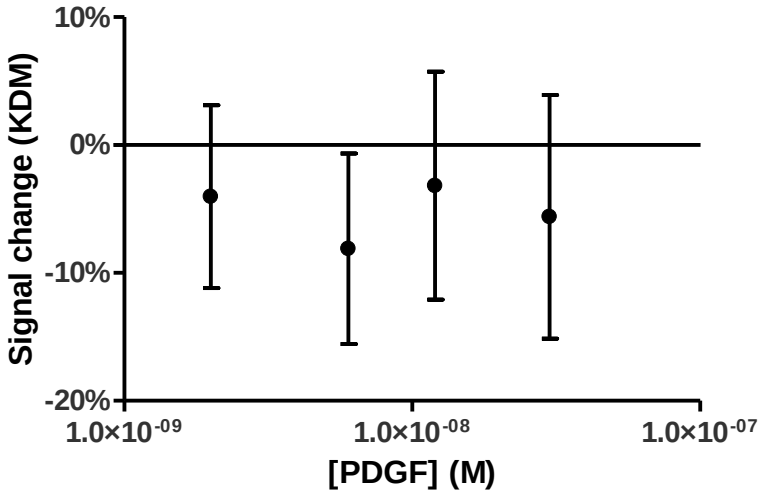

Figure S6.1. Membrane-protected electrodes exhibit signal response within error of zero signal change when challenged with target. Data shown are the mean and standard error of 4 electrodes in flowing whole blood, with KDM using the subtractive difference between 120 Hz and 10 Hz measurements.

C. Materials and methods.

Human recombinant Platelet-derived Growth Factor-BB (expressed in *E. coli*) was purchased from Prospec-Tany Technogene Ltd. (Ness Ziona, Israel) and used as received without further purification. PDGF-BB was dissolved in water to a concentration of 10.3 µM (250 µg/mL) then further diluted for titration in the same media as measurements were performed. 20X phosphate-buffered saline (PBS) was purchased from Sigma Aldrich (St. Louis, MO), diluted to 1X concentration and pH corrected to 7.4 using sodium hydroxide

and hydrochloric acid. Whole bovine blood and bovine plasma were purchased from HemoStat Laboratories (Dixon, CA). Blood was shipped with 3 IU/mL sodium heparin and used within a week of receipt. Gold wire was purchased from A-M Systems (Sequim, WA). Heat-shrink PTFE was purchased from Zeus Labs (Branchburg Township, CA). Polyethersulfone membranes (P/N: C02-E20U-05-N) were purchased as MicroKros Filter Modules from Spectrum Laboratories (Rancho Dominguez, CA). The filter modules were cut open and the hollow membranes were extracted from them. Oligonucleotides were synthesized by Biosearch Technologies (Novato, CA) and purified by dual HPLC. 6-mercapto-1-hexanol and tris(2-carboxyethyl)phosphine were purchased from Sigma Aldrich (St. Louis, MO) and used as received.

Catheters (18G) and 1 mL syringes were purchased from Becton Dickinson (Franklin Lakes, NJ). Silver wire (200 µm diameter) was purchased from Alfa Aesar (Ward Hill, MA); to employ this as a reference electrode it was immersed in bleach overnight to form a silver chloride film. Insulated pure gold and silver wires (100 µm diameter) were purchased from A-M systems. Heat-shrink polytetrafluoroethylene insulation (PTFE, HS Sub-Lite-Wall, 0.02, 0.005, 0.003±0.001 in, black-opaque, Lot # 17747112-3) was purchased from ZEUS (Branchburg Township, CA).

PDGF-BB aptamer sequence.

5’ – 6-carbon thiol linker – `CAGGC TACGG CACGT AGAGC ATCAC CATGA TCCTG` – methylene blue redox tag – 3’

Sensor fabrication and preparation.

Segments of gold wire were cut to 7 cm in length to make sensors. These wires were then insulated by applying heat to shrinkable tubing around the body of the wires. The sensor window (i.e., the region without insulation) was approximately 5-8 mm in length. To increase surface area of these working electrodes (to obtain larger peak currents) the sensor surface was roughened electrochemically via immersion in 0.5 M sulfuric acid followed by jumping between $E_{initial}$ = 0.0 V to E_{high} = 2.0 V vs Ag/AgCl, back and forth, for 100,000 pulses. Each pulse was of 2 ms duration with no "quiet time."

To fabricate sensors an aliquot of the PDGF aptamer was thawed and then reduced for 1 h at room temperature with a 1000-fold molar excess of tris(2-carboxyethyl)phosphine. A freshly roughened gold electrode was then rinsed in di-ionized water before being immersed in a solution of the appropriate reduced DNA construct at 200 nM in 1X PBS for 1 h at room temperature. The sensors were immersed overnight at 4°C for 12 h in 20 mM 6-mercapto-1-hexanol in 1X PBS to coat the remaining gold surface and remove nonspecifically adsorbed DNA. After this the sensors were rinsed with di-ionized water and stored in PBS.

Electrochemical measurements.

Electrochemical measurements were performed at room temperature using a handheld potentiostat (Model 1242 B, CH Instruments, Austin, TX) using a 2-electrode setup in which the reference and counter electrodes were a silver wire coated with a silver chloride film as described above. Square wave voltammetry was performed at 300 Hz using a potential step of 0.001 V, 10 Hz using a potential step of 0.004 V and at 40 Hz using a potential step of 0.001 V, all using an amplitude of 0.025 V.

In vivo Experiments

Animals. Adult male Sprague-Dawley rats (300-500 g; Charles River Laboratories, Wilmington, MA, USA) were pair housed in a temperature and humidity controlled vivarium on a 12-h light-dark cycle and provided *ad libitum* access to food and water. All animal procedures were consistent with the guidelines of the NIH *Guide for Care and Use of Laboratory Animals* and approved by the Institutional Animal Care and Use Committee of the University of California Santa Barbara.

Surgery. For the anesthetized preparation, rats were anesthetized using isoflurane gas inhalation (2.5%) and monitored throughout the experiment using a pulse oximeter (Nonin Medical, Plymouth, MN) to measure heart rate and %SpO2 to insure depth of anesthesia. After exposing both ventral jugular veins, a simple catheter made from a SILASTIC tube (Dow Corning, Midland, MI, USA) fitted with a steel cannula (Plastics One, Roanoke, VA, USA) was implanted into the left jugular vein. 0.1-0.3 mL of heparin (1000U/mL, SAGENT Pharmaceuticals, Schaumburg, IL, USA) were immediately infused through the catheter to prevent blood clotting. The sensor was inserted into the right jugular vein and secured in place with surgical suture. Following drug infusions (see below), animals were euthanized by overdose on isoflurane.

Measurements. A 30 min sensor baseline was established before the first drug infusion. A 3 mL syringe filled with the target drug was connected to the sensor-free catheter (placed in the jugular opposite that in which the sensor is emplaced) and placed in a motorized syringe pump (KDS 200, KD Scientific Inc., Holliston, MA, USA). After establishing a stable baseline, the PDGF-BB protein was infused through this catheter at a rate of 0.2 mL/min.

D. References

1. Anderson, N. L. The Clinical Plasma Proteome: A Survey of Clinical Assays for Proteins in Plasma and Serum. Clin. Chem. 2010, 56, 177–185, doi:10.1373/clinchem.2009.126706.
2. Krisp, C.; Randall, S. A.; McKay, M. J.; Molloy, M. P. Towards clinical applications of selected reaction monitoring for plasma protein biomarker studies. Proteomics - Clin. Appl. 2012, 6, 42–59, doi:10.1002/prca.201100062.
3. Guo, S.; Martin, M. G.; Tian, C.; Cui, J.; Wang, L.; Wu, S.; Gu, W. Evaluation of Detection Methods and Values of Circulating Vascular Endothelial Growth Factor in Lung Cancer. J. Cancer 2018, 9, 1287–1300, doi:10.7150/jca.22020.
4. Hirales Casillas, C. E.; Flores Fernández, J. M.; Camberos, E. P.; Herrera López, E. J.; Pacheco, G. L.; Velázquez, M. M. Current status of circulating protein biomarkers to aid the early detection of lung cancer. Futur. Oncol. 2014, 10, 1501–1513, doi:10.2217/fon.14.21.
5. Kros, J. M.; Mustafa, D. M.; Dekker, L. J. M.; Sillevis Smitt, P. A. E.; Luider, T. M.; Zheng, P.-P. Circulating glioma biomarkers. Neuro. Oncol. 2014, doi:10.1093/neuonc/nou207.
6. Tanase, C.; Albulescu, R.; Codrici, E.; Popescu, I. D.; Mihai, S.; Enciu, A. M.; Cruceru, M. L.; Popa, A. C.; Neagu, A. I.; Necula, L. G.; Mambet, C.; Neagu, M. Circulating biomarker panels for targeted therapy in brain tumors. Futur. Oncol. 2015, 11, 511–524, doi:10.2217/fon.14.238.
7. Liu, Q.; Zhou, Y.; Yang, Z. The cytokine storm of severe influenza and development of immunomodulatory therapy. Cell. Mol. Immunol. 2016, 13, 3–10, doi:10.1038/cmi.2015.74.
8. Clark, I. A.; Vissel, B. The meteorology of cytokine storms, and the clinical usefulness of this knowledge. Semin. Immunopathol. 2017, 39, 505–516, doi:10.1007/s00281-017-0628-y.
9. Stenken, J. A.; Poschenrieder, A. J. Bioanalytical chemistry of cytokines--a review. Anal. Chim. Acta 2015, 853, 95–115, doi:10.1016/j.aca.2014.10.009.
10. Park, K. C.; Gaze, D. C.; Collinson, P. O.; Marber, M. S. Cardiac troponins: from myocardial infarction to chronic disease. Cardiovasc. Res. 2017, 113, 1708–1718, doi:10.1093/cvr/cvx183.
11. Wilson, D. S.; Szostak, J. W. In vitro selection of functional nucleic acids. Annu. Rev. Biochem. 1999, 68, 611–47, doi:10.1146/annurev.biochem.68.1.611.
12. Lubin, A. A.; Plaxco, K. W. Folding-based electrochemical biosensors: the case for responsive nucleic acid architectures. Acc. Chem. Res. 2010, 43, 496–505, doi:10.1021/ar900165x.
13. Somerson, J.; Plaxco, K. Electrochemical Aptamer-Based Sensors for Rapid Point-of-Use Monitoring of the Mycotoxin Ochratoxin A Directly in a Food Stream. Molecules 2018, 23, 912, doi:10.3390/molecules23040912.
14. Swensen, J. S.; Xiao, Y.; Ferguson, B. S.; Lubin, A. A.; Lai, R. Y.; Heeger, A. J.; Plaxco, K. W.; Soh, H. T. Continuous, real-time monitoring of cocaine in undiluted blood serum via a microfluidic, electrochemical aptamer-based sensor. J. Am. Chem. Soc. 2009, 131, 4262–6, doi:10.1021/ja806531z.

15. Arroyo-Currás, N.; Somerson, J.; Vieira, P. A.; Ploense, K. L.; Kippin, T. E.; Plaxco, K. W. Real-time measurement of small molecules directly in awake, ambulatory animals. Proc. Natl. Acad. Sci. 2017, 114, 645–650, doi:10.1073/pnas.1613458114.
16. Lai, R. Y.; Plaxco, K. W.; Heeger, A. J. Aptamer-Based Electrochemical Detection of Picomolar Platelet-Derived Growth Factor Directly in Blood Serum. Anal. Chem. 2007, 79, 229–233, doi:10.1021/ac061592s.
17. Ferguson, B. S.; Hoggarth, D. a; Maliniak, D.; Ploense, K.; White, R. J.; Woodward, N.; Hsieh, K.; Bonham, A. J.; Eisenstein, M.; Kippin, T. E.; Plaxco, K. W.; Soh, H. T. Real-time, aptamer-based tracking of circulating therapeutic agents in living animals. Sci. Transl. Med. 2013, 5, 213ra165, doi:10.1126/scitranslmed.3007095.
18. Li, H.; Dauphin-Ducharme, P.; Ortega, G.; Plaxco, K. W. Calibration-Free Electrochemical Biosensors Supporting Accurate Molecular Measurements Directly in Undiluted Whole Blood. J. Am. Chem. Soc. 2017, 139, 11207–11213, doi:10.1021/jacs.7b05412.
19. White, R. J.; Plaxco, K. W. Exploiting binding-induced changes in probe flexibility for the optimization of electrochemical biosensors. Anal. Chem. 2010, 82, 73–6, doi:10.1021/ac902595f.